

**REMOVING THE KEY TECHNICAL
BARRIER TO WIDESPREAD USE OF
ADVANCED ABSORPTION COOLING**

Prepared For:

California Energy Commission
Public Interest Energy Research Program

Prepared By:

Gas Technology Institute

CONSULTANT REPORT

April 2004
500-04-019

Prepared By:

Gas Technology Institute
1700 South Mount Prospect Road
Des Plaines, IL 60018

Kevin Krist,
Principal Investigator

SRI International
333 Ravenswood Avenue
Menlo Park, CA 94025

Palitha Jayaweera,
Principal Investigator

Contract No. 500-98-029

Prepared For:

California Energy Commission

Chris Scruton,
Project Manager

Nancy Jenkins,
Program Area Lead
Buildings End-Use Energy Efficiency

Terry Surlles,
PIER Program Manager

Robert L. Therakelsen,
Executive Director



DISCLAIMER

This report was prepared as the result of work sponsored by the California Energy Commission. It does not necessarily represent the views of the Energy Commission, its employees or the State of California. The Energy Commission, the State of California, its employees, contractors and subcontractors make no warrant, express or implied, and assume no legal liability for the information in this report; nor does any party represent that the uses of this information will not infringe upon privately owned rights. This report has not been approved or disapproved by the California Energy Commission nor has the California Energy Commission passed upon the accuracy or adequacy of the information in this report.

Acknowledgements

The authors would like to thank Chris Scruton and Eric Stubee of the California Energy Commission for their help and guidance throughout this project. We would also like to thank Ray Reynoldson of Reynoldson Technologies, Australia for his support in the commercialization effort and the scale up process.

Additionally, we would like to thank Angel Sanjurjo, Gopala Krishnan, Kai Lau, Namal Priyantha, and Marc Hornbostel from SRI International for their contributions.

Preface

The Public Interest Energy Research (PIER) Program supports public interest energy research and development that will help improve the quality of life in California by bringing environmentally safe, affordable, and reliable energy services and products to the marketplace.

The PIER Program, managed by the California Energy Commission (Commission), annually awards up to \$62 million to conduct the most promising public interest energy research by partnering with Research, Development, and Demonstration (RD&D) organizations, including individuals, businesses, utilities, and public or private research institutions.

PIER funding efforts are focused on the following six RD&D program areas:

- Buildings End-Use Energy Efficiency
- Industrial/Agricultural/Water End-Use Energy Efficiency
- Renewable Energy
- Environmentally-Preferred Advanced Generation
- Energy-Related Environmental Research
- Strategic Energy Research.

What follows is the final report for the Removing the Key Technical Barrier to the Widespread Use of Advanced Absorption Cooling, Contract Number, 500-98-029 conducted by Gas Technology Institute (GTI). The report is entitled *Removing the Key Technical Barrier to the Widespread Use of Advanced Absorption Cooling*. This project contributes to the Buildings End-Use Energy Efficiency program.

For more information on the PIER Program, please visit the Commission's Web site at: <http://www.energy.ca.gov/research/index.html> or contact the Commission's Publications Unit at 916-654-5200.

Table of Contents

Preface	iv
Abstract	xii
Executive Summary	1
1.0 Introduction	5
1.1 Overview and Project Objectives	5
1.2 Absorption Cycles	6
1.3 Corrosion issues in Advanced Absorption Cycles	7
1.4 Corrosion Protection With Metallic Diffusion Coatings	10
1.5 Fluidized Bed Reactor Chemical Vapor Deposition (FBR-CVD)	11
1.6 Project Focus	12
1.7 Report Organization	13
2.0 Preparation Of Metallic Coatings	15
2.1 Selection of Materials	15
2.1.1 SRI Experience	15
2.1.2 Literature Search	15
2.1.3 Simplified Thermodynamic and Thermochemical Analysis	15
2.2 Selection of Coatings and Coating Techniques	18
2.3 Experimental Procedures	19
2.3.1 SRI Fluidized Bed Reactor Chemical Vapor Deposition (FBR-CVD) Process	19
2.3.2 Preparation of Metallic Coatings by FBR-CVD	21
2.3.3 Electroplating	23
2.3.4 Surface Passivation	27
3.0 Characterization Of Coatings	28
3.1 Analytical Techniques	28
3.2 Surface Analysis And Depth Profile Investigation	28
3.2.1 Cr Coatings on 409 SS by FBR-CVD	28
3.2.2 Cr Coatings on Pure Iron, Carbon Steel (C 1018), and Ni 200	32
3.2.3 Cr + M (M = W or Ni) Coatings on 409 SS by FBR-CVD	35
3.2.4 Ni Coatings on 409 SS by FBR-CVD	39
3.2.5 Ni Coating by Electrodeposition Followed by Cr Deposition by FBR-CVD	41
3.2.6 Ni + M (M = W or Mo) Coating by Electrodeposition Followed by Cr Deposition by FBR-CVD	48
3.3 Effect Of Welding On The Coatings	54
4.0 Corrosion Resistance Evaluation Of Coated Metal Specimens	55
4.1 Corrosion Rate Measurement Techniques	55
4.1.1 Tafel Slope	55
4.1.2 Electrochemical Impedance Spectroscopy	56
4.2 Corrosion Test Results	58

4.2.1.	Ni and Ni + Cr Coatings on 409 SS and C 1018	58
4.2.2.	Cr + Ni + W and Cr + Ni + Mo Coatings on 409 SS and C 1018	60
5.0	Characterization And Corrosion Resistance Evaluation Of Subscale Components	65
5.1.	Uniformity Of Chromium Diffusion Coatings On Subscale Components	65
5.2.	Preliminary Corrosion Experiments	65
5.3.	Electrochemical Corrosion Tests.....	65
5.4.	ASTM Tests for the Determination of localized corrosion	67
5.5.	Effect Of Welding On Subscale Components	69
6.0	Cost And Engineering Projections For Scale-Up Operation	71
6.1.	Triple-Effect Direct-Fired Generator Material Cost.....	71
6.2.	Feasibility Of Technology Commercialization	71
6.2.1.	Industrial Coating Approaches	71
6.2.2.	SRI Preliminary Economic Analysis.....	72
6.3.	Licensing	78
6.3.1.	Selection of a Commercialization Partner	78
6.3.2.	Market Analysis by Quality Heat Technologies.....	79
7.0	Technology Transfer and Commercial Production Process	81
7.1.	Selection of Metal Powders and Suppliers	81
7.2.	Establishing Process Parameters In A Metallined Pilot Scale Fluidized Bed	83
7.2.1.	Process Parameter Issues.....	85
7.2.2.	Equipment Issues.....	87
7.3.	Designing And Building Of Commercial Fluidized Bed Plant For Chromium Coatings	90
7.4.	Establishing Parameters for the Production Metal Lined Fluidized Bed at Bayswater.....	92
7.4.1.	Technical Parameters.....	92
7.4.2.	Consumable Cost Estimates	94
7.5.	Summary and Future Plans for Production of Large Coated Components.....	97
8.0	Component Testing in Prototype Machine.....	101
8.1.	Broad Prototype Design for Cr-Coated 409 SS.....	101
8.2.	Prototype Generator Test Plan.....	102
9.0	Summary And Conclusions.....	105
References	107

List of Figures

Figure 1.	Absorption Chiller (Left) and Inside Tube Bundle (Right).....	8
Figure 2.	Schematic Diagram of a Direct-Fired Generator	9
Figure 3.	Graphical Representation of a Diffusion Coating and Surface Passivation.....	11
Figure 4.	A Typical Metal Diffusion Depth Profile	11
Figure 5.	A Simplified Representation of the Metal-Solution-Vapor System.....	16

Figure 6. Partial Pressure Curves for Metal Halides as a Function of Temperature (e.g., AlCl ₃).....	17
Figure 7. Measured Mass Spectrometric Signals for Silicon Bromides as a Function of Temperature.....	18
Figure 8. Simplified Schematic Diagram of a Fluidized Bed Reactor With RF (Radiofrequency) Heating	20
Figure 9. Laboratory Setup for FBR-CVD Coatings with Electric Heating.....	20
Figure 10. Cr-Coated Steel Tubes Prepared by SRI's FBR-CVD Process.....	21
Figure 11. Microstructure of As-Received 409 SS.....	29
Figure 12. Microstructure of Cr-Coated 409 SS Prepared By FBR-CVD	29
Figure 13. Cr Diffusion Depth Profile of Cr-Coated 409 SS Samples	30
Figure 14. Cr-Coated 409 SS Surface	31
Figure 15. Cr-Coated 409 SS Surface at a Higher Magnification, Showing Attached Cr Particles and Grain Boundaries.....	31
Figure 16. Cr Diffusion Profiles of a Cr Coated 409 SS (Runs #1 And #5)	32
Figure 17. Surface Morphology of a Cr-Coated Iron (99.99%) Specimen	33
Figure 18. Surface Morphology of A Cr-Coated C 1018 Specimen	33
Figure 19. Surface Morphology of A Cr-Coated Ni 200 Specimen	34
Figure 20. Cr Diffusion Profile in the Diffusion Region of Cr-Coated Iron (99.99%)	35
Figure 21. Cr Diffusion Profile in the Diffusion Region of Cr-Coated C 1018	36
Figure 22. Metal Concentration Profiles in the Diffusion Region of Cr-Coated Ni 200 Alloy.....	36
Figure 23. Typical EDX Spectrum of a Cr + W Coated 409 SS Surface	37
Figure 24. SEM Photograph of W on a Cr-Coated 409 SS Surface	38
Figure 25. SEM Photograph of W on a Cr-Coated 409 SS Surface at a Higher Magnification.....	38
Figure 26. Cr Diffusion Profiles in 409 SS Before and After Deposition of Ni (Runs #5 And #10; See Table 2 and Table 3).....	39
Figure 27. Surface Morphology of a Ni Coating on 409 SS (Ni Coating #1)	40
Figure 28. Surface Morphology of a Ni Coating on 409 SS (Ni Coating #2)	41
Figure 29. Ni Diffusion Profile of a Ni-Coated 409 SS Specimen.....	41
Figure 30. Surface Morphology of a Ni + Cr Coating on 409 SS	42
Figure 31. Cross-section of an Electrodeposited Ni Coating on 409 SS Before FBR-CVD Cr Coating and Annealing.....	43
Figure 32. Cross-section of an Electrodeposited Ni Coating on 409 SS After FBR-CVD Cr Coating and Annealing.....	44
Figure 33. Ni and Cr Diffusion Profiles of a Dual-Metal-Coated 409 SS Specimen.....	44
Figure 34. Surface Morphology of an Electrodeposited Ni + FBR-CVD Cr-Coated C 1018 Specimen	45
Figure 35. EDX Spectrum of an Electrodeposited Ni + FBR-CVD Cr-Coated C 1018 Specimen.....	46
Figure 36. Cross-Section of an Electrodeposited Ni + FBR-CVD Cr-Coated C 1018 Specimen.....	47
Figure 37. Cr, Fe, and Ni Diffusion Depth Profiles of an Electrodeposited Ni + FBR-CVD Cr-Coated C 1018 Specimen.....	47
Figure 38. Cr, Fe, and Ni Diffusion Depth Profiles of an Electrodeposited Ni + FBR-CVD Cr-Coated C 1018 Specimen.....	49
Figure 39. An Edge View of Ni + W Coating on 409 SS Specimen #2.....	50
Figure 40. Cross-sectional Image of a Ni + W Electrodeposited C 1018 Specimen #10.....	51
Figure 41. Diffusion Depth Profiles of Cr, Ni, W, and Fe in a C 1018 Sample Prepared by Ni + W Electrodeposition, Followed by FBR-CVD Cr Coating	53
Figure 42. Electrochemical Corrosion Testing Set-Up for Rapid Screening of Coatings.....	56

Figure 43. A Current Versus Potential Curve Tafel Slope Measurements For As-Received 409 SS in 90% Lithium Zinc Bromide Solution at 260°C	57
Figure 44. Nyquist Plot for As-Received 409 SS in 90% Lithium Zinc Bromide Solution at 260°C ..	58
Figure 45. Nyquist Plots for Coated and As-Received C 1018 Specimens in LiBr/LiOH Solution at 165°C	59
Figure 46. Nyquist Plots for Coated and As-Received 409 SS Specimens in the Measured Frequency Range (10 kHz to 10 mHz) in LiBr/LiOH Solution at 165°C	59
Figure 47. Nyquist Plots for Coated and As-Received 409 SS Specimens. Expanded Graph from Figure 48 Focusing on the Low Impedance Region to View the Comparison Between As-Received and Coated Specimens.....	60
Figure 48. Nyquist Plot for Ni + Mo Electrodeposited and then Cr FBR-CVD Coated 409 SS in 90% LZB Solution at 260°C Under N ₂ Saturated Atmosphere.....	61
Figure 49. Nyquist Plot for Coated C 1018 Specimens in 90% LZB at 260°C Under N ₂ Saturated Atmosphere. Top: Ni + Mo Electroplated and then Cr FBR-CVD Coated. Bottom: Ni + W Electroplated and then Cr FBR-CVD Coated.....	63
Figure 50. Potential–Logarithmic Current Relationships (Tafel Plots) of As-Received and Cr-Coated 409 SS Tubular Specimens in LiBr/LiOH at 165°C. The Surface Area of the 409 SS Electrode was 11.80 cm ²	66
Figure 51. Nyquist Plots for Cr-Coated and As-Received 409 SS Tubular Specimens in LiBr/LiOH Solution at 165°C in an N ₂ Atmosphere.....	67
Figure 52. Surface of a Cr-Coated 409 SS Specimen After Exposure to 6% FeCl ₃ Solution at 50°C for 72 H (Scale Bar has 1-mm Divisions).....	69
Figure 53. Cr-Coated 409 SS Tube Welded to AL6XN®, after 1000 H of Exposure to 90% LZB at 260°C	70
Figure 54. Schematic Diagram for the Fluidized Bed Chromizing Process.....	73
Figure 55. Heat Treatment of Large Gear Assembly in a Fluidized Bed Furnace.	78
Figure 56. The Cost of Cr Coating of 409 SS Tubes by the FBR-CVD Process	79
Figure 57. Diffusion Profile of Cr in 409 SS Prepared by Using Fe/Cr Metal Powder	82
Figure 58. Diffusion Profile of Cr in 409 SS Prepared by Using Cr/X Alloy and Cr Metal Powders .	82
Figure 59. Representative Cr Diffusion Achieved in QHT Fluidized Bed at Knoxfield.....	87
Figure 60. Top Distributor Showing Coarse Grit and Sintering.....	89
Figure 61. Sintered Cr Powder Recovered from Above the Flexible Tile	89
Figure 62. Schematic Diagram of the Fluidized Bed Furnace.....	91
Figure 63. QHT’s New Plant for Fluidized Bed Coating at Bayswater, Australia.....	92
Figure 64. Loaded Tube Basket Ready for Processing at Bayswater.....	93
Figure 65. Cr Profile of Coated 409 SS Tube Resulting from a Trial at Bayswater	93
Figure 66. View of Distributor Showing Sintered Powder and Sticking of Powder to Distributor	94
Figure 67. Simplified Diagram of a Broad Triple-Effect Advanced Absorption Chiller	101
Figure 68. Simplified Diagram of the Broad Triple-Effect Generator	102

List of Tables

Table 1. Metal Composition of Commonly Used Alloys (wt%).....	10
Table 2. Experimental Conditions for Deposition of Cr on 409 SS	22
Table 3. Experimental Conditions for Deposition of a Second Metal on Cr-Coated 409 SS.....	23
Table 4. Composition of the Plating Bath and Other Experimental Parameters	24
Table 5. Initial Compositions of Electroplating Baths	26
Table 6. Surface Composition and Average Thickness of Electrodeposited Ni + W Coatings	52
Table 7. Percentages (w/w) of Cr, Ni, W, Mo, and Fe on the Surface of Electrodeposited Alloys	54
Table 8. Rates of Corrosion of Uncoated and Coated Metal in LiBr/LiOH Solution at 165°C and N ₂ Atmosphere	60
Table 9. Polarization Resistance (R _p) and Rate Of Corrosion of As-Received and Coated Steel Specimens.....	62
Table 10. Rate of Corrosion of Subscale Tubes, as Determined According To ASTM G48-76	68
Table 11. Material Cost Comparison for the Triple-Effect Generator	72
Table 12. Capital Cost of the Chromium Coating Process (150,000 Tubes Per Year)	75
Table 13. Annual Operating Costs (150,000 Tubes Per Year).....	77
Table 14. Comparison of 1-Inch-Diameter Tubing Costs per Linear Foot	80
Table 15. SRI Parameters for Cr Coating.....	84
Table 16. Comparison of QHT and SRI Cr Coating Parameters.....	86
Table 17. Comparison of SRI and QHT Fluidized Bed Process	88
Table 18. Cost of Various Consumables in Cr Coating of Steel	95
Table 19. Options for Full Scale Cr-Coated Tube Production	99

Abstract

Increased use of natural gas fired, absorption-chillers could help to mitigate the high cost and potential for outages associated with the peak summer electric loads in California. The introduction of high efficiency, advanced versions of this technology could eventually improve the market prospects. This project addressed a key technical barrier to the use of advanced absorption cycles—the corrosion of practical materials of construction when exposed to the aggressive fluids and high temperatures involved. Currently, super alloys or thicker-walled materials that significantly increase system cost are required in parts of the system.

The project developed an approach to reduce material cost by diffusing corrosion-resistant metal compositions into the surface of inexpensive substrate steels using fluidized-bed reactors. Corrosion resistance comparable to that of super alloys was obtained with laboratory coupons in concentrated lithium bromide fluids up to temperatures of 260°C. One-foot long tubes were then produced in a laboratory reactor, and subsequently, the process was adapted to practical industrial reactors. This led to the successful production of tubes up to two feet in length and considerable progress on making full-scale tubes for an advanced absorption cycle prototype generator. The partners in this project were the Gas Technology Institute (GTI) and SRI International. GTI and SRI are continuing to develop the technology and are seeking commercialization partners for absorption chiller and other applications.

Executive Summary

Background

On hot summer afternoons in California, peak electrical demand topping 50,000 megawatts can put tremendous stress on the statewide electrical system and cause blackouts and brownouts. Nearly 15% of this peak demand is due to commercial air conditioning, providing a strong incentive to develop alternatives to electric powered cooling. In recent years electricity prices have also risen sharply, motivating large electrical energy consumers to search for ways to reduce their electric bills.

In this energy market, an advanced natural gas-fired absorption chiller for air conditioning applications could be an attractive candidate. The share of natural gas fired absorption chillers in the chiller market has increased slowly from about 3.8% in 1990 to about 7% in 2003. The significantly higher efficiency of more advanced systems could increase the rate of market penetration. California electric ratepayers would benefit through reduced demand for, and therefore cost of, electricity as well as reduced potential for outages.

A number of technical challenges apply to the market introduction of advanced absorption chillers. A key challenge involves the expensive alloys such as AL6XN® and SeaCure® typically required to resist the corrosion caused by high temperatures and concentrated lithium bromide solutions used in advanced machines, driving up already high equipment costs.

Goals and Objectives

The overall goal for this project was to lower the cost of advanced gas-fired absorption chillers by developing less expensive materials of construction. Specific technical goals for the chiller materials were:

- Tolerance of temperatures up to 260°C
- Same thermal conductivity as base metal
- Durability of 20 years
- Corrosion of not more than 0.0001 inch per year

A goal for the advanced chiller to be built was a coefficient of performance (COP) of 1.4 to 1.6, where COP is defined as the ratio of cooling provided to heat added by burning natural gas. The project had the following specific economic goals:

- Coating costs of less than \$10 per ft² for generators
- Coating costs of less than \$3 per ft² for absorber heat exchangers
- Reduce the manufactured cost of generators and absorbers for triple effect chillers by at least 25%

Project Approach

The technical approach was to modify the surface of a low-cost steel alloy to provide the corrosion protection required in an advanced absorption cycle environment. The surface was to be modified by diffusing a corrosion resistant metal into the bulk substrate using a process known as Fluidized Bed Reactor Chemical Vapor Deposition (FBR-CVD). In the FBR-CVD process, the substrate to be coated is immersed in a powder bed containing the required coating metal, such as chromium. An inert carrier gas mixed with HCl and H₂ at high temperature is blown upward through the powder bed, causing it to fluidize. Volatile metal halides are generated *in situ* that subsequently decompose on the base metal substrate to form a coating. The deposited metal diffuses into the substrate at high temperatures, producing a coating with a gradient composition that extends deeply into the substrate. Diffusion coatings can be applied uniformly onto large and complex geometric shapes.

The FBR-CVD process was first to be demonstrated on a laboratory scale, and then scaled up in a production environment to a more practical size. The completed components were to be assembled into an absorption chiller generator and performance tested. The Gas Technology Institute (GTI) and SRI International (SRI) were to perform the research and development effort, which would be scaled up by an industrial partner. Trane Corporation, and later Broad USA, a major chiller manufacturer, planned to perform tests of prototype advanced absorption chillers they would construct using the new materials.

Project Results

Coated components were prepared on a laboratory scale at SRI using the FBR-CVD technology. Completed samples had the same thermal conductivity as the base material and showed less than 0.00005 inch per year of corrosion in concentrated LiBr at 260°C, surpassing the goal for corrosion resistance and equaling the performance of expensive super alloys. Methods were developed to diffuse other elements that could prevent additional modes of corrosion, should this be necessary.

Due to unrelated economic factors, early in the project the Trane Corporation decided to terminate their participation. The Commission temporarily halted the project until a viable market partner could be found. After some delay Broad USA stepped forward as a market partner and the project was re-started.

Scaling up the process to a practical size by the industrial partner proved to be technically challenging. First 1- and then 2-ft tubes with the requisite uniformity and Cr content were prepared. After resolving most of the technical production problems, full-scale 4-ft tubes were ultimately prepared which were very close to the desired specifications.

The industrial partner came under financial stress during the course of the contract and was unable to fully complete the project. SRI and GTI continued some limited activities. The construction of a prototype chiller generator with processed materials, although not yet implemented, appears to be feasible once components are available.

Economic analysis by SRI indicates that the cost of production for a plant producing 150,000 tubes of 1.5" diameter by 40" length, including coating materials, labor, plant capital costs

and quality control laboratory overhead, would be \$5.12 per tube. Each of these tubes has a surface area of about 2.4 ft², giving a cost of \$2.13 per ft² of coating, surpassing the project goal of less than \$10 per ft² for generator coatings and \$3 per ft² for other heat exchanger coatings.

A 500 ton absorption generator using AL6XN® was projected to have \$40,500 in material costs. The cost of the processed materials was estimated to be 37% that of AL6XN® alloy, which would yield a savings of over \$25,000 on generator material costs. While precise generator manufacturing costs are not available, this seems likely to reduce the manufactured cost of absorber generators by more than the goal of 25%.

An additional outcome has been significant interest in the diffusion coating process by manufacturers of other cost sensitive equipment requiring corrosion resistance, such as high efficiency condensing gas furnaces and water heaters. These manufacturers clearly see benefits in a process that promises to lower their costs and improve equipment performance.

Conclusions

This project was able to create diffusion coatings on inexpensive materials that meet the demanding requirements for corrosion and temperature resistance in lithium bromide absorption and many other harsh environments. The technology was shown to be scalable in a production environment and cost effective. Although the project did not construct and test an advanced chiller generator as originally planned, it has substantially prepared the way for this outcome. Manufacturing firms have expressed interest in using the process in other applications where aggressive fluids are involved, such as condensing furnaces and water heaters, furnace vents, and food, pharmaceutical, and seawater applications.

1.0 Introduction

1.1 Overview and Project Objectives

In California, a significant amount of energy is used for air conditioning on hot summer days, with large fluctuations in the electricity demand. This peak electricity demand put a tremendous stress on the grid, causing blackouts and brownouts. In this market, natural gas fired, absorption chillers can play a major role by reducing the peak electrical energy demand and associated high costs.

The share of natural gas fired, absorption chillers in the gas and electric chiller market has increased slowly, from ~3.8% in 1990 to ~6.4% today. Wider use of absorption chillers would greatly benefit the California electric ratepayer by reducing the very high cost of electricity and the potential for outages associated with the peak summer electric load in California. The high efficiencies of advanced absorption chillers under development could significantly improve the prospects for this market. However, the high temperature and concentrated lithium bromide fluids associated with these machines drastically increase the corrosion rates of the construction materials. To mitigate corrosion, special alloys such as AL6XN® are currently required, but the alloy cost compromises the potential benefits gained from increased chiller efficiency. Therefore, the technical goal of this project was to develop lower cost materials that are corrosion resistant in lithium bromide fluids in order to accelerate the introduction of advanced absorption cooling technology. The approach to reduce the material cost is to introduce diffusion coatings of corrosion-resistant metal compositions into the surface of low-cost substrate steels by using fluidized bed reactors. An initial laboratory phase was completed previously under the support of the Gas Technology Institute (GTI). The present three-year project focused mainly on completion of laboratory development of the coating process and prototype testing of coated specimens. The specific technical objectives were:

- Microscopic and X-ray examination of the low-cost coating/substrate systems to determine physical coating properties and optimum fabrication conditions.
- Corrosion rate screening of coating/substrate system coupons in the fluids and under operating conditions for advanced chillers to confirm selections identified in previous research and to attempt to identify better systems.
- Fabrication and successful corrosion rate testing of subscale tubes at SRI.
- Engineering/cost projections for scale-up operation, which indicate that investment in pilot-scale operation is warranted.
- Successful testing of full-scale tubes in a prototype direct-fired generator for a Broad absorption chiller.
- A production readiness plan, which identifies the processes, facilities, manpower, support systems, and other issues needed to introduce low-cost, diffusion-coated materials into chiller equipment.

The technical criteria for successful components include (1) corrosion rates of < 0.1 mil per year; (2) temperature tolerance up to 500°F; (3) negligible influence on the thermal conductivity of the substrate steel; (4) projected durability of 20 years; and (5) reliable operation in chillers having coefficients of performance up to 1.4-1.6.

The current estimated cost criteria for successful components include (1) generator tube cost of < \$3/ft for 1-inch-diameter tubes (equivalent to < \$10/ft²), and (2) 25% cost reductions to manufacture advanced generators. Advanced designs may also increase operating temperature or aggressive conditions in other parts of the chiller, such as the absorber or evaporator. Diffusion coatings may benefit these components as well.

The current project effort was focused on the development of corrosion protective diffusion coatings, process scale-up and production of tubes for a prototype generator, and field tests with the prototype advanced absorption chiller. The project team members were Gas Technology Institute for project management and commercialization, SRI International for technical development and testing, Quality Heat Technologies for coating process scale-up and coated tube production for prototype chillers, and Broad USA for prototype chiller fabrication and testing.

1.2. Absorption Cycles

Absorption cycles or chemical heat pumps transfer heat from a low-temperature source (e.g., a room) to a high-temperature sink (e.g., a cooling tower) by circulating refrigerants and absorbents through numerous heat exchangers. Such a transfer requires a thermodynamic input in the form of either work or heat, as explained by the second law of thermodynamics [1]. Absorption cycles are widely used in large industrial space conditioning applications. Recent advances in absorption cooling technology have improved the coefficient of performance (COP) of absorption cycles. The new generation of absorption cycles, commonly known as advanced absorption cycles fueled by natural gas, can offer significant advantages over conventional heating, cooling, and refrigeration systems [2-4]. These advanced cycles include double-effect, triple-effect, and generator absorber heat exchange (GAX) cycles [5-7]. High-performance advanced absorption cycles reduce energy consumption and thereby make it economical to use natural gas in air-conditioning and refrigeration.

The advanced absorption cycle consists of carefully designed, multistage heat exchanger loops that transfer heat by using one or two refrigerant/absorbent pairs. The triple-effect chiller has a 30% to 60% higher COP than a double-effect cycle chiller using equivalent heat exchangers. The triple-effect chiller has the potential to be less expensive than double-effect chillers because the triple-effect chillers (1) can use several existing absorption fluids, (2) use conventional heat exchangers, and (3) need less total heat exchanger per unit capacity than single- or double-effect cycles.

Water/LiBr, water/LiBr with additional absorbents (e.g., ZnBr₂, LiCl), ammonia/water, and ammonia/water with other salts (e.g., LiBr) are some of the widely used absorbents and refrigerants [2-4]. Conventional cycles operate at 93°-177°C (200°-350°F), but the triple-effect and other advanced cycles operate at much higher temperatures to transfer absorber heat at

temperatures up to 149°C (300°F). Because the condenser is also operating at about 93°C (200°F), the generator temperatures must be very high, typically over 232°C (450°F). Under these conditions, highly concentrated absorption fluids are generated and circulated in advanced absorption cycle components.

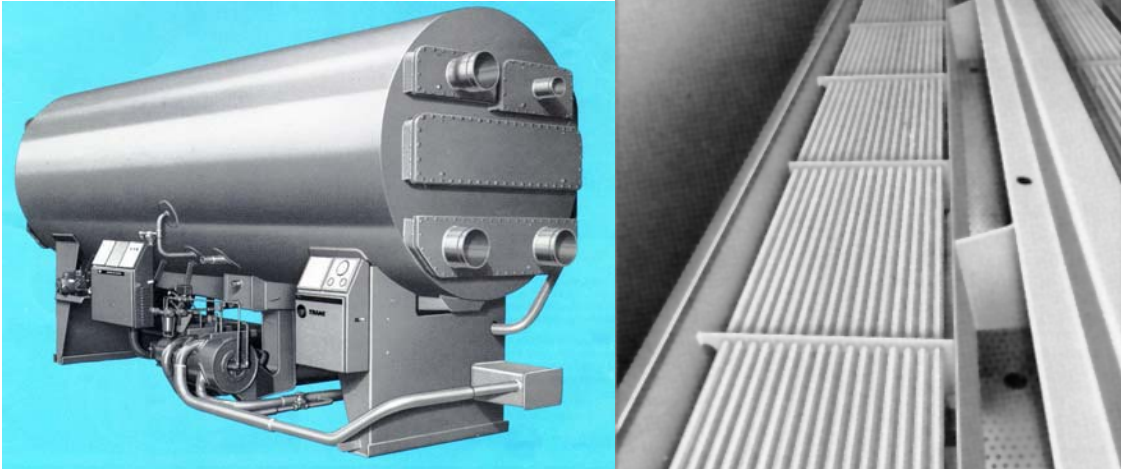
1.3. Corrosion issues in Advanced Absorption Cycles

The major components of an absorption cycle, heat exchangers, require relatively large areas in contact with the absorbent and refrigerant to transfer heat from one source or sink to another. The absorbent mixtures used in chillers are corrosive toward preferred construction materials for heat exchangers. The higher operational temperatures of advanced double- and triple-effect cycles significantly increase the corrosion rate in heat exchangers and thereby reduce their service life and effectiveness, offsetting the savings of gas consumption. Currently, unavailability of reliable corrosion control technologies is one of the major barriers to the commercialization of these advanced absorption cycles.

Advanced absorption cycles are at late stages of development, and prototypes such as triple-effect chillers are being tested for their COP. The triple-effect absorption chiller under development at Trane is essentially two single-effect chillers connected in tandem. They have two independent circulating fluid loops. LiBr/water is used in the low-temperature stage. Because the high *pH* of the fluid (~12-13) keeps the metals passivated, no major corrosion problems are expected in the low-temperature stage.

Trane proposes to use LiBr/ZnBr₂ (LZB) absorption fluid in the high-temperature loop to operate the machine at ambient pressure. However, use of LiBr/ZnBr₂ and higher operating temperatures make the fluid extremely corrosive to commonly used metals. Bivalent Zn²⁺ hydrolyzes in water [$\text{Zn}^{2+} + 2\text{OH}^- \rightarrow \text{Zn}(\text{OH})_2$], decreasing the *pH*. The *pH* of the solution cannot be increased sufficiently to decrease the corrosion rate without precipitating zinc hydroxides. Although the *pH* of the fluid is about 5.6-6.0 at room temperature, it may be much lower at the operating temperature (for pure water, *pH* is decreased by about 1.4 units when the temperature is increased from 25° to 260°C, according to the *pK_w*-temperature relationship [8]), making the fluid extremely corrosive to economical alloys such as mild steel or 409 SS.

Although the high-temperature absorber is also subjected to some degree of corrosion, the high-temperature generator is the critical component of triple-effect absorption chillers subject to severe corrosion (Figure 1). In the Trane design, the generator is directly fired rather than steam-driven as in other designs. Figure 2 shows the major components of a direct-fired generator. In the current prototype design, relatively expensive chromium/molybdenum alloys and stainless steels are used to avoid the corrosion problems encountered in the high-temperature stage.



Courtesy of The Trane Company

Figure 1. Absorption Chiller (Left) and Inside Tube Bundle (Right)

In the Trane prototype direct-fired generator, shell components and the tube bundle are made of AL6XN[®] and SeaCure[®] alloys, respectively. Both these alloys are expensive, high-chromium alloys and cost \$6 to \$7/lb. A major cost saving can be achieved if these chromium/molybdenum super alloys can be replaced with 409 SS, which costs only \$0.80 to \$1.00/lb. This will decrease the material cost of an average generator from ~\$45,000 to ~\$6,500, according to Trane's estimates. Because the generators vary in size, the cost and savings are expressed per ton of cooling capacity. The use of 409 SS will save \$100 to \$150 per ton of cooling capacity.

The high-temperature absorber shell components of the prototype triple-effect chiller are made of 409 SS. An additional cost saving of \$25 to \$50 per ton of cooling capacity can be obtained by replacing 409 SS in the absorber with mild steel (C 1018). The metal compositions of AL6XN[®], SeaCure[®], 29-4C, 409 SS, and C 1018 are given in Table 1.

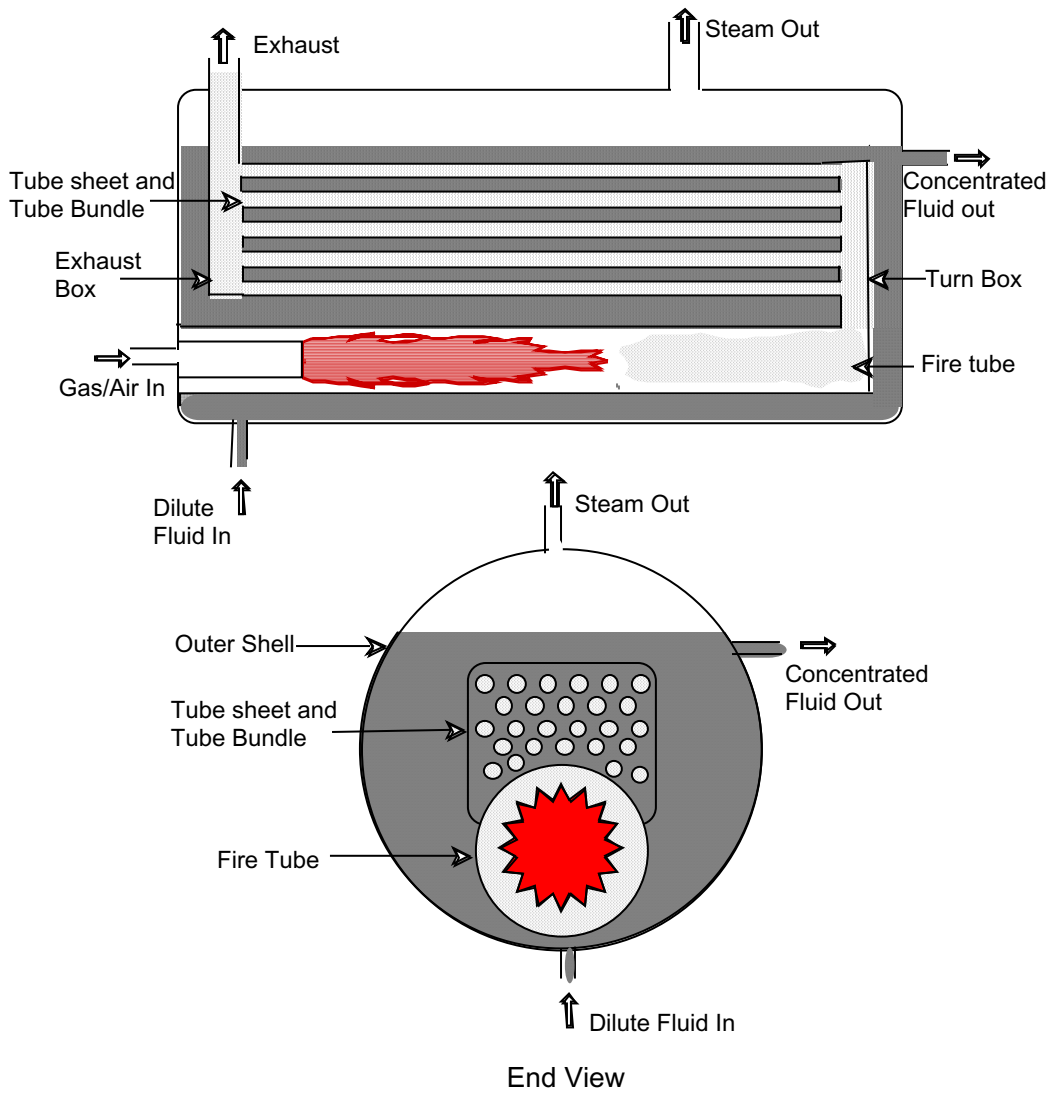


Figure 2. Schematic Diagram of a Direct-Fired Generator

Table 1. Metal Composition of Commonly Used Alloys (wt%)

Alloy	Ni	Cr	Mo	C	Mn	Si	P	S	N	Fe	Other
AL6XN®	23.5-24.5	20.0-22.0	6.00-7.00	0.30 max.	2.00 max.	1.00 max.	0.04 max.	0.03 max.	0.18-0.25	bal.	
SeaCure® (SC-1)	1.50-3.50	25.0-27.0	2.50-3.50	0.025 max.	1.00 max.	1.00 max.	0.04 max.	0.03 max.	0.035 max.	bal.	Nb+Ti 0.2+4(C+N)-0.8
29-4C	1.0 max.	28.0-30.0	3.60-4.20	0.03 max.	1.00 max.	1.00 max.	0.04 max.	0.03 max.	0.045 max.	bal.	Nb+Ti 6(C+N) 0.2-1.0
409 SS	0.50 max.	10.5-11.75	---	0.08 max.	1.00 max.	1.00 max.	0.045 max.	0.045 max.	-	bal.	Ti 6XC-0.75
C 1018	0.25	0.20	---	1.20	0.15	0.25	0.035	0.03	---	bal.	

1.4. Corrosion Protection With Metallic Diffusion Coatings

In an earlier project funded by GTI (GTI 5095-260-3561), we successfully demonstrated that metallic diffusion coatings could be used for corrosion protection of low-cost steels in advanced absorption environments [9]. The diffusion of a reactive metal such as Cr or Ni into steel increased its corrosion resistance significantly [10, 11]. Subsequently, the metal surface was further inactivated by passivation (controlled oxidation or nitridation), as shown in Figure 3. The most simple and benign surface passivation technique is controlled oxidation, in which a thin protective oxide film is formed on the surface. For example, SiO₂ is formed to passivate the metal surface of Si diffusion-coated surfaces.

Figure 4 shows a typical diffusion depth profile of a Cr-coated 409 SS specimen. Diffusion coatings of Cr, Mo, Ni, and W were considered effective in the high-temperature LZB triple-effect environment. In the current project, our research effort was mainly focused on coating 409 SS and C 1018 because a major cost saving can be achieved by replacing nickel/chromium/molybdenum alloys in the generator with 409 SS, and by replacing 409 SS in the absorber with mild steel.

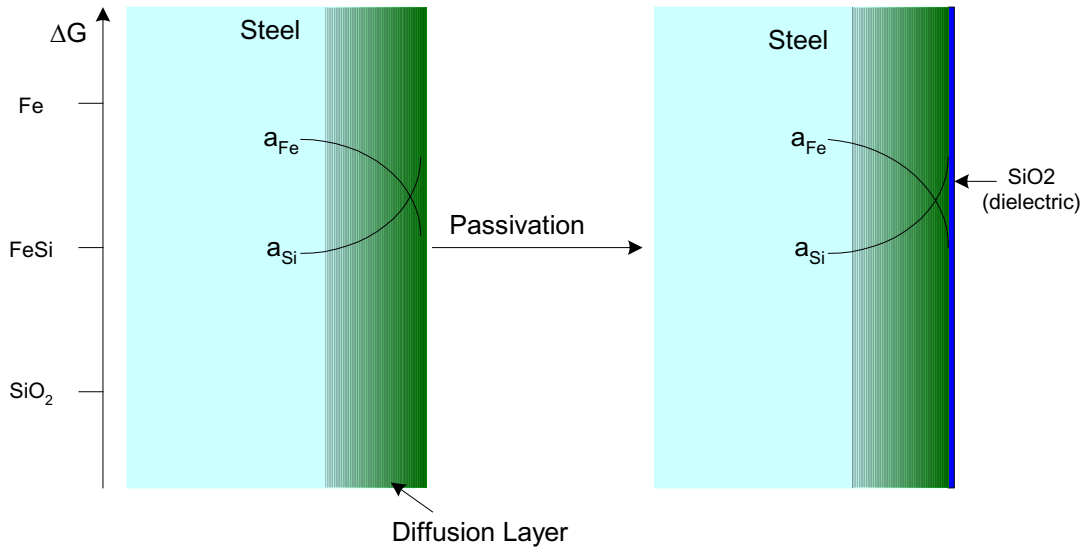


Figure 3. Graphical Representation of a Diffusion Coating and Surface Passivation

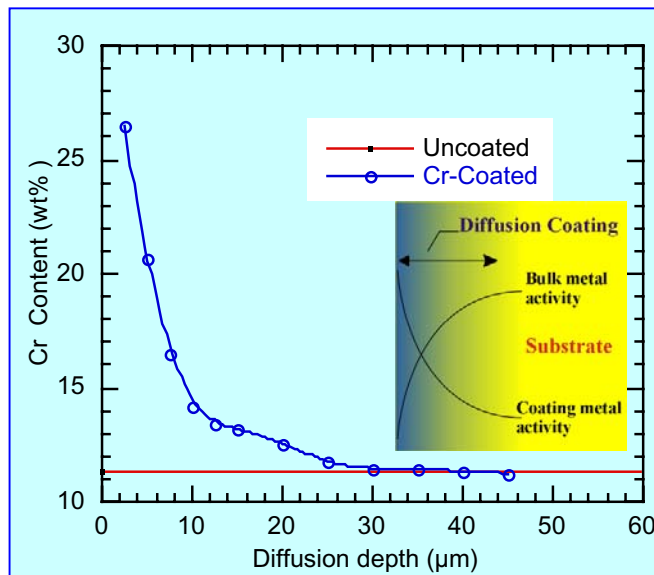


Figure 4. A Typical Metal Diffusion Depth Profile

1.5. Fluidized Bed Reactor Chemical Vapor Deposition (FBR-CVD)

To form diffusion coatings on metallic substrates, we used SRI's fluidized bed reactor chemical vapor deposition (FBR-CVD) technique or an adaptation of it [12-14]. Briefly, in this technique, a source metal powder bed (e.g., Cr) is fluidized with a carrier gas (e.g., Ar), and reacted with HCl and H_2 . When the reactor is operated at a temperature and conditions appropriate for the coating metal, volatile metal halides (e.g., $CrHCl_3$, CrH_2Cl_2 , $CrCl_2$) are

generated *in situ* that subsequently decompose on the substrate (e.g., 409 SS) to form a metallic coating. The substrate acts as a sink because the activity of the coating metal (e.g., Cr) in it is typically very low (< 1%) while the gas is saturated. In many cases, such coatings are deposited on substrate materials at much lower temperatures than are possible with other coating techniques. Deposition and diffusion are very fast in the initial stages, as the activity of the depositing metal is low in the substrates, and eventually become slower as the surface concentration of the depositing metal increases. The deposited metal (e.g., Cr) is diffused into the substrate during the coating and subsequent annealing process, producing diffusion coatings with gradient composition that extend to the bulk of the substrate. In these diffusion coatings, the interfacial stress between the coated phase and the substrate is minimized, and thus they provide excellent corrosion protection of the underlying substrate for high-temperature applications, where thermal effects accelerate delamination of overlay coatings. Because the CVD process is not a line-of-sight coating technique, it can be applied uniformly on complex geometric shapes.

1.6. Project Focus

The current project effort was focused on continued development of the corrosion protective diffusion coating, process scale-up, and field tests in prototype advanced absorption chillers. We addressed the corrosion protection of generator and absorber components in LiBr/water absorbent/refrigerant combinations and evaluated the corrosion rate of coated steels at elevated temperatures up to 500°F (260°C). We demonstrated the effectiveness of the diffusion coatings on test elements simulating the generator and the absorber of an advanced absorption cycle. During this project, planar and tubular 409 SS and C 1018 specimens were coated with corrosion-resistant metals (individual metals or combinations of them) for testing in simulated triple-effect and double-effect environments.

We also demonstrated that the diffusion coating process could be scaled up economically to a production level to be used in absorption cycles and a wide variety of other applications. The experimental parameters for industrial scale production were optimized for the best corrosion resistant diffusion coating. We produced Cr-coated 409 SS test specimens of 1.25-inch diameter and up to 4 ft length in an industrial fluidized bed. The coated tubes are to be welded to the tube sheet to fabricate the heat exchanger tube bundle by using corrosion-resistant weld materials such as Incovar[®] or ARMACOR[®]. Both these weld materials resist corrosion at high temperatures in HCl environments. Diffusion coatings are not expected to be damaged during welding because they are truly surface alloys and do not have a well-defined and stressed interface. The weldability and corrosion resistance of coated 409 SS specimens have been previously tested in LZB at 500°F, a typical triple-effect generator operating condition [9].

We could not complete the field testing of a prototype generator built with coated tubes as planned because of management changes at the coating subcontractor, Quality Heat Technologies (QHT). We plan to work with other potential high temperature coating manufacturers to commercialize the technology. We expect that corrosion protection coatings will permit the use of low-cost steels in advanced absorption cycles and an increase in operating temperatures to improve the coefficient of performance (COP). We expect the service life of the equipment will be significantly extended, thereby reducing maintenance and replacement costs.

1.7. Report Organization

This report is organized as follows:

Project Approach	Section 2.0
Project Outcomes	Sections 3.0, 4.0, & 5.0
Conclusions	Sections 6.0, 7.0, 8.0 & 9.0

2.0 Preparation Of Metallic Coatings

2.1. Selection of Materials

We selected materials for the preparation of metallic diffusion coatings to be tested for their corrosion resistance in LZB and LiBr/LiOH environments based on SRI's experience, literature searches, and simple thermochemical modeling. From the results of these activities, we selected a number of metals and alloys for laboratory testing.

2.1.1. SRI Experience

SRI has more than 15 years of experience in preparation and characterization of a variety of diffusion coatings on different metallic substrates [9, 11, 13, 15].

In a previous project, we found that high Cr-Fe alloys, high Si-Fe alloys, and nitrided Ti-Ni alloys exhibited good corrosion resistance in concentrated LiBr solutions used in chemical heat pumps. Also, we have shown that diffusion coatings of Si or Ti on steel or Cu increase the corrosion resistance by orders of magnitude and thus significantly extend the projected life [11, 13]. Similarly, Cu and Cu-Ni alloys can be protected by siliconizing their surfaces to form Si-bronzes that are more resistant to corrosion, simulating the high-Si alloys used in industry for acidic environments.

During an earlier project funded by GTI, Si and/or Cr diffusion coatings were extensively investigated as candidates for mitigating corrosion in the triple-effect generator environment. These metallic coatings have excellent heat transfer properties and a good thermal match with the substrate material, and thus they are expected to resist thermal shock.

2.1.2. Literature Search

We conducted a literature search on coatings and corrosion inhibitors for LiBr chemical heat pump applications at the beginning of the project to find any reference to applications similar to triple-effect generator corrosion problems. We found very little published literature pertaining to corrosion mitigation in the LZB environment. Several general sources, including corrosion handbooks and articles in the molten salt literature, indicate that Ta, W, and Mo are resistant to corrosion in halide environments below 149°C (300°F). The chemical industry uses Duriron® (Fe 85%, Si 15%), and several patents have been filed on techniques for siliconizing the steel surface to increase its corrosion resistance in hot sulfuric and hydrochloric acid applications [16, 17]. We did not find any metallic coatings that have been proven to resist corrosion in LZB at elevated temperatures, although there were a few reports on the development of diffusion coatings [18].

2.1.3. Simplified Thermodynamic and Thermochemical Analysis

The steel surfaces of the heat exchanger are exposed to vapors of H₂O and HBr, concentrated LiBr and ZnBr₂ solution, and the vapor-liquid interface (solution line). This metal-solution-vapor system is illustrated in Figure 5. Corrosion at the vapor-solid interface above the liquid is dominated by the reaction of HBr and water vapors with the metal or metal oxide surface. From these reactions, products such as bromides, oxides, and oxybromides are expected to form with a free energy of formation more negative than the

original surface compound. Note that this is an acidic environment, and that H_2 is generated when HBr or H_2O reacts with the metal until equilibrium or steady-state is reached.

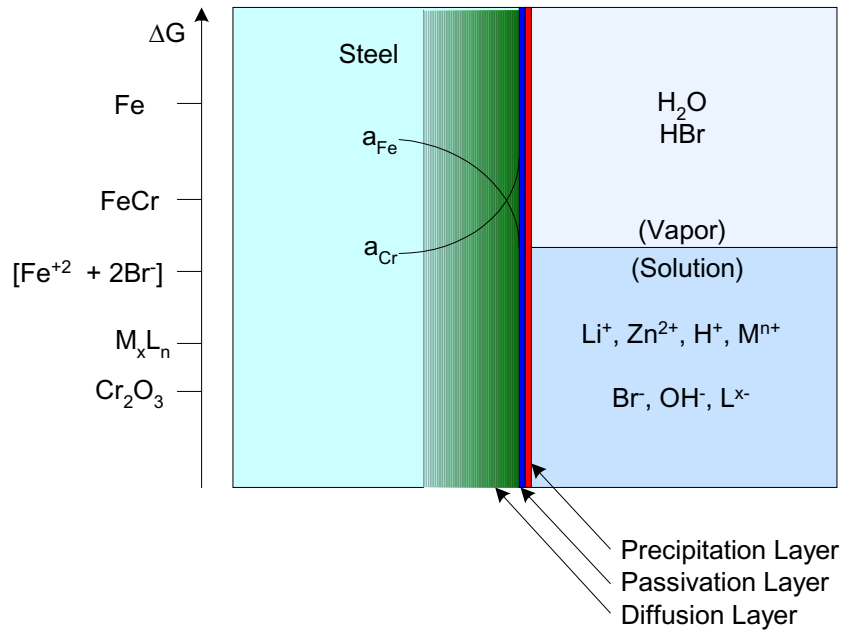


Figure 5. A Simplified Representation of the Metal-Solution-Vapor System

At the liquid-solid interface, the thermodynamic force for the metal to corrode is further driven by the potential for the bromides to form complex ions in the solution. The strategy here is to select coatings with compositions that do not have soluble, stable bromide complexes. This approach includes elements such as Si, which does not form a stable $SiBr_6^{2-}$, or large atoms such as W, which may form an insoluble bromide complex that precipitates at the interface. Figure 5 shows the simple model of this approach and the layers formed. The additives or inhibitors in the solution may act by blocking sites by either adsorption or precipitation of an insoluble compound, thus restricting the electronic transfer and hence the corrosion. Typical examples are oxyanions of transition metals with multiple degrees of oxidation states, such as MoO_4^{2-} , and WO_4^{2-} . These anions may form insoluble compounds upon reaction with the substrate surface.

Obtaining a diffusion coating and a proper microstructure is the most important step in passivating the surface of the substrate metal. Several chemistries were used in an effort to select the best combination of reactants, process conditions, and process economics for the production of corrosion-resistant coatings. A preliminary selection was made by thermochemical modeling. Figure 6 shows a typical variation of estimated metal halide equilibrium vapor pressure with temperature. For most applications, we used a fluidized bed of powders of the elements to be coated (e.g., Si, Cr). The metal powder bed is fluidized

with a carrier gas such as Ar. Volatile halide species are generated *in situ* by a trace of HCl in the carrier gas. The reactor is operated at a previously determined optimal temperature for fast and uniform deposition. The halide species transport the reactive element and deposit it on the substrate, forming a coating. Figure 7 shows the effect of temperature on vapor pressure, measured by mass spectrometry for the silicon bromide gas phase reaction. Similar measurements were performed for other potential metals to determine the optimal temperature for chemical transport of gaseous species.

Based on the findings of the above activities, promising candidates were chosen for the preparation of highly corrosion-resistant diffusion coatings.

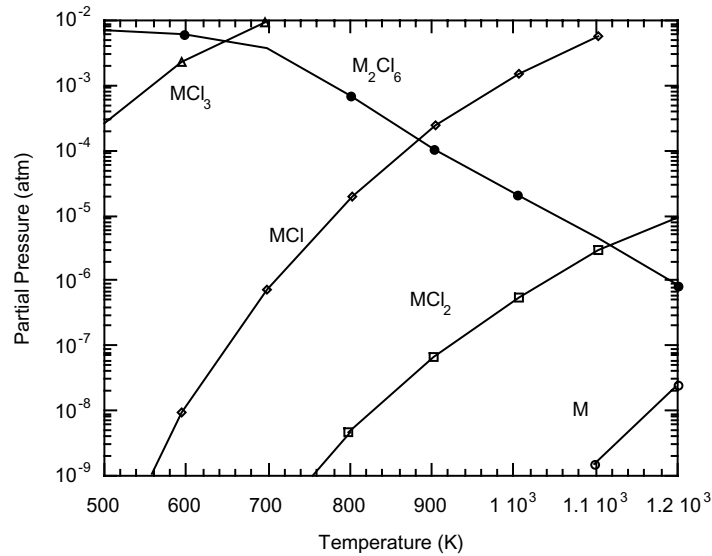


Figure 6. Partial Pressure Curves for Metal Halides as a Function of Temperature (e.g., AlCl₃)

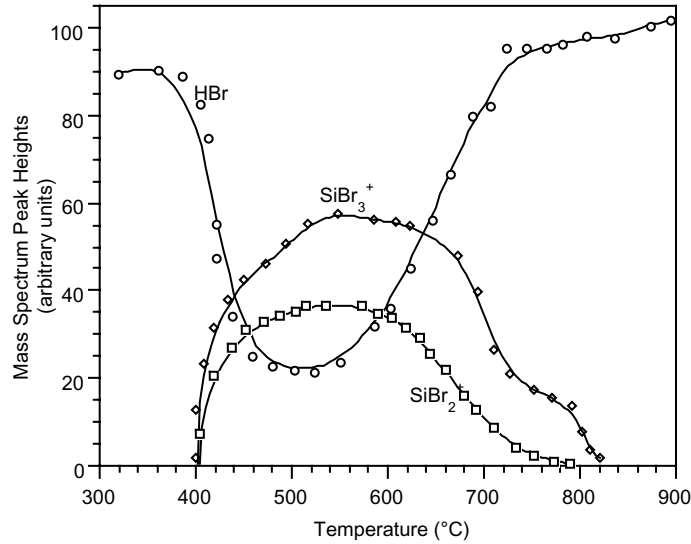


Figure 7. Measured Mass Spectrometric Signals for Silicon Bromides as a Function of Temperature

2.2. Selection of Coatings and Coating Techniques

The main criteria used to select an appropriate coating and a coating technique were the following:

1. It should be able to coat three-dimensional structures and reach every point on the surface to provide the required corrosion resistance.
2. It should result in a pinhole-free coating.
3. It should protect the surface to a certain depth to avoid corrosion, if scratching or erosion occurs.
4. It should be relatively inexpensive.
5. It is desirable that it does not interfere with welding or other fabrication steps.

We selected several variations of diffusion coatings by chemical vapor deposition (CVD) because these techniques satisfy the above criteria. We selected deposition in fluidized beds at atmospheric pressure because of the fast heat and mass transfer rates in the bed. Thus, in fluidized beds, homogeneous coatings are deposited at faster rates or at lower temperatures than in conventional CVD. The temperature required for deposition is generally high enough to help interdiffusion at the coating-substrate interface, which helps to produce adherent and pinhole-free coatings, but not high enough to seriously affect the microstructure and strength of the substrate.

In some cases we performed multiple element coating experiments. In these experiments, the deposition of a metal such as Cr with sub-halide chemistry was followed by the deposition of a second metal, such as Ni or W, by decomposition of its metal halides. This approach introduced composite diffusion coatings consisting of more than one metal. In

certain cases, an electroplating step was also introduced before the fluidized bed treatment, to deposit metals such as Ni, Mo, and W that are readily electroplated. Many advances have been reported recently for the preparation of composite coatings by electrodeposition [22, 23]. Nevertheless, electrodeposited coatings by themselves do not provide sufficient corrosion protection in the triple-effect environment, as they generally form overlay structures that tend to delaminate with long-term exposure. Therefore, electrodeposited coatings must be treated at high temperatures to form diffusion coatings of Cr and electrodeposited metal(s).

2.3. Experimental Procedures

2.3.1. SRI Fluidized Bed Reactor Chemical Vapor Deposition (FBR-CVD) Process

SRI International's FBR-CVD technique can be used to coat fibers, particles, and powders. Because the CVD process is not a line-of-sight coating technique, it can be applied uniformly on complex geometric shapes such as fabricated parts. A simplified schematic diagram of a fluidized bed reactor is shown in Figure 8. The reactor is a cylindrical vessel incorporating a porous plate that serves the dual function of supporting the bed of granular or powdered material and distributing the flow of gas uniformly over the cross-sectional area of the bed. The velocity of gas necessary to levitate the particles in the bed is a function of the particle diameter, shape, and density of the bed material. When fluidization takes place, the bed of particles expands and acts like a liquid in that it seeks its own level and assumes the shape of the containing vessel. Furthermore, during fluidization, the flow of gas through the bed is locally turbulent, favoring high rates of heat and mass transfer that result in very low thermal and concentration gradients within the bed. The technique is potentially applicable to a great variety of coating/substrate systems because it is open to many permutations of bed geometry, thermal conditions, fluid flow rates, precursor chemistry, and modes of injection. Figure 9 shows a photograph of one of our laboratory experimental setups for FBR-CVD. Figure 10 shows some 409 SS tubes coated with Cr by SRI's FBR-CVD process. Industrial scale fluidized beds for coating large parts or large quantities of small parts are already available.

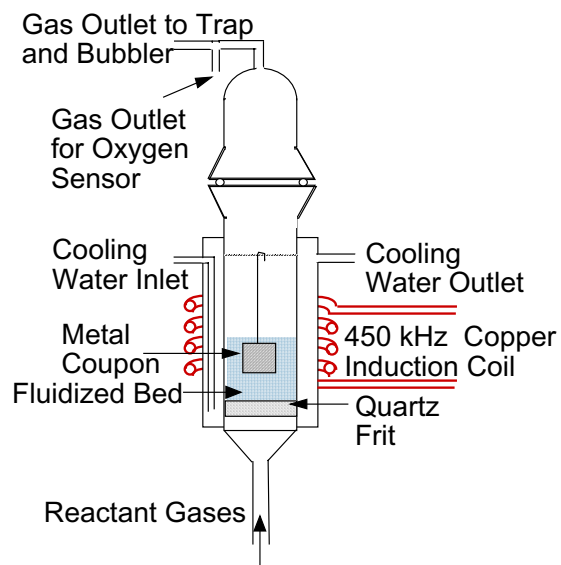


Figure 8. Simplified Schematic Diagram of a Fluidized Bed Reactor With RF (Radiofrequency) Heating

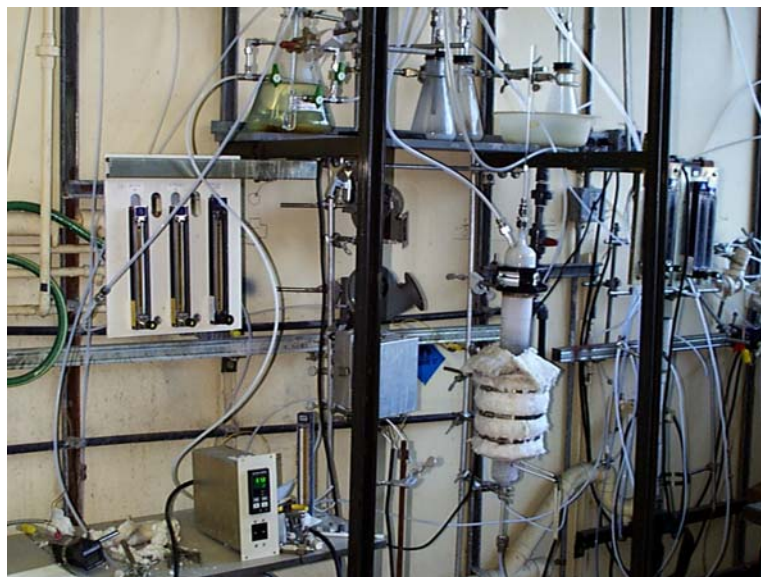


Figure 9. Laboratory Setup for FBR-CVD Coatings with Electric Heating



Figure 10. Cr-Coated Steel Tubes Prepared by SRI's FBR-CVD Process.

2.3.2. Preparation of Metallic Coatings by FBR-CVD

Cr Coatings on 409 SS by FBR-CVD

The main goal of coating steels with metals such as Cr, Ni, Mo, and W is to obtain a surface composition similar to corrosion resistant super alloys. For example, Cr coatings on low-cost steel would provide a surface with corrosion-resistant properties similar to high chromium stainless steel. During this project, we coated a number of 409 SS and C 1018 metal coupons with Cr in the fluidized bed reactor shown in Figure 9. These Cr diffusion coatings were prepared at 900° to 1000°C in a powder bed consisting of Cr powder, a Cr alloy, and Al₂O₃. The bed was fluidized with Ar, and the reactant gases (H₂ and HCl) were introduced to the Ar gas stream when the bed temperature reached the coating temperature (e.g., 1000°C). Typically, the Cr deposition was carried out for about 2 h. The coated samples were kept in the fluidized bed, usually at the same temperature as the Ar flow, for an additional 30 min to 1 h for annealing before cooling down to room temperature.

The detailed experimental conditions for Cr deposition on 409 SS are summarized in Table 2. We used metal powders with two proprietary Cr alloy compositions (5% X and 20% X), both of which yielded similar coating characteristics.

Table 2. Experimental Conditions for Deposition of Cr on 409 SS

Run #	Substrate	Coating	Precursor	Coating Time (min)	Coating Temp. (°C)	Annealing Time (min)	Annealing Temp. (°C)
1	409 SS	Cr/X	3.06 g Cr (5%X) + 3.15 g Cr	129	1000	30	1000
5	409 SS	Cr/X	0.765 g Cr (20%X) + 5.445 g Cr	126	1000	35	1000

Cr Coatings on Fe, C 1018, and Ni (Ni 200) by FBR-CVD

Cr coatings on iron (99.99%), C 1018, and nickel (Ni 200) were prepared at 1000°C and ambient pressure. The metal powder bed was fluidized with Ar, and reactive gases (H₂ and HCl) were introduced into the Ar gas stream to deposit and diffuse Cr on substrates. Samples were treated in the fluidized bed for 2 h for Cr coating, and annealed for 1 h in the Ar flow.

Cr + M (M = W or Ni) Coatings on 409 SS by FBR-CVD

We performed a number of experiments to introduce a second corrosion-resistant metal into the Cr-coated surface to further reduce the corrosion rate. The objective of these experiments was to increase the hydrogen overpotential and/or deactivate grain boundaries, which would improve the corrosion resistance. For these experiments, first we coated 409 SS coupons with Cr at 1000°C for 2 h, using the already optimized conditions (see Table 2 for details), followed by deposition of a second metal (W or Ni) for a shorter time period at different annealing temperatures, as given in Table 3. Specimens were analyzed after each step to obtain surface microstructure and Cr diffusion profiles.

Many variations were introduced to the experimental procedure for coating W on Cr-coated specimens. The idea of these experiments was to optimize conditions to obtain well-adhering, halide-free tungsten films. We managed to improve the quality of the tungsten film on Cr-coated 409 SS progressively in these experiments. The W coating obtained in Run #8 was strongly bonded to the surface and free of any trapped residual halides from the decomposed precursor.

Table 3. Experimental Conditions for Deposition of a Second Metal on Cr-Coated 409 SS

Run #	Substrate	Coating	Precursor	Coating Time (min)	Coating Temp. (°C)	Annealing Time (min)	Annealing Temp. (°C)
2	Run #1	W	2.1 g WCl ₆	105	1000	45	1000
3	Run #1	W	0.142 g WCl ₆	20	545	25	625
4	Run #1	W	0.777 g WCl ₆	50	600	35	630
6	Run #5	W	0.185 g WCl ₆	26	470	120	625
7	Run #5	W	0.406 g WCl ₆	57	480	60	685
8	Run #5	W	0.406 g WCl ₆	55	900	31	950
9	Run #5	Ni	0.715 g NiCl ₂	73	900	60	950
10	Run #5	Ni	1.850 g NiCl ₂	60	900	60	950

2.3.3. Electroplating

Ni + Cr Coatings on 409 SS and C 1018

We used a standard Ni plating bath (NiCl₂, NiSO₄, H₃BO₃) with a Ni anode at 60°C for Ni deposition on C 1018 or 409 SS metal specimens [24]. Typically, samples were coated for 0.5 to 1 h with ~5 mA cm⁻² current density. After Ni plating, metal specimens (both 409 SS and C 1018) were placed in a fluidized bed reactor containing a proprietary component and Cr powder. The metal specimens were first heated to diffuse the overlay Ni coating. Then, the reactive gases (H₂ and HCl) were introduced to deposit and diffuse Cr on the Ni-coated specimens. The coated specimens were left in the fluidizing bed reactor for an additional hour under the Ar flow for annealing.

Ni + W Coatings on 409 SS and C 1018

We prepared Ni + W alloy coatings on 409 SS and C 1018 specimens in electroplating baths containing Na₂WO₄, NiSO₄, and citric acid, together with a Ni anode. The pH of the bath was maintained above 7 with ammonia, and the operating temperature range was maintained between 55° and 70°C. It was difficult to get a significant W loading in the coatings, as previously reported in the literature [25]. In our initial experiments, we observed very low currents in electroplating baths of concentrated W and Ni salts, even at potentials more negative than -1.0 V. However, we managed to increase the deposition current by 2 orders of magnitude by adding a proprietary constituent to the bath (Additive A). Factors contributing to the increase in deposition rate (current) are believed to be understood. We performed a number of experiments to further optimize the electrochemical deposition conditions. Experimental conditions employed for the preparation of some electrodeposited specimens are given in Table 4. Experimental

variations include substrate pretreatment in acid, application of an initial potential pulse, *pH*, and bath temperature.

Table 4. Composition of the Plating Bath and Other Experimental Parameters

Sample	Plating Bath	Temp (°C)	Pot. (V)	Current (mA/cm ²)	Time (h)	<i>pH</i> (initial)
Specimen #1 409 SS (AR)	40 g/L NiSO ₄ .6H ₂ O + 50 g/L Na ₂ WO ₄ .2H ₂ O + 66 g/L citric acid + Additive A	60 - 65	-0.9	1.94 - 2.78	3.5	8.0
Specimen #2 409 SS (AR)	32.5 g/L NiSO ₄ .6H ₂ O + 50 g/L Na ₂ WO ₄ .2H ₂ O + 66 g/L citric acid + Additive A	57 - 63	-1.03	1.87 - 2.91	4.33	8.0
Specimen #3 409 SS (AR)	Bath used in #2 above + 0.5 g NiSO ₄ (for 120 mL)	60 - 65	-1.03	2.45 - 3.23	3	8.2
Specimen #4 Acid-cleaned 409 SS	Bath used in #3 above + 0.5 g NiSO ₄ .6H ₂ O + 0.025 g Na ₂ WO ₄ .2H ₂ O (for 120 mL)	60 - 65	-1.03	1.87 - 2.13	3	8.2
Specimen #5 Acid-cleaned 409 SS	25 g/L NiSO ₄ .6H ₂ O +50 g/L Na ₂ WO ₄ .2H ₂ O + 66 g/L citric acid + 2x Additive A	62.5 - 68	-1.05	1.81 - 5.23	2.75	8.2
Specimen #6 Acid-cleaned 409 SS	25 g/L NiSO ₄ .6H ₂ O + 50 g/L Na ₂ WO ₄ .2H ₂ O + 66 g/L citric acid + 2x Additive A	65.5 - 69	-1.05	1.61 - 7.81	2	7
Specimens #7 #8, #9 & #10 Acid-cleaned C 1018	25 g/L NiSO ₄ .6H ₂ O + 50 g/L Na ₂ WO ₄ .2H ₂ O + 66 g/L citric acid + 2x Additive A	66-72	-1.05	2.58-7.04	2	8

Further optimization of experimental parameters was necessary to develop mechanically stable Ni + W alloy coatings on 409 SS and C 1018, because electrodeposited coatings should be treated in the fluidized bed with the Cr metal powder to form diffusion coatings. This process was expected to produce highly corrosion-resistant Ni + W + Cr diffusion coatings. Electroplating baths that consisted of 20 g L⁻¹ NiSO₄.6H₂O, 50 g L⁻¹ Na₂WO₄.2H₂O, 66 g L⁻¹ citric acid, and Additive A were used in these experiments. Thorough pretreatment was necessary, especially for 409 SS specimens, in order to remove its oxide layer. Given below are the specific conditions and experimental parameters, determined after a series of well-controlled experiments, used for the preparation of mechanically stable, electrodeposited Ni + W coatings on both types of electrodes.

a. Ni + W Coatings On C 1018 Specimens

Surface pretreatment: Acetone cleaning, followed by 5 min treatment in 6 M H₂SO₄ acid.

Temperature range 65–73°C

Potential -1.05 V

Time duration 2 h

Initial *pH* 8

b. Ni + W coatings on 409 SS specimens

Surface pretreatment: Acetone cleaning, 10 min treatment in 6 M H₂SO₄ acid, polished with a soft sandpaper, followed by further acid treatment for 5 min.

Temperature range 48–51°C

Current ~ 4 mA cm⁻² (potential was usually ~ -1.05 V)

Time duration 2 h

Initial *pH* 8

It should be stressed that, although the current passed was higher at elevated temperatures, electroplating was accomplished at 50°C. Higher temperatures resulted in delamination of electrodeposited layers, probably due to the faster rate of deposition. All deposits obtained using this procedure were shiny and gray.

Ni + Mo Coatings on 409 SS and C 1018

We also prepared Ni + Mo alloy coatings on 409 SS and C 1018 specimens in electroplating baths containing Na₂MoO₄·2H₂O and NiSO₄·6H₂O with a Ni anode. The experimental conditions detailed in Table 5 [26, 27] produced thin gray deposits on both C 1018 and 409 SS specimens. However, the deposit did not have a sufficient amount of Ni and Mo, according to X-ray fluorescence measurements. Changes in experimental conditions, such as use of additives, increase in the Ni(II) salt or Mo(VI) salt concentration, increase in temperature, application of potential pulses, acid treatment of specimens, etc., did not significantly improve the Ni and Mo loading of deposits, although the current passed was increased during these changes.

Table 5. Initial Compositions of Electroplating Baths

Ni(II) Conc. (M)	Mo(VI) Conc. (M)	Citrate Conc. (M)	Other Additives (M)	pH	Temp. (°C)	Potential (V)
0.10	0.10	0.20	---	5.0	25	1.0
0.10	0.10	0.20	---	5.0	70	-1.0
0.05	0.03	0.10	Glycine, 0.10 M	10.5	30	-2.2

This was probably due to the lack of adhesion of Ni on the surface of the alloys in the presence of Mo in solution. If Ni was not deposited, codeposition of Mo would not take place, as deposited Ni layers would act as a catalyst for the deposition of Mo. This problem was addressed by altering the electroplating bath composition and other experimental parameters to ensure Ni coating. The following changes were made in the procedure reported in Table 5:

- Increased concentration of Ni(II) (as NiSO₄·6H₂O) to 0.2 M.
- Decreased concentration of Mo(IV) (as Na₂MoO₄·2H₂O) to 0.03 M.
- Decreased electroplating temperature to about 40°C.
- Decreased deposition potential below -3.0 V vs. a Ni anode.
- Decreased deposition time to about 1 h.
- Used citric acid in place of sodium citrate.

In addition to alterations in the experimental procedure, more efficient surface pretreatment methods were used in order to enhance the adhesion between the electrodeposits and the electrode surface. The 409 SS specimens required more rigorous treatment than C 1018 specimens, as discussed below.

- a. 409 SS specimens: 10 min treatment with 6 M H₂SO₄, polish the surface with sandpaper, followed by further 5 min treatment with 6 M H₂SO₄.
- b. C 1018 specimens: 20 min treatment with 6 M H₂SO₄.

These conditions would facilitate the initial formation of an electrodeposited layer of Ni, followed by the deposition of Mo. It should also be noted that, in the case of 409 SS, the specimens were spot-welded with a Hastelloy® rod for electrical connection after the specimen was polished with sandpaper. In addition to the alterations mentioned above, the concentrations of citric acid and ammonia were maintained at 0.95 M and 0.28 M, respectively. The pH was measured to be 9.9 with these constituents. More importantly, the deposition potential was adjusted (but always kept more negative than -3.0 V) to maintain a current density of 54–62 mA cm⁻² throughout the experiment. Although hydrogen evolution was aggressive at such high negative potentials, stable, shiny metallic colored deposits resulted under these conditions.

One probable reason for earlier failures to obtain stable deposits was the use of citric acid instead of sodium citrate, since the acid required a larger amount of ammonia to maintain

an initial pH of about 10, and excess ammonia may form amine complexes with metal ions, preventing electrodeposition.

After successful completion of electroplating experiments, representative specimens of (a) Ni + W coated 409 SS, (b) Ni + Mo coated 409 SS, (c) Ni + W coated C 1018, and (d) Ni + Mo coated C 1018 were treated in a fluidized bed that consisted of Cr powder, a Cr alloy, and alumina at 1000°C for 3 h, followed by annealing for about 1 h. The flow rates of the gases were 3 L min⁻¹ Ar, 300 mL min⁻¹ H₂, and 13 mL min⁻¹ HCl. The objective of this experiment was to form diffusion coatings that consisted of Cr, Ni, and W or Mo. These specimens were then tested in the LiBr/ZnBr₂ solution at 500°F, simulating the advanced absorption environment. Electrochemical impedance spectroscopic and Tafel measurements were conducted to determine the rate of corrosion.

2.3.4. Surface Passivation

According to thermochemical arguments, nitrided and oxidized surfaces of Si- or Ti-coated specimens should show better corrosion resistance than untreated specimens. Nevertheless, no significant improvement was achieved on the corrosion resistance of FBR-CVD Cr-coated 409 SS specimens after nitridization. This was partly due to the already low corrosion rates of the coated materials, and thus the improvements were masked by the detection limits of measurement techniques. Thus, it is not necessary to include an additional surface passivation step, if the diffusion coatings are highly corrosion-resistant.

3.0 Characterization Of Coatings

3.1 Analytical Techniques

Coated specimens were analyzed by scanning electron microscopy (SEM), energy dispersive x-ray spectroscopy (EDX), Auger spectroscopy (Auger), and X-ray fluorescence spectroscopy (XRF) to determine their microstructure, composition, and diffusion profile. SEM was used to determine the grain growth and microstructure of the coated surface, and that of the bulk. For cross-sectional analysis, metal specimens were cut, polished, and etched to enhance the morphology of the surface. EDX was extensively used to determine the surface composition and the diffusion depth profile of the depositing metal. The specimens were placed in the SEM equipped with an EDX attachment, and the metal compositions were determined at 5 μm intervals to obtain the concentration profile of the diffusing metal in the substrate.

3.2 Surface Analysis And Depth Profile Investigation

3.2.1 Cr Coatings on 409 SS by FBR-CVD

Microstructure of the Substrate

The grain growth is a concern when substrates are heated to a high temperature during a coating process, and thus it must be carefully monitored and controlled to avoid changes in the microstructure, which is strongly related to the mechanical properties of the substrate material. As the grains become large, the material becomes hard but brittle. Ideally, the coating process should not have any effect on the microstructure. However, high-temperature coating processes invariably lead to some grain growth in the substrate material. The key is to minimize the grain growth by optimizing the time-temperature budget so that coating process does not have any adverse effects on the mechanical properties of the substrate.

To study the effect of high-temperature coating processes on the microstructure of substrates, we compared as-received 409 SS and coated coupons by using SEM. Figure 11 shows an SEM photograph of the cross-section of an as-received 409 SS specimen. We cut, polished, and etched the surface to enhance the microstructure. The average grain size of the as-received specimen is about 10-20 μm . Figure 12 shows an SEM photograph of a Cr-coated 409 SS specimen prepared by the FBR-CVD process. The average grain size of this specimen is about 30-40 μm , indicating some grain growth during the coating process. This minimal grain growth is unlikely to affect the physical properties of the substrate, and thus it should be acceptable in most applications. It should be noted that the pack cementation diffusion coating process produces significant grain growth in the substrate material as a result of the higher temperature and longer coating time compared with the FBR-CVD process. In a previous project, we observed an average grain growth up to about 200-500 μm in the substrate for coatings prepared by pack cementation. This could be a concern in some applications. However, coatings prepared by pack cementation showed deeper diffusion profiles due to the exposure to high temperatures for long periods.

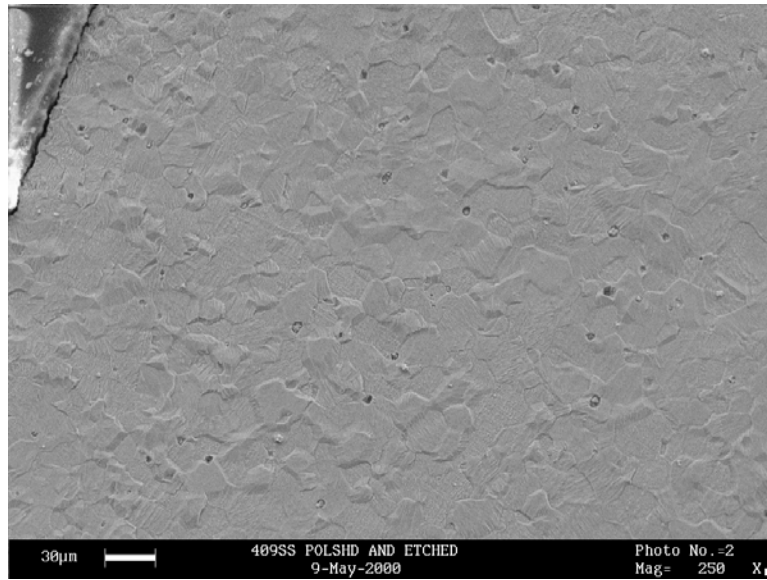


Figure 11. Microstructure of As-Received 409 SS

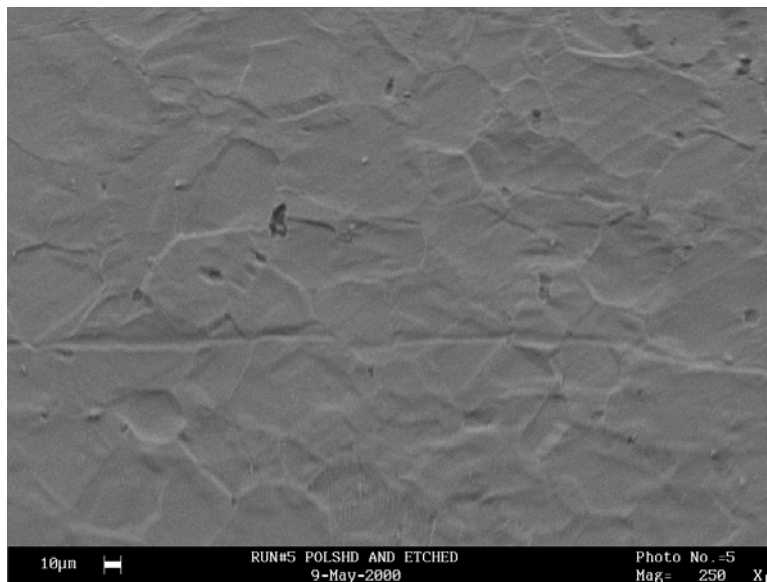


Figure 12. Microstructure of Cr-Coated 409 SS Prepared By FBR-CVD

Surface Structure and Diffusion Profiles

We performed a series of experiments for optimization of experimental conditions to obtain the best Cr diffusion profile with the lowest time-temperature budget. The effect of

temperature and time on the Cr diffusion profile is illustrated in Figure 13. The 409 SS coupons were 1 inch square. The coupon referred to as #6 was coated with Cr in the fluidized bed reactor for 5 h at 930°C, and the coupon referred to as #10 was coated with Cr in the fluidized bed reactor for 2 h at 1000°C. The surface morphology of both Cr-coated coupons was found to be generally similar. However, their diffusion depth profiles were different depending on experimental parameters. Specimen #10, coated at 1000°C for 2 h, had a deeper diffusion profile than that for specimen #6, coated at 930°C for 5 h. The diffusion depth improvement is prominent between the depths of 5 and 45 μm . This indicates that we can reduce the coating time by a factor of 2 compared to the coating time for specimen #6 and still get a better diffusion depth if we increase the temperature to 1000°C. This observation would allow us to optimize the temperature and time and thus reduce the cost of coating. By reducing the coating time, we could increase the throughput of the process and/or lower the labor cost.

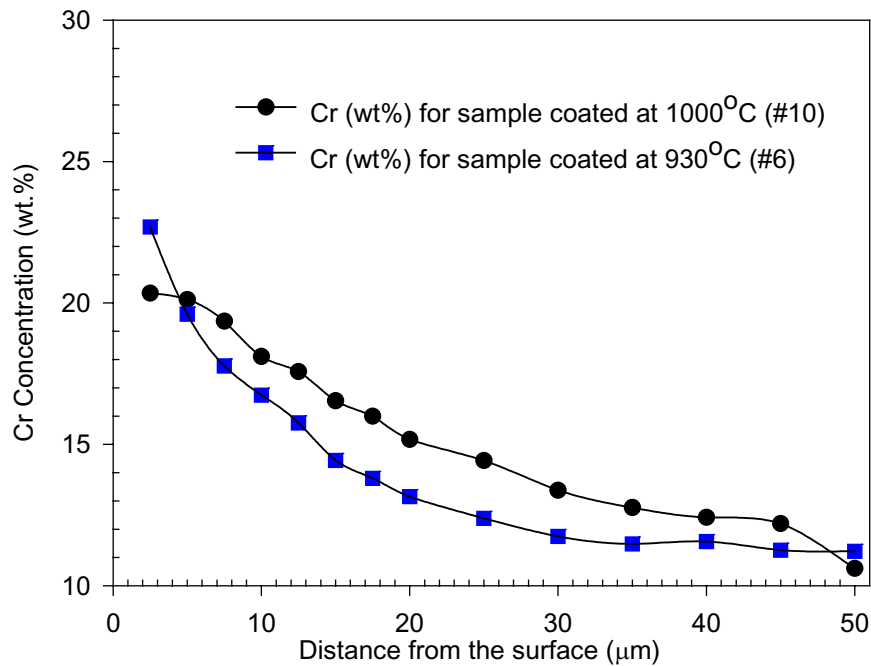


Figure 13. Cr Diffusion Depth Profile of Cr-Coated 409 SS Samples

Figure 14 and Figure 15 show SEM photographs of a Cr-coated 409 SS surface. The particles attached to the surface are Cr powder from the fluidized bed. The photograph taken at a higher magnification (Figure 15) also shows the grain structure and size on the surface. The grains are about 10-20 μm in diameter – much smaller than the grains observed in coatings prepared by the pack cementation process.

Coated samples were also analyzed for coating composition and diffusion depth profile (Figure 16). According to diffusion profiles, both specimens (Runs #1 and #5) show deep chromium diffusion. Run #5, conducted with a different Cr alloy composition (see Table 2), shows marginally better diffusion depth. However, the diffusion profiles are similar in both cases.

In a separate set of experiments, we coated 409 SS samples with Cr using N₂ as the fluidizing gas. The objective was to study the possibility of using low-cost N₂ in place of Ar. However, at high temperatures, Cr formed nitrides and prevented diffusion into the Fe substrate. Therefore, the diffusion of Cr was shallow in these coatings, compromising the corrosion protection.

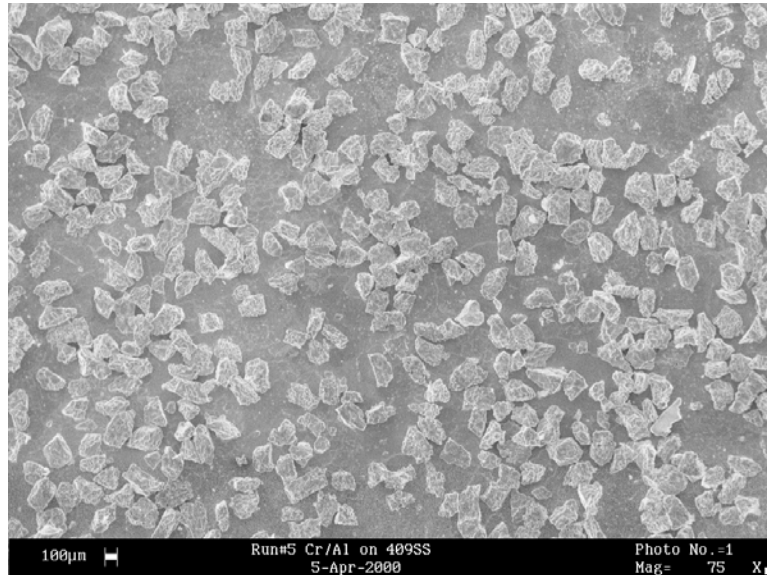


Figure 14. Cr-Coated 409 SS Surface

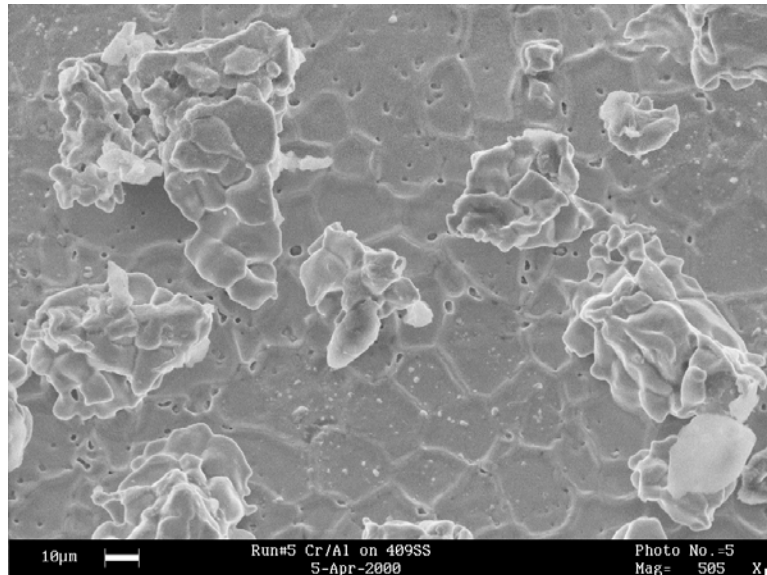


Figure 15. Cr-Coated 409 SS Surface at a Higher Magnification, Showing Attached Cr Particles and Grain Boundaries

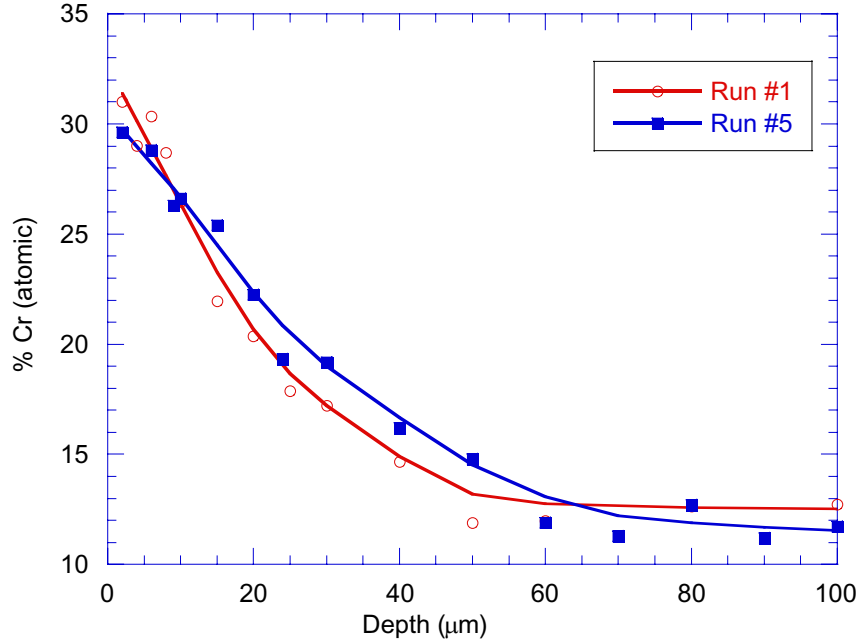


Figure 16. Cr Diffusion Profiles of a Cr Coated 409 SS (Runs #1 And #5)

3.2.2. Cr Coatings on Pure Iron, Carbon Steel (C 1018), and Ni 200

To study the diffusion behavior of Cr in various important substrate matrices, we prepared Cr coatings on iron (99.99%), C 1018, and nickel (Ni 200). The objective of these experiments was to explore whether we could form corrosion-resistant alloy-like surfaces by the fluidized bed process, in particular, Inconel®-like surfaces on Ni200. The experimental procedure used for the preparation of these coatings is given in Section 2.2.

Figure 17 shows the surface morphology of an iron specimen coated with Cr. Particles attached to the surface are Cr powder from the fluidized bed. We have made similar observations with Cr coatings on 409 SS as well.

Figure 18 shows the surface morphology of a Cr-coated C 1018 sample. As is apparent, the surface of the specimen was roughened by the particle bombardment in the fluidizing bed. Figure 19 shows the surface morphology of a Cr-coated Ni 200 specimen.

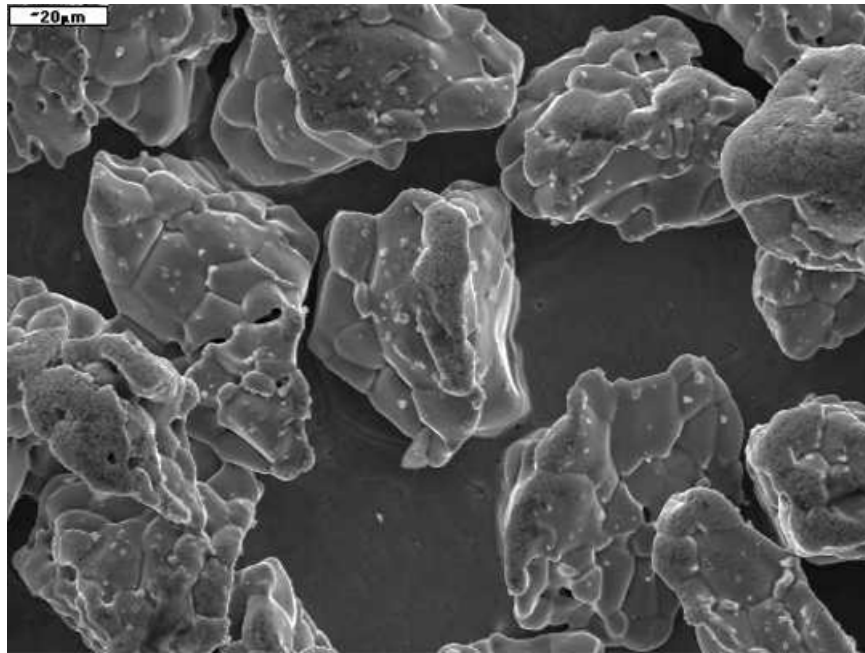


Figure 17. Surface Morphology of a Cr-Coated Iron (99.99%) Specimen

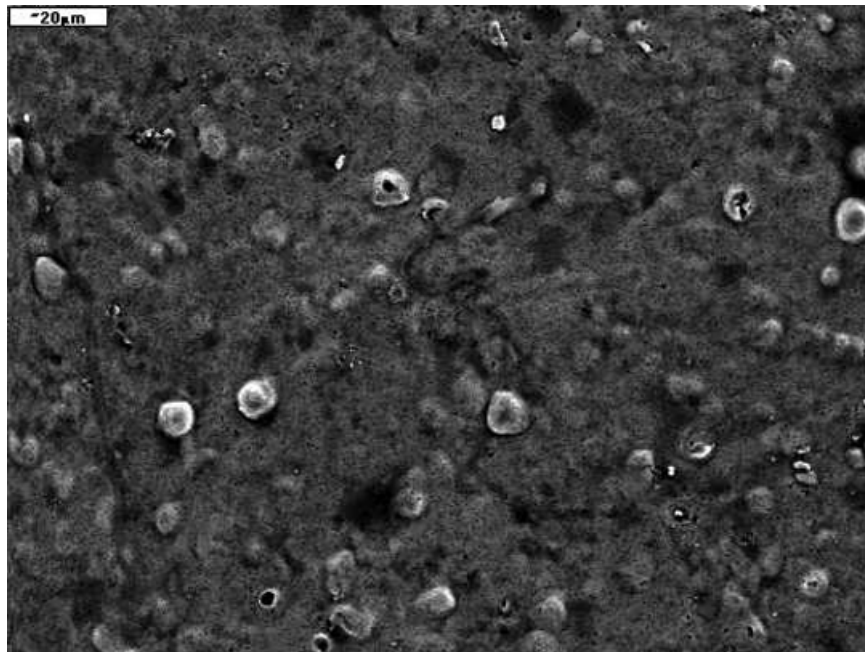


Figure 18. Surface Morphology of A Cr-Coated C 1018 Specimen

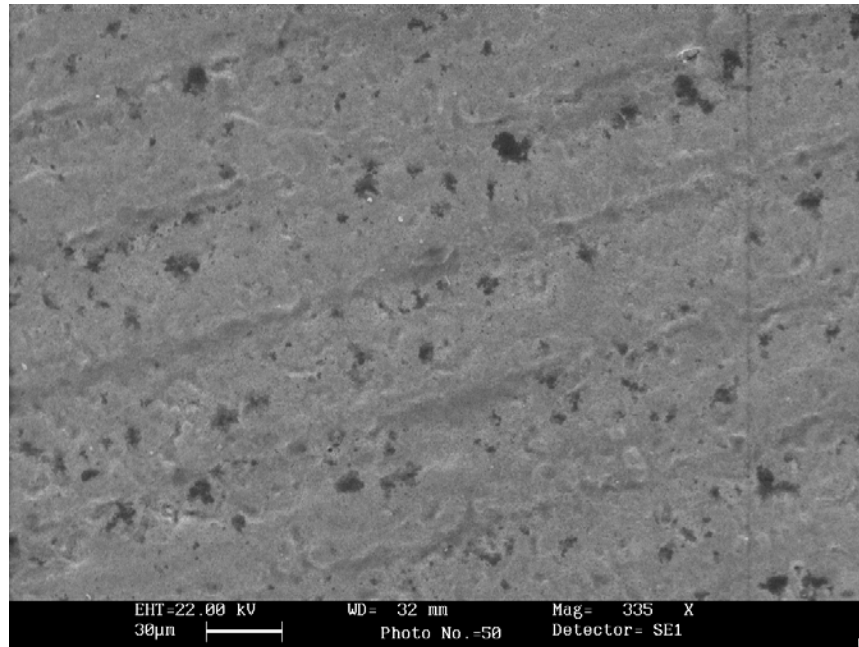


Figure 19. Surface Morphology of A Cr-Coated Ni 200 Specimen

Figure 20 shows the diffusion profiles of Cr and Fe for a Cr coating on pure iron (99.99%). The Cr concentration on the surface is about 30%. Most importantly, we have managed to diffuse Cr up to 25 μm deep into the substrate. Figure 21 shows the Cr diffusion profile in the Cr-coated C 1018 specimen. The diffusion profile in C 1018 is very similar to that in pure iron, indicating that carbon in steel does not interfere significantly with the Cr diffusion process. However, in other experiments, we found that the high carbon content in C 1018 interferes with Cr diffusion, presumably due to the formation of carbides, resulting in shorter diffusion depths. In both pure iron and C 1018 specimens, the Cr diffusion depths and concentration profiles were sufficient to provide excellent corrosion protection in the advanced absorption cycle environment.

Figure 22 shows the concentration profiles of metals in the diffusion region of the Cr-coated Ni 200 specimen. The Cr diffusion profile is considerably shallower in Ni than in C 1018 or 409 SS. We have observed similar behavior in previous experiments where attempts were made to diffuse Cr in Ni films electroplated on 409 SS. It is believed that Ni significantly reduces the Cr diffusion rate, and consequently, Cr tends to build up on Ni surfaces rather than diffusing into the bulk. The surface composition of the Cr-coated Ni 200 specimen was found to be ~25% Fe, 15% Ni, and 70% Cr. The surface Cr concentration on the Cr-coated Ni 200 (~70%) is much higher than that observed in Cr-coated 409 SS or C 1018 surfaces (30-40%).

According to the diffusion profiles in Figure 22, the Fe content on Ni 200 diminishes rapidly within about 2 μm from a surface concentration of about 25%. Although we did not add any Fe powder to the fluidized bed, C 1018 and 409 SS samples that were placed adjacent to the Ni 200 specimen must have acted as a source of Fe. These observations are reasonable,

given the partial molar enthalpies of 6 kCal/g.at. for the Fe-Cr system, -1 kCal/g.at. for the Fe-Ni system, and -4.2 kCal/g.at. for the Ni-Cr system.

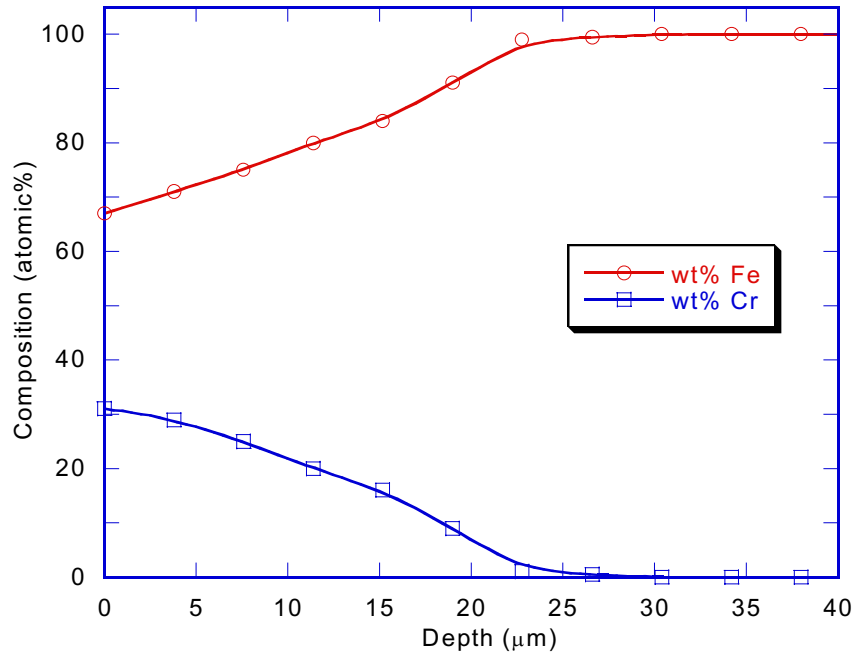


Figure 20. Cr Diffusion Profile in the Diffusion Region of Cr-Coated Iron (99.99%)

3.2.3. Cr + M (M = W or Ni) Coatings on 409 SS by FBR-CVD

An EDX spectrum of a W-coated surface over a Cr-coated 409 SS surface is shown in Figure 23. This coating has a surface elemental composition of 41% Cr, 48% Fe, and 11% W according to X-ray fluorescence (XRF), which is used mainly as a preliminary analysis tool to obtain a rapid qualitative reading of the surface composition.

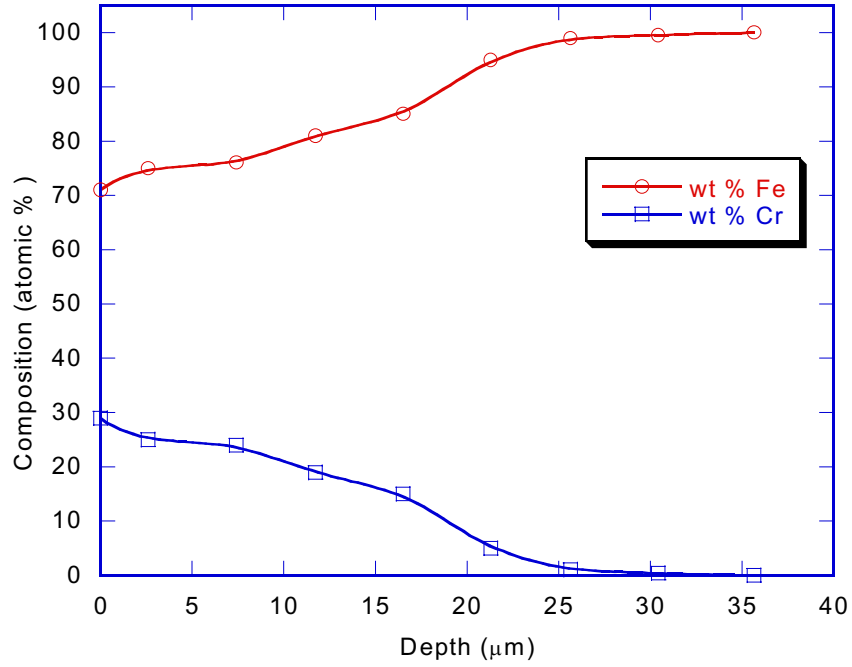


Figure 21. Cr Diffusion Profile in the Diffusion Region of Cr-Coated C 1018

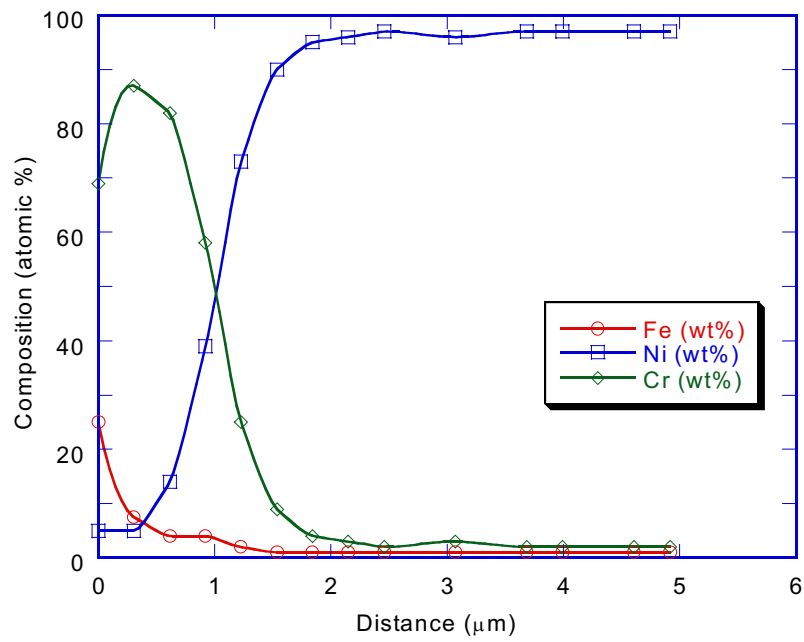


Figure 22. Metal Concentration Profiles in the Diffusion Region of Cr-Coated Ni 200 Alloy

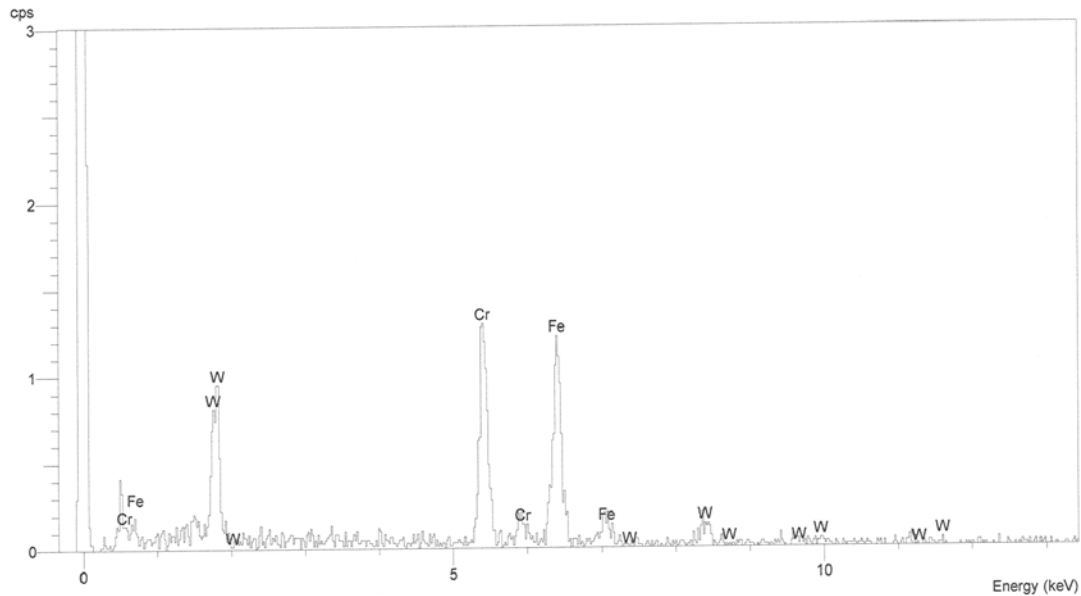


Figure 23. Typical EDX Spectrum of a Cr + W Coated 409 SS Surface

The SEM photograph in Figure 24 shows the microstructure of the W + Cr-coated 409 SS surface. The grain structure is not clear even at higher magnification (Figure 25), in contrast to the Cr-coated 409 SS surface shown in Figure 15. Tungsten seems to stay on the surface and anchors most probably through grain boundaries. XRF and XRD (X-ray diffraction) confirmed the presence of W in the coated 409 SS. However, W deposited on Cr-coated 409 SS was concentrated mostly on the surface. We did not see any W in the bulk according to diffusion profile measurements, indicating very low diffusion of W into the 409 SS substrate.

The presence of Ni in coatings where Ni was deposited over Cr-coated 409 SS was also confirmed by XRF and XRD. As with W coatings on Cr-coated 409 SS, we did not notice any Ni in the bulk according to diffusion profiles (Figure 26), indicating very low diffusion. Apparently Ni was concentrated mostly on the surface. However, diffusion profiles obtained before and after deposition of Ni on Cr-coated 409 SS specimens indicate that the previously diffused Cr is pulled back to the surface after Ni deposition. This could be attributed to the migration of the Cr to the surface to alloy with the incoming Ni, presumably by the favorable partial molar enthalpy of mixing. This indicates that dual coatings of Cr + W or Cr + Ni may not be as efficient as Cr coatings on 409 SS for long-term corrosion protection, although Ni and W are known to exhibit strong corrosion resistant properties. This suggests that a different approach should be developed for the preparation of such dual metallic coatings.

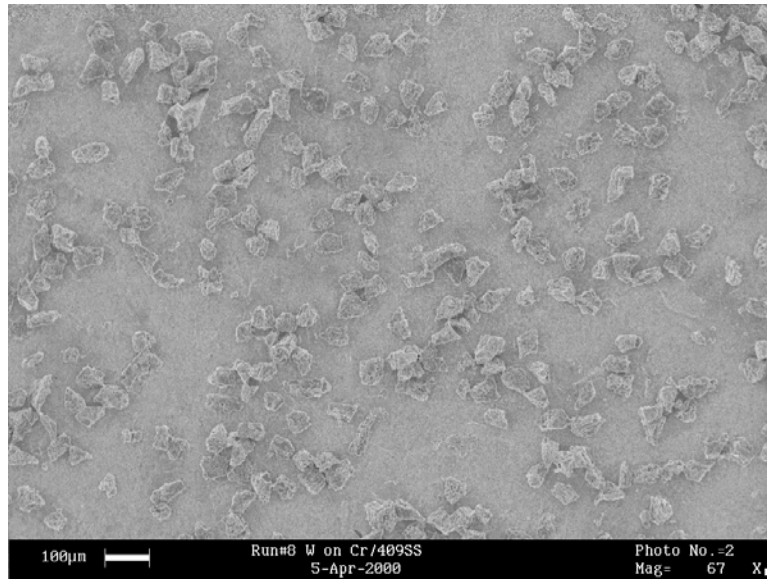


Figure 24. SEM Photograph of W on a Cr-Coated 409 SS Surface

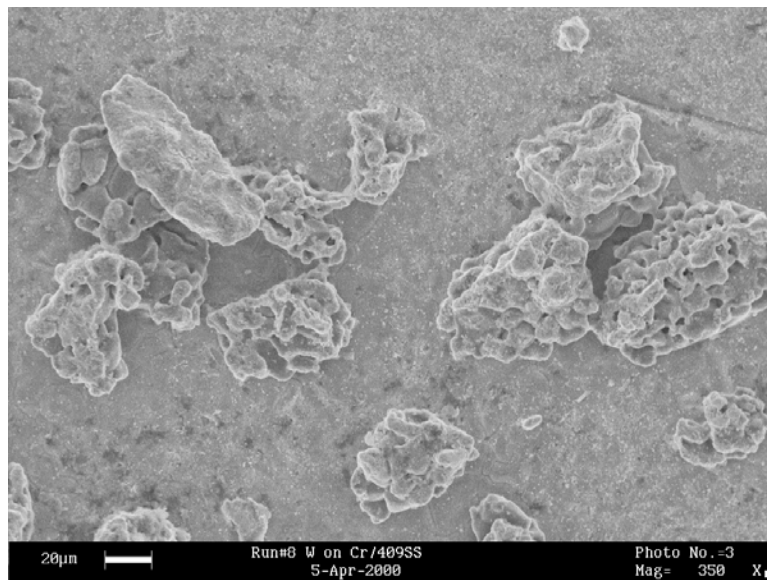


Figure 25. SEM Photograph of W on a Cr-Coated 409 SS Surface at a Higher Magnification

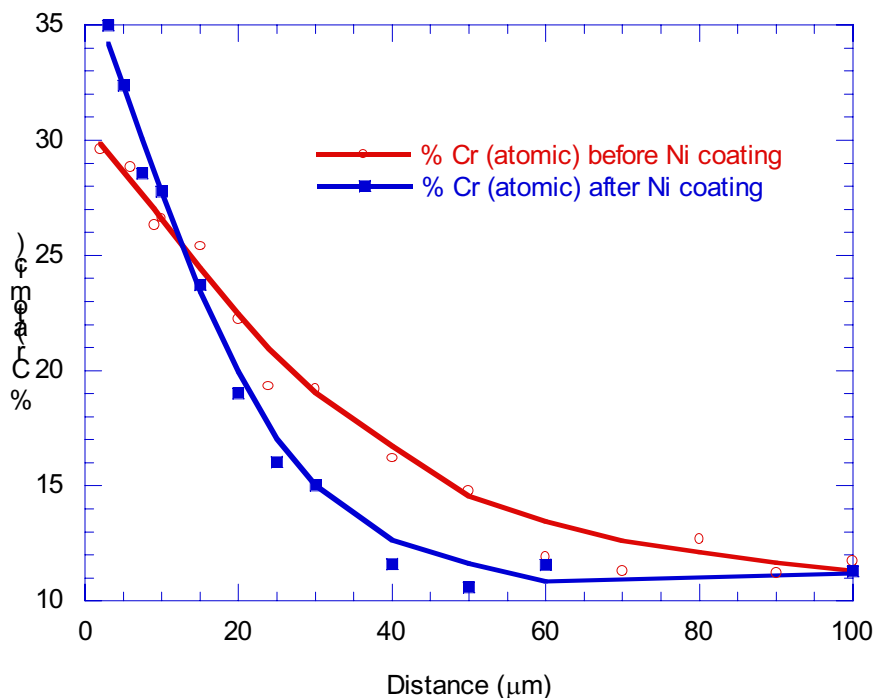


Figure 26. Cr Diffusion Profiles in 409 SS Before and After Deposition of Ni (Runs #5 And #10; See Table 2 and Table 3)

3.2.4. Ni Coatings on 409 SS by FBR-CVD

We prepared a number of Ni coatings on 409 SS, as Ni is known for its corrosion resistance properties in LiBr/LiOH based absorption fluids. It is difficult to deposit Ni from a Ni powder fluidized bed because of powder sintering during the deposition process. When HCl is introduced, Ni particles become very reactive and thus agglomerate, resulting in loss of fluidization. We evaluated several approaches to overcome this problem. First, we used NiCl₂ as the Ni source in an Al₂O₃ powder fluidized bed. When the alumina fluidized bed reached the deposition temperature, NiCl₂ was gradually introduced to the reaction chamber. NiCl₂ was rapidly reduced by hydrogen to deposit Ni on the substrate, and the Ni diffused into the substrate because of the large activity gradient. However, the alumina powder was completely coated with Ni after a brief coating period, and thus it agglomerated in the presence of halides.

Second, we used tungsten-coated alumina powder. The objective of this experiment was to suppress the agglomeration tendency of the bed and to incorporate tungsten and nickel into the coating in a single experiment. By carefully controlling the fluidizing gas flow rate and the rate of nickel chloride introduction, we managed to obtain a stable fluidized bed, which would be important to maintain high heat and mass transfer characteristics. After Ni deposition, samples were left in the reaction chamber for 1 h at 950°C for annealing and improving the Ni diffusion.

Figure 27 and Figure 28 show the surface morphology of two Ni coatings on 409 SS, prepared under similar conditions in the fluidized bed (using the second method described above). However, for the Ni coating shown in Figure 27, the alumina powder was coated with W. Therefore, the coating contained only a trace of W (1-2%) on the surface. Both Ni-coated surfaces show prominent grain boundaries that are enhanced as a result of the halide chemistry coating process. However, the grains are comparable in size to those in as-received 409 SS, indicating only minimal grain growth during the coating process.

Figure 29 shows the Ni diffusion profile for the #2 Ni coating on 409 SS. Unlike Cr coatings, Ni showed only marginal diffusion into the 409 SS substrate. We believe that the initial Ni deposition on the surface is insufficient, and that a strong Ni concentration gradient could not be established to assist deep diffusion during the annealing. It is worth repeating that Ni did not show deep diffusion on Cr-coated 409 SS substrates in earlier experiments (see Section 3.2.3). Thus, fluidized bed treatment would not be a good approach to obtain a significant diffusion profile for Ni, and consequently, electrochemical Ni deposition followed by heat treatment would be a better option.

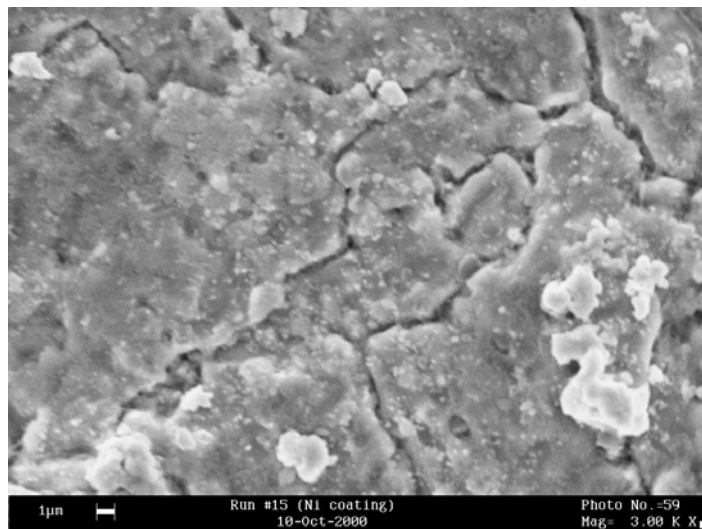


Figure 27. Surface Morphology of a Ni Coating on 409 SS (Ni Coating #1)

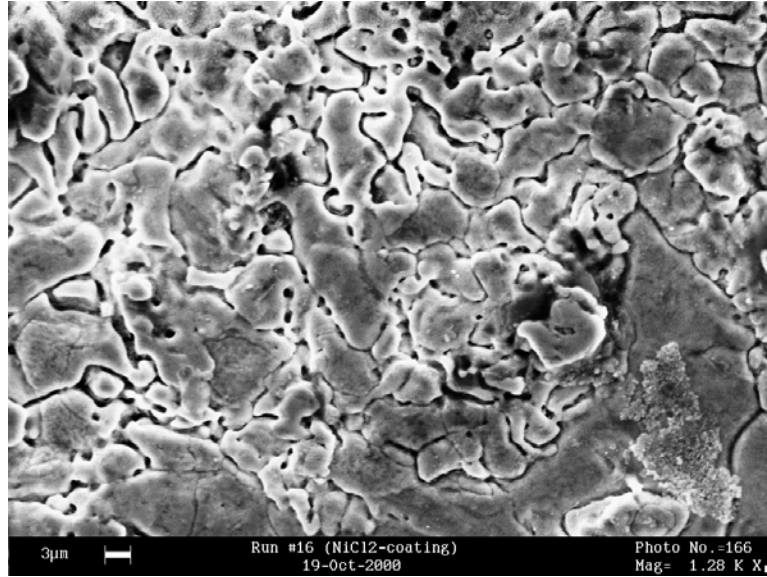


Figure 28. Surface Morphology of a Ni Coating on 409 SS (Ni Coating #2)

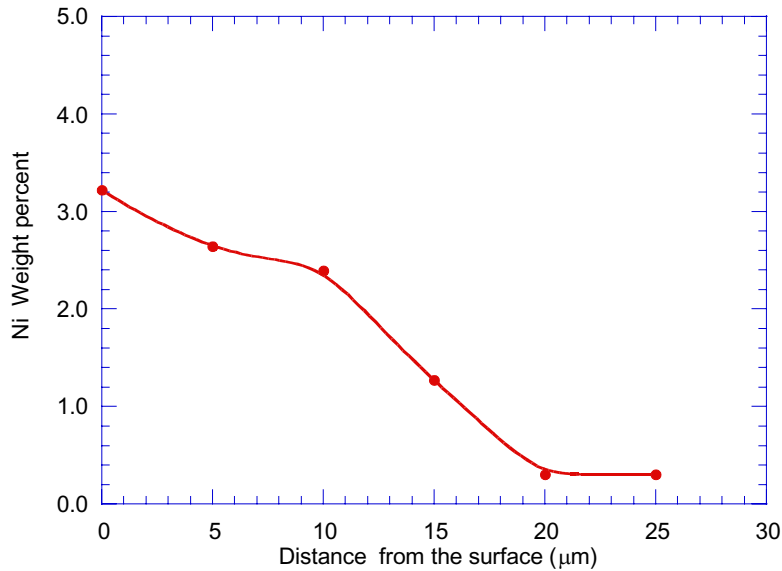


Figure 29. Ni Diffusion Profile of a Ni-Coated 409 SS Specimen

3.2.5. Ni Coating by Electrodeposition Followed by Cr Deposition by FBR-CVD

Ni electroplating is a thoroughly studied subject, and a wealth of information is available in the literature [28-30]. However, electroplating itself does not provide adequate corrosion protection, as this process generally yields overlay coatings that may or may not adhere well to the substrate surface, depending on the surface properties, such as microstructure and cleanliness. Electroplated coatings should therefore be further processed to improve their mechanical stability, especially for high-temperature applications. Our objective in this

project is to combine the advantages of electrodeposition and fluidized bed treatment in such a manner that the two techniques complement each other, using the earlier technique to prepare surface coatings consisting of heavy loadings of highly corrosion-resistant metals, and the latter one as a post treatment process at high temperature to improve interdiffusion of elements between the coating and the substrate. During the post treatment process, a new metal can also be introduced as needed. Such diffusion coatings are expected to exhibit excellent corrosion resistance at high temperatures.

Ni + Cr Coatings on 409 SS

Figure 30 shows the surface morphology of a diffusion coating prepared by electrodeposition of Ni on 409 SS, followed by fluidized bed treatment with a Cr powder. It is expected that the surface consists of Ni-Cr-Fe alloy. The Ni coating surface shows some grain boundaries that are enhanced as a result of the halide chemistry coating process at a high temperature. The grains are comparable in size to as-received 409 SS, indicating only minimal grain growth during the coating process.

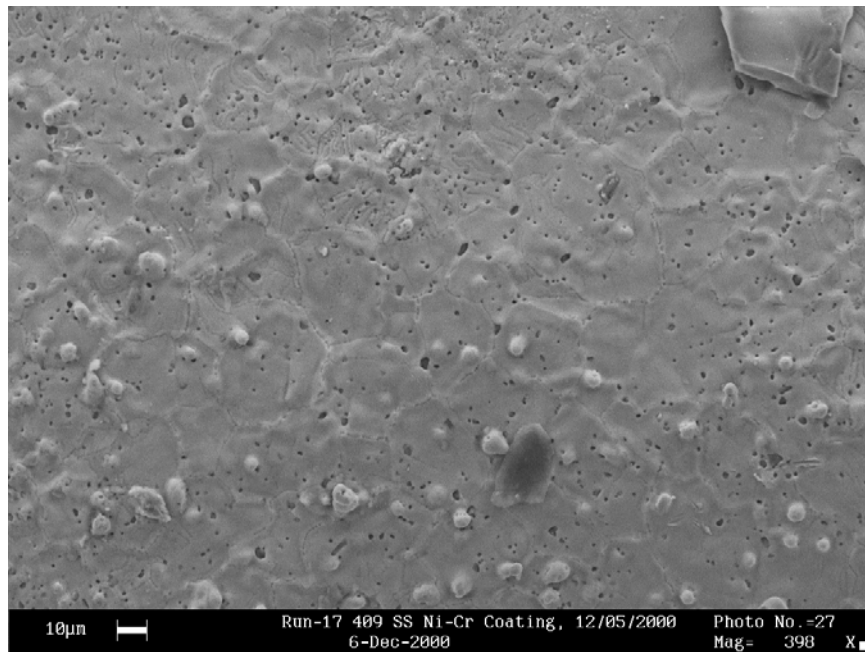


Figure 30. Surface Morphology of a Ni + Cr Coating on 409 SS

Figure 31 shows the Cross-section of an electrodeposited Ni specimen before FBR-CVD Cr coating. As clearly seen in the photograph, overlay Ni coating is loosely bonded to the 409 SS substrate, showing its limitations for corrosion protection. When the overlay Ni coating was annealed followed by Cr deposition in the fluidized bed, the substrate-coating interface disappeared completely, suggesting that a diffusion coating of Ni-Cr-Fe alloy is formed on the 409 SS surface (Figure 32). The photograph shown in the figure was obtained by polishing and etching the Cross-section of the coated specimen to enhance the

microstructure. The etching marks are prominent in the substrate region, but the specimen was hardly etched in the diffusion coating region, indicating its corrosion resistance to acids. Figure 33 shows the diffusion profiles of Ni and Cr in the coated 409 SS. These results confirm the interdiffusion of metals forming a Ni-Cr-Fe alloy on the 409 SS surface. By controlling experimental conditions, we can obtain alloy compositions that are optimized for corrosion resistance for high-temperature applications.

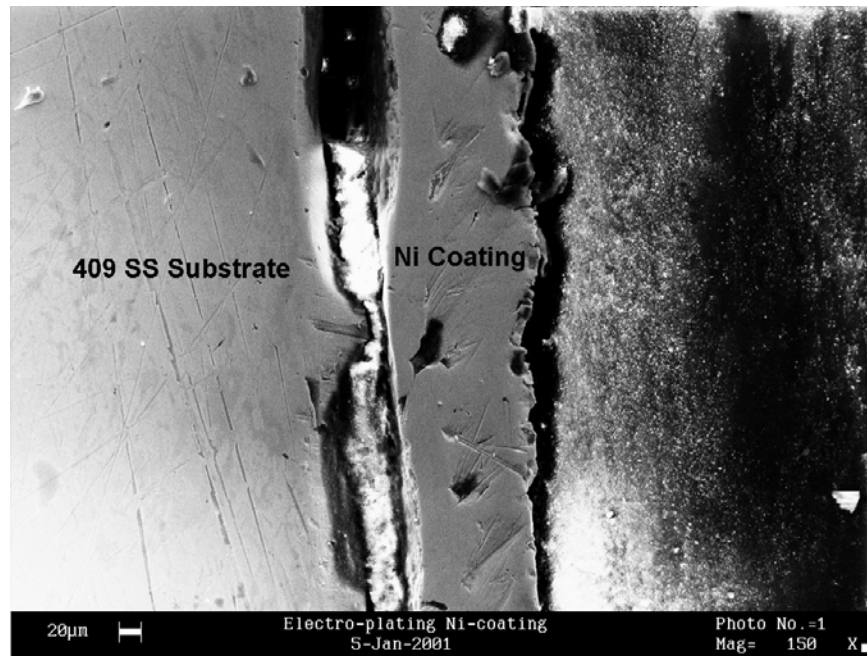


Figure 31. Cross-section of an Electrodeposited Ni Coating on 409 SS Before FBR-CVD Cr Coating and Annealing

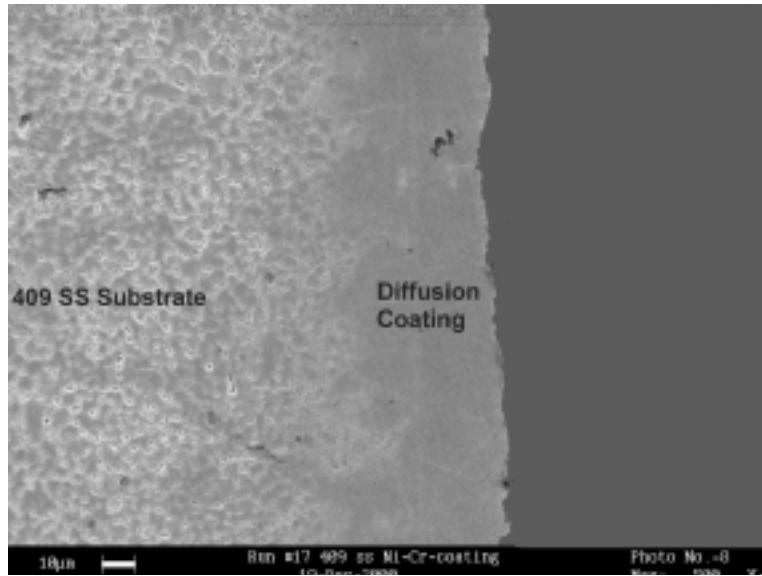


Figure 32. Cross-section of an Electrodeposited Ni Coating on 409 SS After FBR-CVD Cr Coating and Annealing

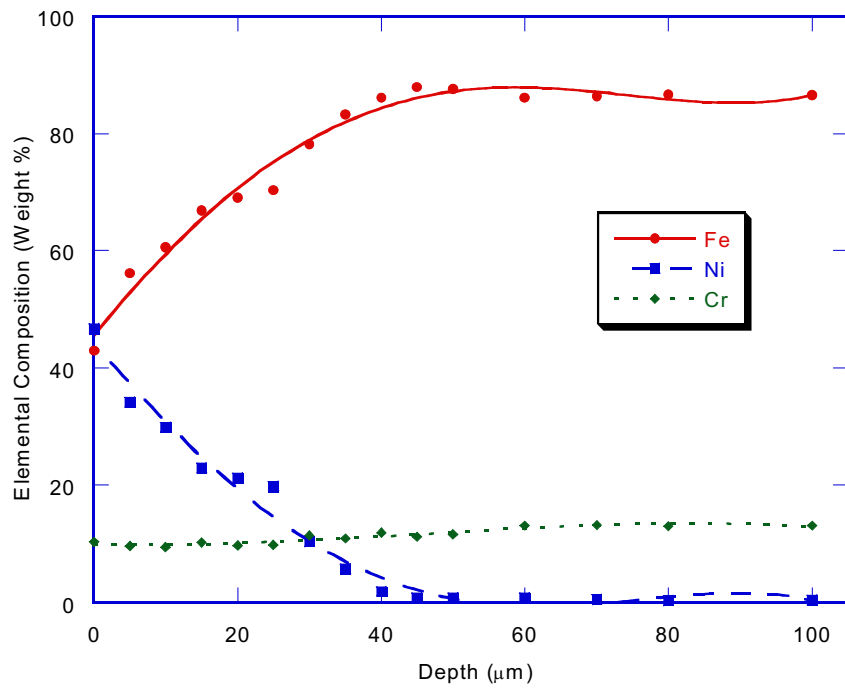


Figure 33. Ni and Cr Diffusion Profiles of a Dual-Metal-Coated 409 SS Specimen

Ni + Cr Coatings on C 1018

Attempts were also made to deposit Ni + Cr diffusion coatings on C 1018, using the procedure developed for 409 SS substrates, as explained earlier, to improve corrosion resistance of C 1018 substrates. Figure 34 shows the surface morphology of a Ni + Cr-coated C 1018 sample prepared by electrodeposition of Ni in a plating bath followed by Cr diffusion in a fluidized bed reactor at 990°C. The surface was rough and showed a dull finish due to particle bombardment during the fluidized bed coating process. The thickness of electrodeposited coatings varies depending on the geometry and arrangement of the electrodes in the electrochemical cell, the current passed, and the deposition time. The uniformity of electrodeposited coatings is improved during the fluidized bed treatment, because FBR-CVD always produces uniform coatings, since the deposition process is performed through gas phase mass transfer.

The EDX spectrum of the Ni + Cr-coated C 1018 specimen shown in Figure 35 indicates that its surface consists of Ni, Cr, and Fe. The average atomic elemental compositions of Ni, Cr, and Fe on the surface were found to be 59%, 8%, and 33%, respectively.



Figure 34. Surface Morphology of an Electrodeposited Ni + FBR-CVD Cr-Coated C 1018 Specimen

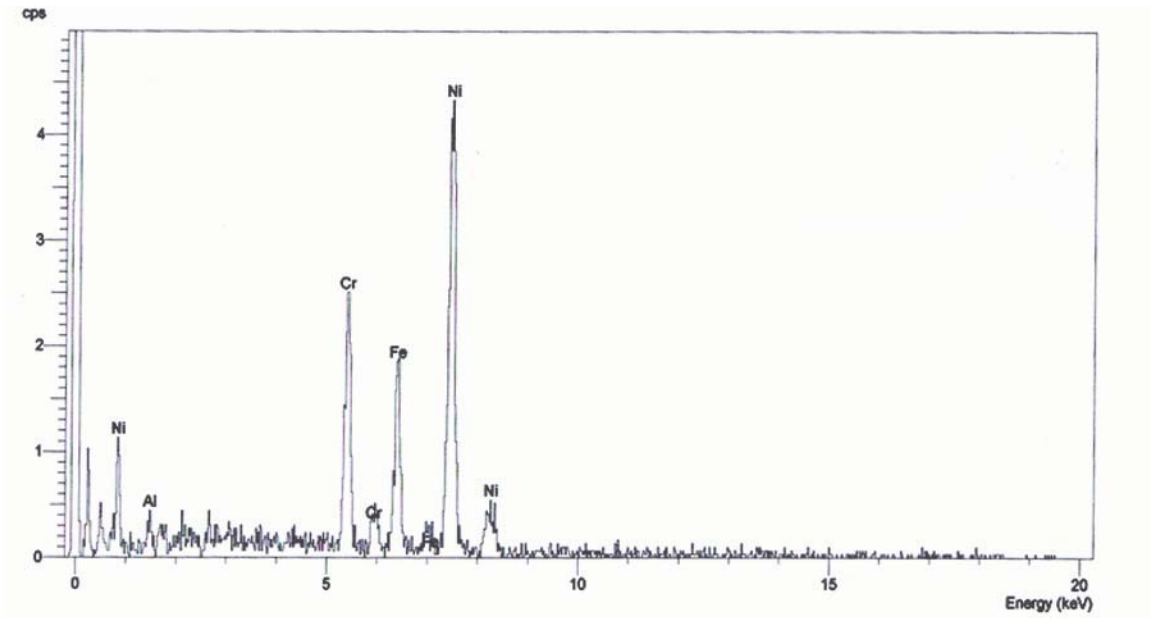


Figure 35. EDX Spectrum of an Electrodeposited Ni + FBR-CVD Cr-Coated C 1018 Specimen

After high-temperature treatment in the fluidized bed during the Cr coating step, Ni, Cr, and Fe are expected to be well inter-diffused to form an alloyed surface coating on C 1018, as observed in the case of 409 SS specimens. Thus, well-defined interfaces are not observed between the coating and the substrate (Figure 36). Diffusion profiles obtained through EDX analysis confirm the presence of Ni, Cr, and Fe in the diffused region, as shown in Figure 37. The diffused layer extends to about 80 μm deep, providing excellent corrosion protection to the substrate material.

Although the diffusion layer is as deep as 80 μm , Cr has diffused up to about 30 μm into the Ni-Fe matrix. It is evident from our experiments where diffusion profiles of elements in Fe, C 1018, and Ni 200 were measured that the diffusion of Cr in Ni is much slower than diffusion of either metal in Fe (Section 0). In fact, the presence of Cr in the substrate, as in the case of 409 SS (Section 3.2.3), hinders diffusion of Ni into the bulk. This again suggests that a strong Cr-Ni alloy is formed on the surface region and blocks the diffusion of atoms to the interior.

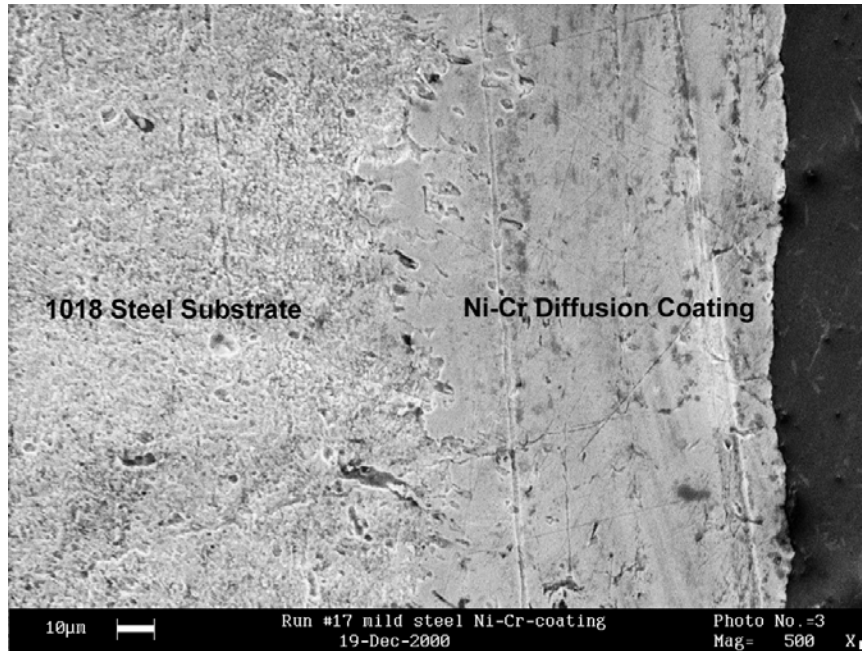


Figure 36. Cross-Section of an Electrodeposited Ni + FBR-CVD Cr-Coated C 1018 Specimen

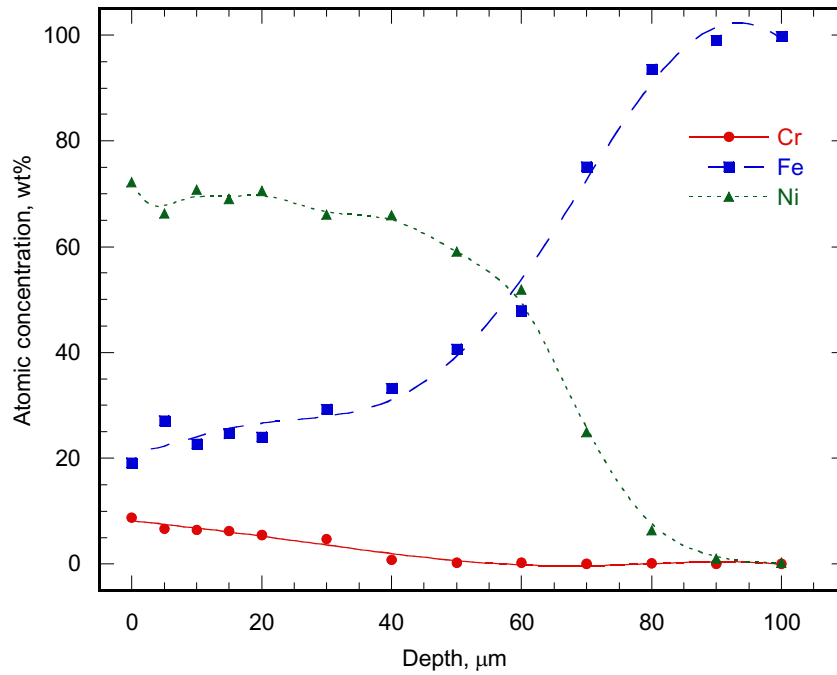


Figure 37. Cr, Fe, and Ni Diffusion Depth Profiles of an Electrodeposited Ni + FBR-CVD Cr-Coated C 1018 Specimen

3.2.6. Ni + M (M = W or Mo) Coating by Electrodeposition Followed by Cr Deposition by FBR-CVD

The goal of these experiments was to extend the electrodeposition – FBR-CVD combination to incorporate two metals in the electrodeposit, in particular Ni + Mo and Ni + W alloy electrodeposits, followed by Cr deposition in the fluidized bed. In earlier experiments, Mo and W coatings prepared by CVD with metal-organic precursors, and Ni-coatings prepared by electrodeposition followed by fluidized bed treatment had shown good corrosion-resistant properties in triple-effect generator environments. Therefore, dual coatings consisting of Ni + Mo or Ni + W should also show excellent corrosion-resistant properties due to the combined corrosion-resistant properties of both metals. Inclusion of Mo or W in the coating should significantly improve the pitting corrosion resistance. The pitting resistance of an alloy is given by an empirical equation, where the pitting resistance equivalent (PRE) [31] is calculated as follows:

$$PRE = \%Cr + 3.3 (\%Mo + 0.5 \times \%W) + a \times \%N$$

The coefficient a ranges from 6 to 30, depending on the nature of the alloy and the conditions of the test. It is clear that alloys of higher PRE show stronger resistance to corrosion, and no pitting is expected when $PRE > 40$.

Ni + W + Cr Coatings

Although W coatings prepared by CVD had shown good corrosion-resistant properties, these coatings have a tendency to delaminate after long-term exposure to corrosive environments. Therefore, an alternative deposition technology, which produces long-term stability in triple-effect generator environments, would be highly desirable. Performance characteristics of coatings prepared by the electrodeposition – FBR-CVD combined technology would meet this demand.

Electrodeposited Ni + W coatings prepared according to the procedure given in Table 4 appeared to be shiny and gray-white. The preliminary characterization of these coatings was performed using SEM and EDX. Figure 38 shows an SEM photograph of the surface morphology of a typical electrodeposited Ni + W coating. Since the SEM was taken before the heat treatment, which would facilitate interdiffusion, the coatings still had an overlay microstructure and could be lifted from the substrate surface to determine its thickness. Figure 39 shows an edge view of a peeled-off Ni + W coating from specimen #2 (see Section 2.2.3 for specimen numbering). One reason for the coating not adhering to the substrate may be the presence of a thick oxide layer.

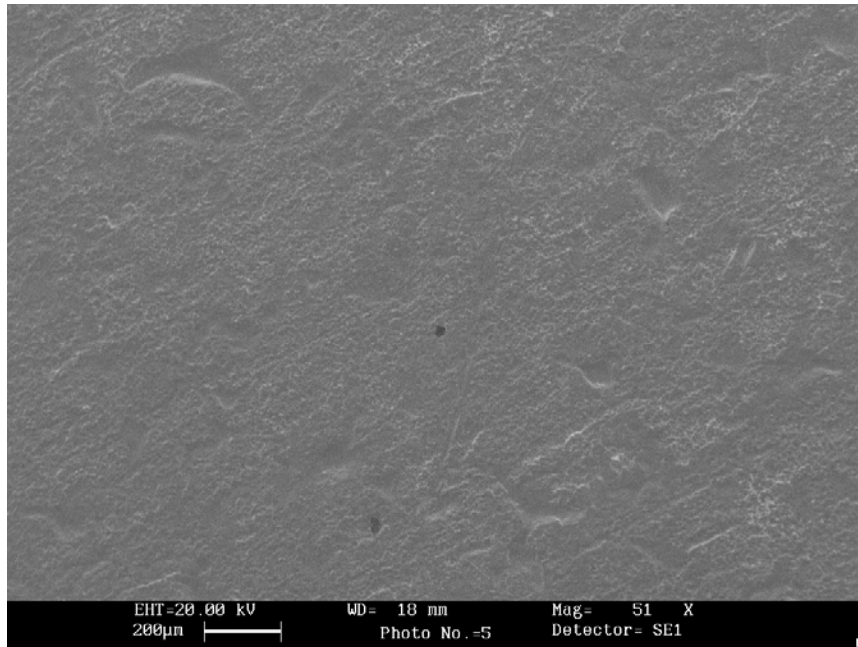


Figure 38. Cr, Fe, and Ni Diffusion Depth Profiles of an Electrodeposited Ni + FBR-CVD Cr-Coated C 1018 Specimen

Treatment of the metal surfaces with mineral acids (for 10 min) did not significantly improve the adhering properties of Ni + W coatings, in particular on 409 SS. However, stronger adhering coatings were observed on C 1018 specimens. A Cross-sectional image of an acid-treated C 1018 specimen after Ni + W electroplating (specimen #10) is shown in Figure 40. The overlay structure is still evident in the figure.

The surface composition of the deposit and the average thickness for some specimens, as determined by SEM and EDX, are shown in Table 6. Addition of an optimum amount of the proprietary substance, Additive A, was found to play a major role in obtaining deposits of high W content. This is clearly evident when the W content of specimens #1 and #2 is compared to the W content of specimen # 3, where the average W loading is decreased by about 32% when 'A' is not added. Acid-cleaning the substrate was not able to improve the W loading, according to the results for specimen # 4 (as compared to Specimen #3). The low W loading of specimens #3 and #4 is attributed to the absence of Additive A, not to acid treatment of the surface. This argument was further supported by the finding that acid-treated 409 SS specimen #5 had the highest W loading, 28%, which was produced by addition of the optimized amount of 'A'. A relative increase in the W concentration in the deposition bath may also have had an impact on this result. The W loading was only a little lower, however, when the *pH* was decreased to 7 (from 8), as observed for specimen #6.

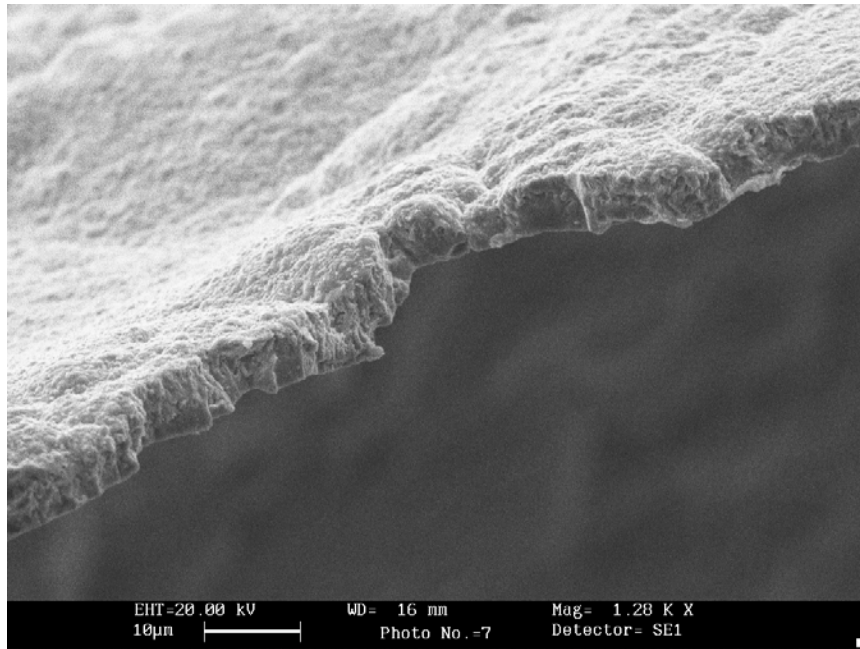


Figure 39. An Edge View of Ni + W Coating on 409 SS Specimen #2

Because specimen #5 showed the highest W content among specimens #1 to #6, it was decided to use the composition of the electrodeposition bath optimized for this specimen to produce Ni + W coatings of significant W loading. However, surface pretreatment procedures should be further optimized to yield coatings with stronger adhering properties. Temperature of the plating bath would be another factor that could easily be controlled, and it was decided to use lower temperatures to produce more stable coatings. At higher temperatures, the deposition rate is faster, resulting in thicker coatings that would easily be peeled off.

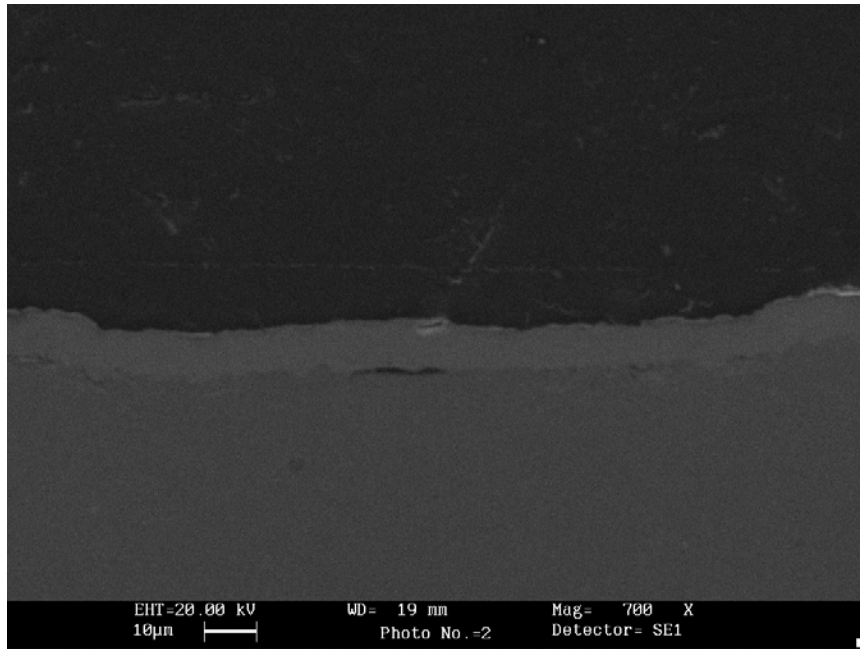


Figure 40. Cross-sectional Image of a Ni + W Electrodeposited C 1018 Specimen #10

Table 6. Surface Composition and Average Thickness of Electrodeposited Ni + W Coatings

Sample	%W at Different Locations (w/w)	Average %W (w/w)	Thickness (μm)
Specimen #1 409 SS (AR)	22.99 (bottom), 25.18 (middle), 31.50 (top)	27	4.5
Specimen #2 409 SS (AR)	29.93 (dark area), 18.36 (surrounding), 11.55 (clear area)	20	3.0
Specimen #3 409 SS (AR)	21.86 (top), 11.28 (middle)	16.5	4.8
Specimen #4 409 SS (acid-cleaned)	12.06, 13.64, 14.92, 11.81, 9.93, 15.67, 15.92, 14.15 (random positions)	13.5	---
Specimen #5 409 SS (acid-cleaned)	--	28	--
Specimen #6 409 SS (acid-cleaned)	--	21	--

After a series of experiments, Ni + W electrodeposits on 409 SS with stronger adhering properties were prepared with a thorough acid cleaning process (15 min acid cleaning, compared to 5 min cleaning for C 1018 specimens). Although the deposit seemed to adhere better, there was no visual difference. These coated specimens (on both 409 SS and C 1018) were treated in the fluidized bed with Cr powder to yield Ni-W-Cr surface alloy composition with gradient diffusion coatings. Such coated specimens were analyzed using SEM, EDX, and XRF to determine the microstructure, diffusion profile, and metal composition. Average surface composition of each electrodeposited coating before and after fluidized bed treatment is given in Table 7. Electrochemical corrosion testing of these coated specimens was performed at 260°C in the LZB solution to demonstrate their corrosion resistance properties (See Chapter 5.0 for details).

The diffusion depth of Cr in the multi-element coated C1018 specimen (Ni + W electrodeposited, followed by Cr deposition in FBRthe fluidized bed reactor) is shown in Figure 41. However, the surface Cr content is lower because of the presence of Ni and W that replace Cr in the coating. The diffusion depths of Ni, W, and Cr in the specimen were found to be 25, 20, and 15 μm , respectively.

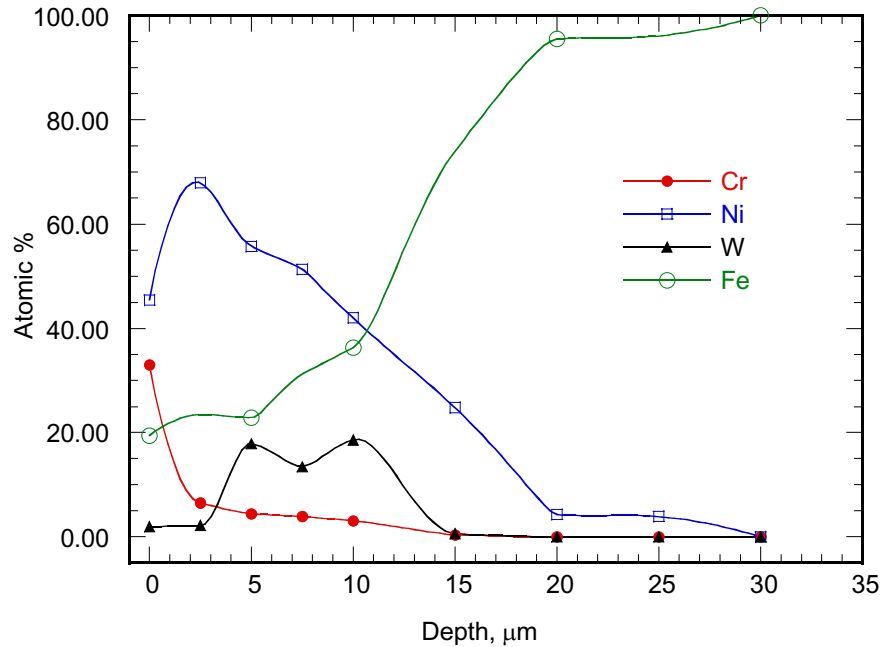


Figure 41. Diffusion Depth Profiles of Cr, Ni, W, and Fe in a C 1018 Sample Prepared by Ni + W Electrodeposition, Followed by FBR-CVD Cr Coating

As the surface condition was a key factor in the preparation of mechanically stable electrodeposits, surface characterization of C 1018 and 409 SS specimens was conducted before and after acid treatment. The grain structure was clearly visible in the acid-treated (10 min in 6 M H₂SO₄ acid) specimens, as compared to the as-received specimens.

Ni + Mo + Cr Coatings

Application of optimized experimental conditions (see Section 2.2.3) produced mechanically stable, shiny, gray Ni + Mo coatings on both 409 SS and C 1018 specimens. After treatment of electrodeposited specimens in the fluidized bed to incorporate Cr into the diffusion layer, surface characterization was carried out using SEM. The average surface composition of these coatings is given in Table 7.

Table 7. Percentages (w/w) of Cr, Ni, W, Mo, and Fe on the Surface of Electrodeposited Alloys

Specimen	Cr	Ni	W	Mo	Fe	Al
Before fluidized bed treatment						
Ni/W coated 409 SS	--	69.3	29.4	--	1.7	--
Ni/Mo coated 409 SS	--	55.1	--	42.7	2.2	--
Ni/W coated C 1018	--	76.6	23.3	--	--	--
Ni/Mo coated C 1018	--	49.2	--	47.2	3.6	--
After fluidized bed treatment						
Ni/W coated 409 SS	20.7	30.6	7.3	---	25.7	15.6
Ni/Mo coated 409 SS	43.4	3.3	--	0.6	42.3	10.4
Ni/W coated C 1018	29.2	37.5	3.0	--	11.7	18.5
Ni/Mo coated C 1018	18.0	58.1	--	3.7	3.5	16.6

3.3. Effect Of Welding On The Coatings

The weldability of coated specimens was tested by welding coated 409 SS coupons together, using tungsten-inert-gas welding (TIG) with 625 weld filler. The 625 weld wire is resistant to corrosion in 90% LZB. Welded samples were tested in 90% LZB solution at 260°C for a period of one month, then examined by SEM for corrosion damage in the vicinity of the weld (heat affected zone, HAZ). We did not see any sign of local corrosion on the coated surface in the HAZ. This observation is critical for field applications where welding is most likely to be part of the assembly process. In many applications, components would have to be coated separately, as the finished product is geometrically too complicated or bulky for the diffusion coating reactors.

4.0 Corrosion Resistance Evaluation Of Coated Metal Specimens

4.1. Corrosion Rate Measurement Techniques

We used electrochemical techniques such as Tafel slope measurements and electrochemical impedance spectroscopy (EIS) to determine the rate of corrosion and thus to evaluate the coatings' performance in aggressive media. Specifically, measurements were obtained in LiBr/LiOH solution at 165°C (330°F) or in LiBr/ZnBr (lithium zinc bromide, LZB) solution at 260°C (500°F). Figure 42 shows the electrochemical cell and the instrumental set-up used for these measurements. The electrochemical cell contained the appropriate bromide solution under an N₂ atmosphere. N₂ gas was saturated with water to compensate for the loss of water due to evaporation. We used a custom designed Ag/AgBr/LiBr electrode as the reference electrode. The counter electrode was a 1-inch² tantalum foil. The test electrode was a 1-inch² metal specimen or a tubular specimen (coated or as-received to be used as a control). The electrical contacts to the test and counter electrodes were made by a spot welded tantalum wire as shown in Figure 42.

4.1.1. Tafel Slope

In the Tafel slope technique, the potential of the coated metal specimen is scanned about ± 100 mV from the corrosion potential (open circuit potential) at a slow scan rate of 0.2 mV s^{-1} , and the resulting current is measured. Typically, the data are presented in a E vs. $\log I$ plot as shown in Figure 43. By using the Stern-Geary equation for the corrosion process and applying non-linear regression analysis to the data, Tafel slopes, corrosion current, and corrosion rate are determined. We used a software package, SoftCorr[®] (EG&G Princeton Applied Research), for experiment control and for data acquisition and analysis. One drawback of this technique is that the coated specimen surface is stressed because a large electrochemical potential (± 100 mV) is applied to the specimen during the scan. Thus, Tafel slope technique is not very desirable for continuous monitoring of long-term performance.

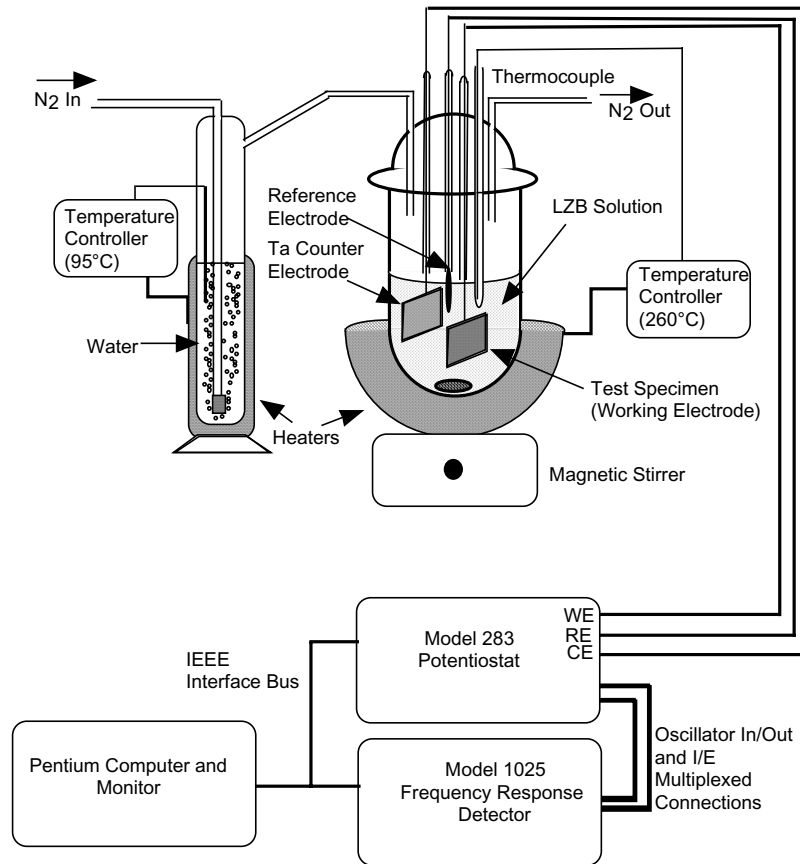


Figure 42. Electrochemical Corrosion Testing Set-Up for Rapid Screening of Coatings

4.1.2. Electrochemical Impedance Spectroscopy

In electrochemical impedance spectroscopy (EIS), a small sinusoidal waveform (± 10 mV) is applied on the coated specimen at the corrosion potential. The frequency of the waveform is varied typically from 10 kHz (1×10^4 Hz) to 10 mHz (1×10^{-2} Hz), and the resulting current is measured with its phase relationship to the applied waveform. From these measurements, impedance characteristics of the coated surface can be determined, which in turn gives a measure of corrosion resistance properties. The results are generally presented in a Nyquist plot as shown in Figure 44. The data are typically fitted to a semicircle and extrapolated to intercept the x-axis. The difference between the x-axis intercepts of the impedance curve is the polarization resistance (R_p), which is inversely proportional to the corrosion rate. The proportionality constant is a function of anodic and cathodic Tafel slopes, and thus the absolute corrosion rate can be calculated if the Tafel slopes are known, using the following equations.

$$\text{Corrosion Rate (mpy)} = 1.287 \times 10^5 \times (eqw/d) \times (I_{corr}/A) \quad (1)$$

$$I_{corr} = \beta_a \beta_c / [2.3 R_p (\beta_a + \beta_c)] \quad (2)$$

Where mpy is mils per year, eqw is the equivalence weight of the sample in g mol^{-1} , d is the density of the substrate in g cm^{-3} , I_{corr} is the corrosion current in amperes, A is the surface area exposed in cm^2 , R_p is the polarization resistance in ohm cm^2 , β_a is the anodic Tafel slope in V per decade, and β_c is the cathodic Tafel slope in V per decade.

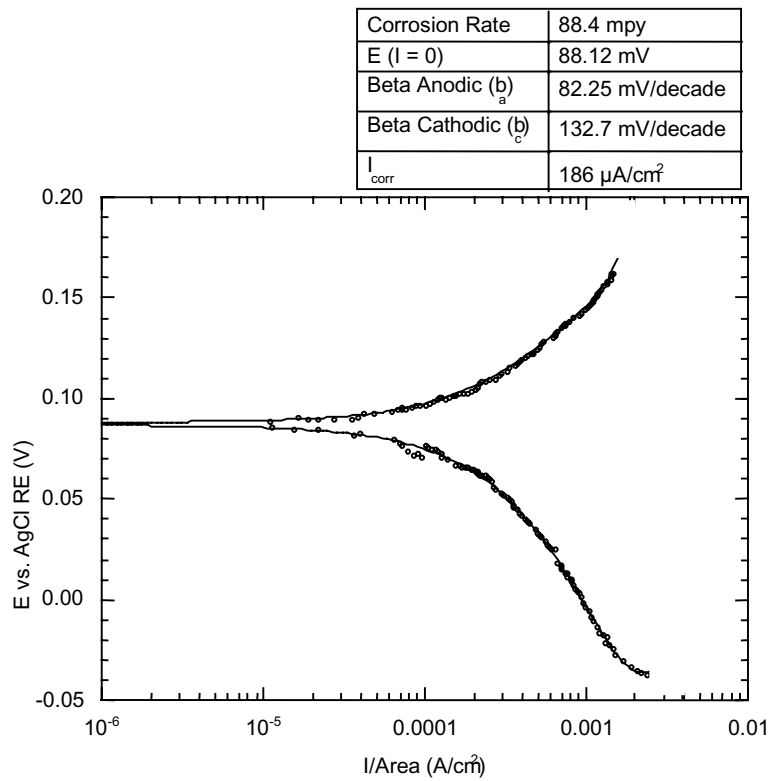


Figure 43. A Current Versus Potential Curve Intafel Slope Measurements For As-Received 409 SS in 90% Lithium Zinc Bromide Solution at 260°C

In most cases, relative corrosion rates are sufficient, as what is needed is the comparison of corrosion rates before and after coating. In EIS, the electrochemical potentials applied on the coated specimen are very small (5-10 mV), and thus the coating experiences only a minimal stress. Thus, we used EIS for long-term corrosion monitoring of coated samples. The EIS and Tafel slope methods of corrosion rate measurement resulted in comparable rates.

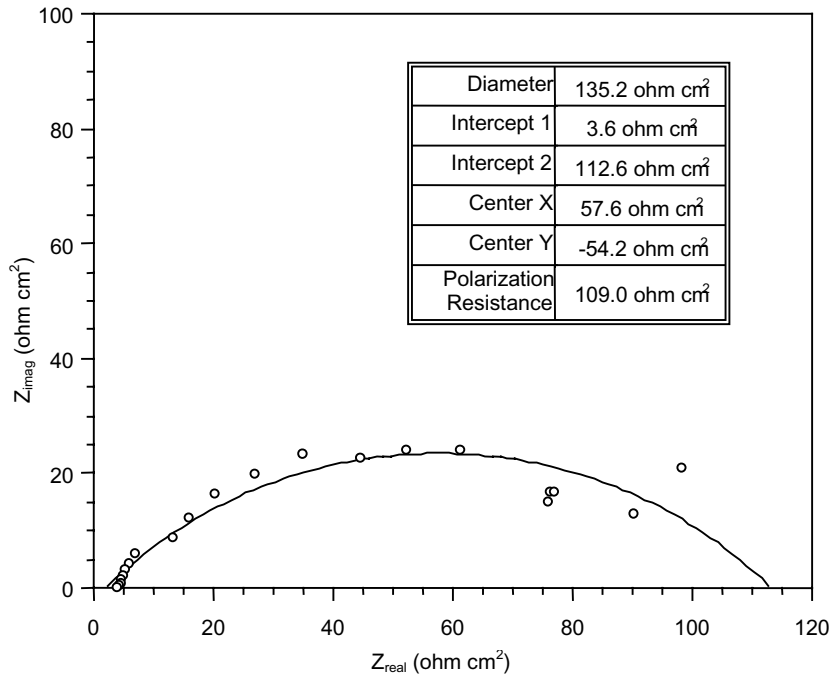


Figure 44. Nyquist Plot for As-Received 409 SS in 90% Lithium Zinc Bromide Solution at 260°C

4.2. Corrosion Test Results

4.2.1. Ni and Ni + Cr Coatings on 409 SS and C 1018

Figure 45 shows the Nyquist plots for as-received and Ni + Cr-coated (electrodeposited Ni + FBR-CVD Cr) C 1018 planar (1-inch²) specimens. As seen clearly in the figure, the polarization resistance of the coated steel specimen is orders of magnitude higher than that of uncoated steel, indicating the excellent corrosion protection provided to the substrate by the Cr + Ni diffusion coating. The calculated corrosion rates of as-received and Ni + Cr coated C 1018 specimens were 62.6 and 1.84 mpy, respectively.

Figure 46 and Figure 47 show Nyquist plots for as-received, Cr-coated, Ni-coated, and Ni + Cr-coated, 1-inch², planar 409 SS specimens. The polarization resistance of 409 SS was increased orders of magnitude by Cr, Ni, or Ni + Cr coatings. Ni + Cr shows a little improvement over either pure Ni or pure Cr diffusion coatings. The calculated corrosion rates of as-received, Cr-coated, Ni-coated, and Cr + Ni-coated 409 SS were 1.94, 0.09, 0.1, and 0.06 mpy, respectively. Table 8 summarizes the rates of corrosion of various coated and uncoated planar steel samples in LiBr/LiOH solution at 165°C under N₂ deaerated conditions.

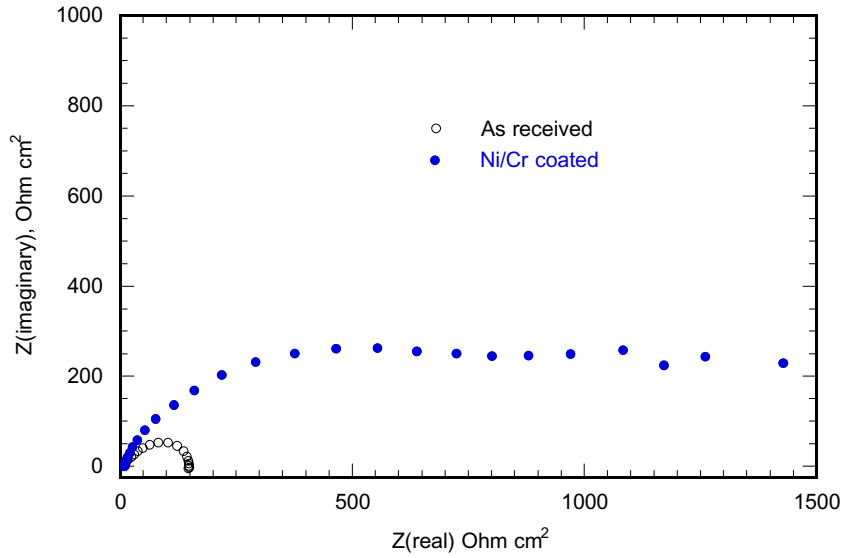


Figure 45. Nyquist Plots for Coated and As-Received C 1018 Specimens in LiBr/LiOH Solution at 165°C

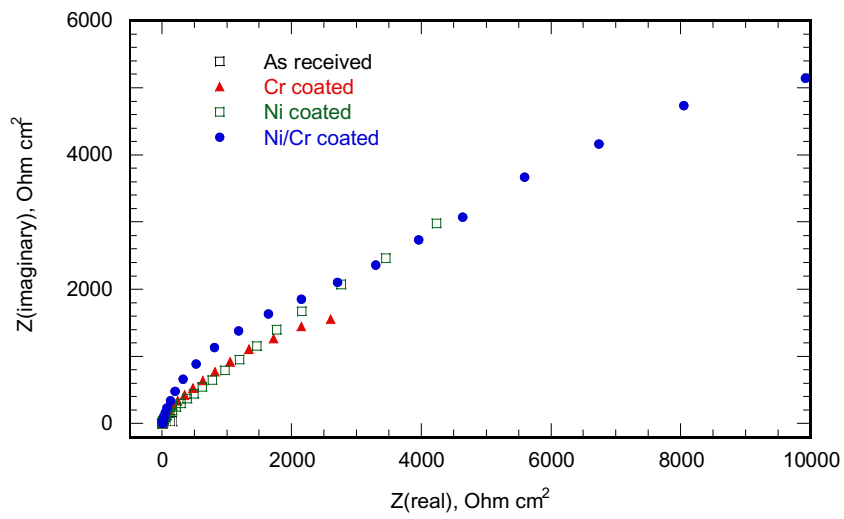


Figure 46. Nyquist Plots for Coated and As-Received 409 SS Specimens in the Measured Frequency Range (10 kHz to 10 mHz) in LiBr/LiOH Solution at 165°C

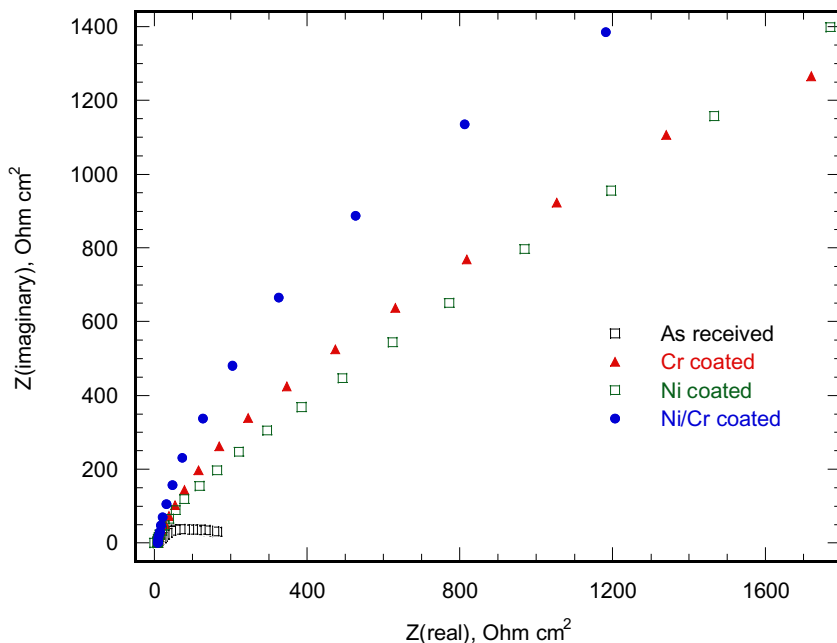


Figure 47. Nyquist Plots for Coated and As-Received 409 SS Specimens. Expanded Graph from Figure 46 Focusing on the Low Impedance Region to View the Comparison Between As-Received and Coated Specimens

Table 8. Rates of Corrosion of Uncoated and Coated Metal in LiBr/LiOH Solution at 165°C and N₂ Atmosphere

Sample	Corrosion Rate (mpy)
Carbon steel (C 1018) specimens	
As-received C 1018	62.6
Ni-coated C-1018	1.84
Si + Ti-coated C-1018	14.4
409 SS specimens	
As-received 409 SS	1.94
Cr-coated 409SS	0.087
Ni-coated 409 SS	0.111
Ni + Cr-coated 409 SS	0.056

4.2.2. Cr + Ni + W and Cr + Ni + Mo Coatings on 409 SS and C 1018

Coated specimens prepared by simultaneous electrodeposition of Ni + W or Ni + Mo coatings, followed by FBR-CVD coatings of Cr to produce multi-elemental corrosion-resistant diffusion coatings, were tested in the LZB solution at 260°C, simulating the advanced absorption environment. Electrochemical impedance spectroscopic and Tafel measurements were conducted to determine the rate of corrosion.

Specimens placed under these aggressive conditions for more than three days had no visible discoloration, but surface changes had occurred at a few places along the edges of some specimens.

The Nyquist plot obtained for a Ni + Mo + Cr-coated 409 SS planar specimen of surface area 14.22 cm² is shown in Figure 48. The polarization resistance of the as-received 409 SS specimen (109 ohm cm²) has been increased tremendously, to an estimated value of more than 1 × 10⁸ ohm cm² after coating. This is a 6-fold increment, which demonstrates the excellent corrosion resistance properties of Ni + Mo + Cr diffusion coatings on 409 SS (Table 9).

The polarization resistance (R_p) of as-received C 1018 is too small to be measured under the simulated advanced absorption environment, according to our past experience. However, Ni + Mo + Cr- or Ni + W + Cr-coated C 1018 specimens show R_p values greater than 10³ ohm cm². The Nyquist plots of coated C 1018 specimens are shown in Figure 49. The exact R_p values and corrosion rates determined are shown in Table 9.

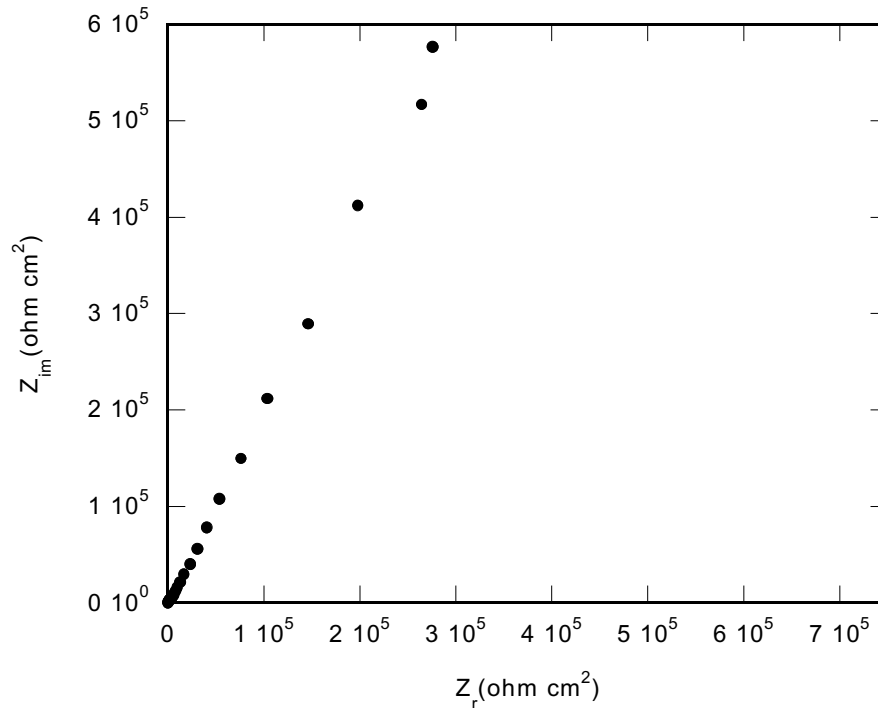


Figure 48. Nyquist Plot for Ni + Mo Electrodeposited and then Cr FBR-CVD Coated 409 SS in 90% LZB Solution at 260°C Under N₂ Saturated Atmosphere

Table 9. Polarization Resistance (R_p) and Rate Of Corrosion of As-Received and Coated Steel Specimens

Specimen	R_p (ohm cm²)	Rate of corrosion (mpy)
As-received 409 SS	109	94.8
As-received C 1018	Too small	Very high (>500 mpy)
Ni + Mo + Cr 409 SS	$> 1 \times 10^8$	< 0.001
Ni + Mo + Cr C 1018	3.8×10^5	0.026
Ni + W + Cr C 1018	3.6×10^3	2.76

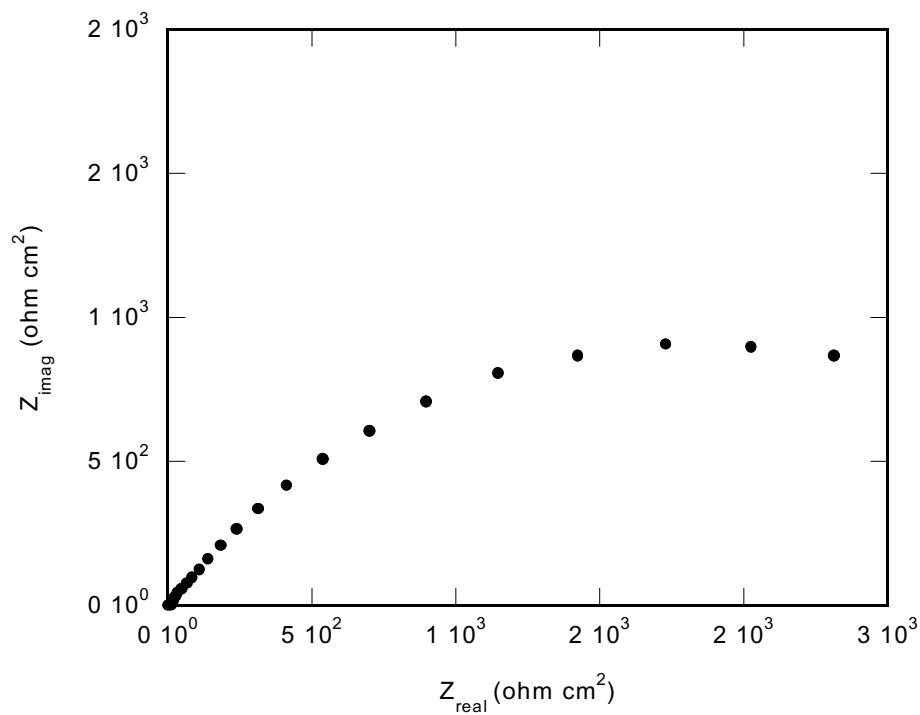
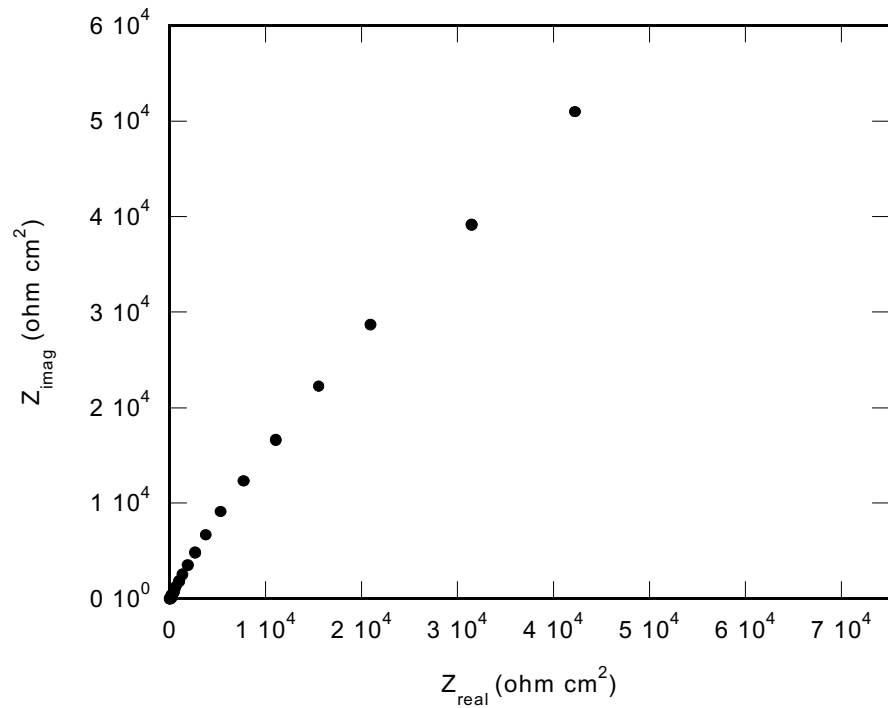


Figure 49. Nyquist Plot for Coated C 1018 Specimens in 90% LZB at 260°C Under N₂ Saturated Atmosphere. Top: Ni + Mo Electroplated and then Cr FBR-CVD Coated. Bottom: Ni + W Electroplated and then Cr FBR-CVD Coated

5.0 Characterization And Corrosion Resistance Evaluation Of Subscale Components

5.1. Uniformity Of Chromium Diffusion Coatings On Subscale Components

We coated a number of 10-inch \times 5/8-inch OD tubes and a 24-inch \times 1.25-inch OD 409 SS tube with Cr by FBR-CVD at 1000°C for 2 h to demonstrate the feasibility of coating narrow, long, and full-scale specimens. Coated tubes have a rough metallic finish, as shown in Figure 2.7 (in Chapter 2.0). The Cross-sections of the tubes were analyzed by EDX, and the Cr coating was found to be uniform on both the inside and the outside surface of these tubes. The surface concentration of Cr in all the specimens investigated was about 25% (wt) and gradually decreased toward the interior, as expected. The coated full-scale tubes show a deep Cr diffusion depth, up to 50 μm .

5.2. Preliminary Corrosion Experiments

Initially, Cr-coated 409 SS tubes (0.5-inch diameter) were tested under advanced double-effect conditions by exposing them to LiBr solution at 150°C (300°F) for 10 days. They were carefully inspected for corrosion damage, and we found that the Cr-coated tubes did not show any signs of corrosion under these conditions.

Additionally, we completed a four-week-long test of Cr-coated 409 SS, 5/8-inch OD tubes in LZB solution at 260°C and used weight loss measurements to determine the corrosion rate. The average corrosion rate of Cr-coated 409 SS over the four-week testing period was determined to be 0.05 mpy. Electrochemical experiments were also performed on these specimens to gather quick, quantitative information, which showed close agreement with the weight loss measurements.

We also prepared a number of Cr-coated tubes using F.W. Winter bulk metal powders, and tested them in the LiBr/LiOH solution at 165°C and in the LZB solution at 260°C. The objective of these experiments was to optimize the coating parameters for using a bulk Cr powder source, as size, alloy composition, and trace metals can affect the coating process. F.W. Winter is one of the powder suppliers to QHT. We successfully coated 6-inch-long tube specimens using the bulk Cr alloy powder, and the coated tubes did not show any sign of corrosion in high-temperature bromide solutions.

5.3. Electrochemical Corrosion Tests

The coated tubular specimens prepared with pure Cr metal powder in the fluidized bed were exposed to the LiBr/LiOH solution at 165°C in an N_2 atmosphere, and their corrosion rates were measured using the electrochemical techniques explained in Section 4.0. Figure 50 illustrates the Tafel characteristics of Cr-coated and as-received 409 SS specimens. The polarization current associated with the Cr-coated specimen is an order of magnitude lower than that of the uncoated 409 SS specimen between the potentials of -0.60 V and -0.35 V (with respect to the custom-designed Ag/AgBr/saturated LiBr reference electrode), indicating high corrosion resistance after Cr coating.

Figure 51 shows the Nyquist plots for Cr-coated and uncoated 409 SS specimens. The significant increase observed in the polarization resistance of the coated specimen, compared to the uncoated specimen, indicates the excellent corrosion resistance of Cr-coated specimens. The measured corrosion rates for as-received and Cr-coated specimens in the LiBr/LiOH solution at 165°C under N₂ atmosphere were 4.62 and 0.06 mpy, respectively, so the corrosion resistant ability improved 2 orders of magnitude after Cr coating.

We also performed corrosion testing of the Cr-coated 409 SS specimens in 90% LZB solution at 260°C, which indicated that the rates of corrosion of all these Cr coatings were below 0.1 mpy. These findings clearly confirm that the above-described diffusion coatings can be safely used in bromide-based advanced absorption chiller environments to protect low-cost steels.

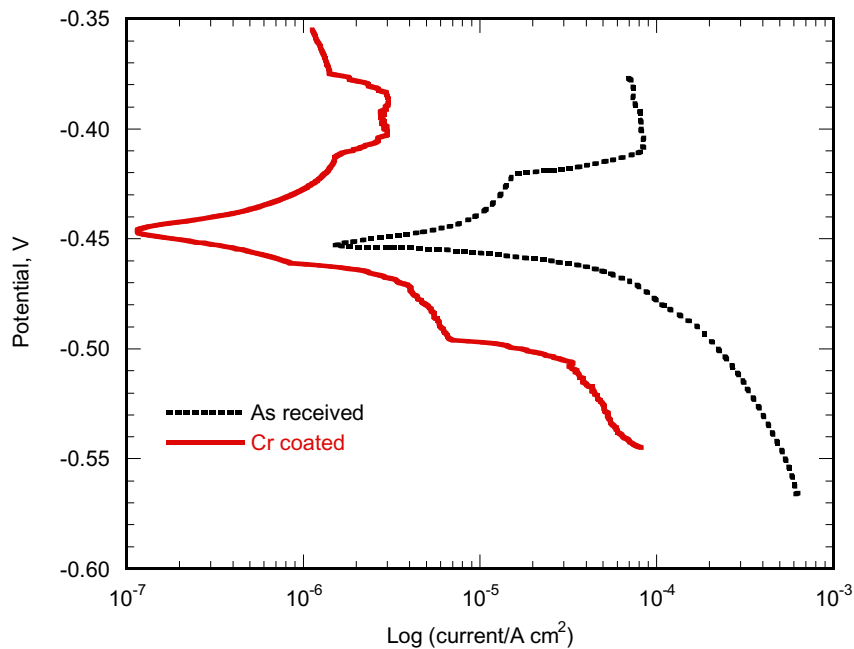


Figure 50. Potential–Logarithmic Current Relationships (Tafel Plots) of As-Received and Cr-Coated 409 SS Tubular Specimens in LiBr/LiOH at 165°C. The Surface Area of the 409 SS Electrode was 11.80 cm²

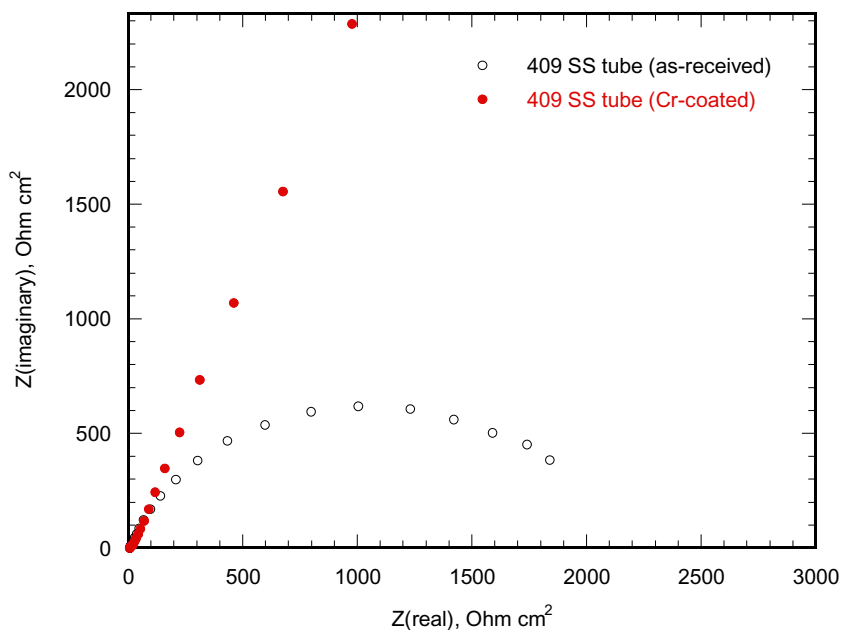


Figure 51. Nyquist Plots for Cr-Coated and As-Received 409 SS Tubular Specimens in LiBr/LiOH Solution at 165°C in an N₂ Atmosphere

5.4. ASTM Tests for the Determination of localized corrosion

We performed several ASTM tests to determine localized corrosion (pitting and crevice corrosion), as they are considered benchmark tests in the industry to qualify materials. The simplest method, used for stainless steels and related alloys, is to expose the materials to a strong oxidizing chloride environment. An aqueous FeCl₃ solution is recommended for this purpose, as this solution is highly corrosive. For corrosion-resistant alloys, this test can be performed at higher temperatures. If a specimen can survive in this environment for a few days, it is believed to be resistant to pitting corrosion in less corrosive environments for an extended period of time.

In this project, we conducted ASTM tests for as-received and Cr-coated 409 SS tubular specimens in 6% FeCl₃ solution at room temperature [32] to investigate the susceptibility of the specimens to pitting and crevice corrosion. In this test, Cr-coated tubes were exposed to the Fe(III) solution at 20°C and 50°C for 72 h. Corrosion rates were determined by measuring the difference in weight during the treatment period under air saturated conditions. Alloys 29-4C, 316L, 316SS, and 304 were also investigated under identical conditions for comparison, and the corrosion rates calculated are listed in Table 10. It is clear from these measurements that the corrosion resistance of 409 SS is greatly enhanced (by a factor of about 36) when specimens are coated with Cr. In fact, the measured weight losses of this sample were heavily influenced by the corrosion damage to the cut edges of the tube where the substrate was exposed to the FeCl₃ solution, thus resulting in a high apparent corrosion rate.

The corrosion resistance of Cr-coated 409 SS is much stronger than that of many types of stainless steel in the 300 series, according to the results in Table 10. Figure 52 shows the surface of the Cr-coated 409 SS tubular specimen after the exposure to the FeCl₃ solution. The clear absence of signs of any pitting confirms the excellent corrosion resistance properties of the Cr coating.

Table 10. Rate of Corrosion of Subscale Tubes, as Determined According To ASTM G48-76

Alloy	Corrosion Rate at RT (mpy)
409 SS AR	491
Cr/409 SS	13.7
29-4C AR	0.114
316 L	84.2
316 SS	162
304	119

Another important parameter used to predict the corrosion resistance of a metal is the critical pitting temperature (CPT), which is defined as the temperature at which the current measured at a predetermined potential shows an abrupt increment during a linear temperature ramp experiment. For the determination of CPT, specimens were cathodically conditioned at -1.1 V vs. SCE (standard calomel electrode) for 1 min, held at open circuit potential for 10 min, and then potentiostatically controlled at +0.7 V vs. SCE for 10 min at room temperature (RT). Following this period, the solution temperature was increased at 1.0°C min⁻¹ while both cell temperature and cell current were monitored. CPT was then determined by plotting the cell current vs. cell temperature.

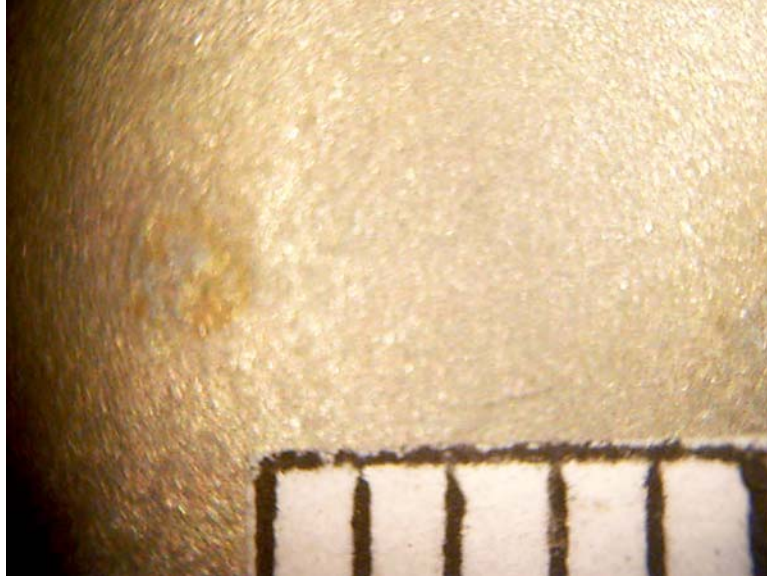


Figure 52. Surface of a Cr-Coated 409 SS Specimen After Exposure to 6% FeCl₃ Solution at 50°C for 72 H (Scale Bar has 1-mm Divisions)

Highly corrosion-resistant alloys typically have high CPT values. We found that AL29-4C and Cr-coated 409 SS specimens had similar CPT values, about 75°C. This confirms that the corrosion resistance of Cr-coated specimens is similar to that of super alloys.

5.5. Effect Of Welding On Subscale Components

The testing of weldability of coated 409 SS specimens, and the corrosion resistance performance of welded specimens in 90% LZB at 500°F have already been discussed in Section 3.3. In addition, we performed a long-term exposure test in 90% LZB at 500°F of a Cr-coated 409 SS subscale component welded to an AL6XN tube sheet. The test specimen was prepared by welding a Cr-coated 409 SS 6-inch × 1.25-inch OD tube to an AL6XN tube sheet, using a tungsten inert gas welding process and 625 weld wire. The welded piece was then exposed to 90% LZB at 500°F for 1000 h, simulating field conditions. Figure 53 shows the LZB-exposed welded piece. Except for the slight changes in color, the welded specimen did not show any sign of corrosion at or near the welded area after this exposure, indicating that we could indeed weld-coat 409 SS steel without reducing its corrosion resistance. Thus, a generator manufacturer will be able to precut and shape tubes, tube sheets, and other components; send them to a coating company for application of the necessary corrosion-resistant coating; and receive and assemble the coated parts at the absorption chiller manufacturing facility. This finding thus has a significant impact on the usability of metallic diffusion coatings in various industrial applications.

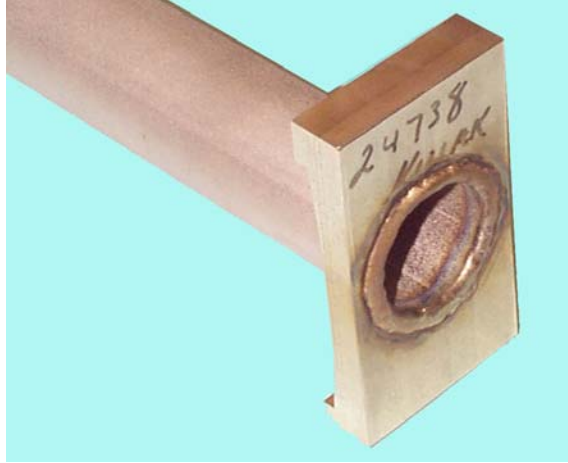


Figure 53. Cr-Coated 409 SS Tube Welded to AL6XN®, after 1000 H of Exposure to 90% LZB at 260°C

6.0 Cost And Engineering Projections For Scale-Up Operation

6.1 Triple-Effect Direct-Fired Generator Material Cost

The cost information for the triple-effect generator can be broken down into the cost for inexpensive materials in non-corrosive areas, such as legs, stands, and exhaust lines, and the cost associated with the brine-exposed areas. In these areas, some triple-effect generator designs use expensive AL6XN[®] (flat sheet) and SeaCure[®] tubes. The high percentage of corrosive areas in triple-effect generators means that the total material cost is dictated mainly by the cost of expensive alloys. Thus, the comparison of total costs with the costs of cheaper alternative materials is strongly related to the ratio of the material costs.

Table 11 shows an approximate comparison of material costs for a developmental Trane triple-effect design. Because the generators are built in different sizes, the cost information is averaged over each ton of cooling capacity. The average cost of AL6XN[®] and SeaCure[®] is about \$6 per pound, whereas the cost of 409 SS is about \$1 per pound. For a 500-ton generator, \$33,250 can be saved by changing the construction material from AL6XN[®] and SeaCure[®] to 409 SS. Even if the corrosion protection measures cost \$10,000 per generator, using 409 SS is far more economical than using AL6XN[®] – the savings is about \$23,250.

6.2 Feasibility Of Technology Commercialization

6.2.1 Industrial Coating Approaches

The two possible approaches for applying a diffusion coating to a direct-fired generator are to (1) coat the assembled generator in a modified fluidized bed or (2) coat precut individual components in a standard fluidized bed. Coating a completely assembled generator would need significant development of the fluidized bed reactor system. Although this method may be extremely efficient and cost effective in the long term for high-volume manufacturing, much more research and development work would be needed to optimize a production-scale coating process.

Table 11. Material Cost Comparison for the Triple-Effect Generator

	AL6XN® and SeaCure® Alloys (\$ per ton capacity)	409 SS (\$ per ton capacity)	Total Cost for a 500-ton Capacity Generator	
			AL6XN® and SeaCure®	409 SS
Non-fluid-contact material costs	\$ 3.00	\$ 3.00	\$ 1,500.00	\$1,500.00
Fluid-contact-material costs				
Flat sheet	70.00	11.67	35,000.00	5,835.00
Tubes	11.00	1.83	5,500.00	915.00
Total fluid-contact material costs	<u>81.00</u>	<u>13.50</u>	<u>40,500.00</u>	<u>6,750.00</u>
Grand total	<u>\$84.00</u>	<u>\$16.50</u>	<u>\$41,500.00</u>	<u>\$8,250.00</u>

The second approach, coating individual components and welding them together, is simpler to implement on the industrial scale with already existing or easily modified facilities. We have clearly shown that coated components can be welded, using filler materials such as Alloy 625, without compromising the corrosion resistance. Therefore, we decided that the coat-and-weld approach be the direction for commercializing diffusion coatings for triple-effect applications.

6.2.2. SRI Preliminary Economic Analysis

We conducted a preliminary economic analysis to determine the cost of applying the FBR-CVD Cr diffusion coatings to both the insides and the outsides of steel tubes. We developed a simple, conceptual process flow sheet, as shown in Figure 54, for coating 150,000 tubes per year. In this process scheme, the tubes to be coated are immersed in a fluidized bed consisting of chromium and alumina particles. A carrier gas (e.g., Ar) containing HCl vapor is passed through the fluidized bed. Chromium chloride vapors are generated by the reaction of HCl with chromium particles, and the vapors dissociate or disproportionate on the surface of the tubes, depositing chromium. The unreacted HCl, CrCl₂, and CrCl₃ vapors leave the reactor along with the fluidizing gas.

Our conceptual coating system shown in Figure 54 consists of a fluidized bed reactor, a furnace, a cyclone, a heat exchanger, a waste heat boiler, and a scrubber system. Different parts of the equipment are described below.

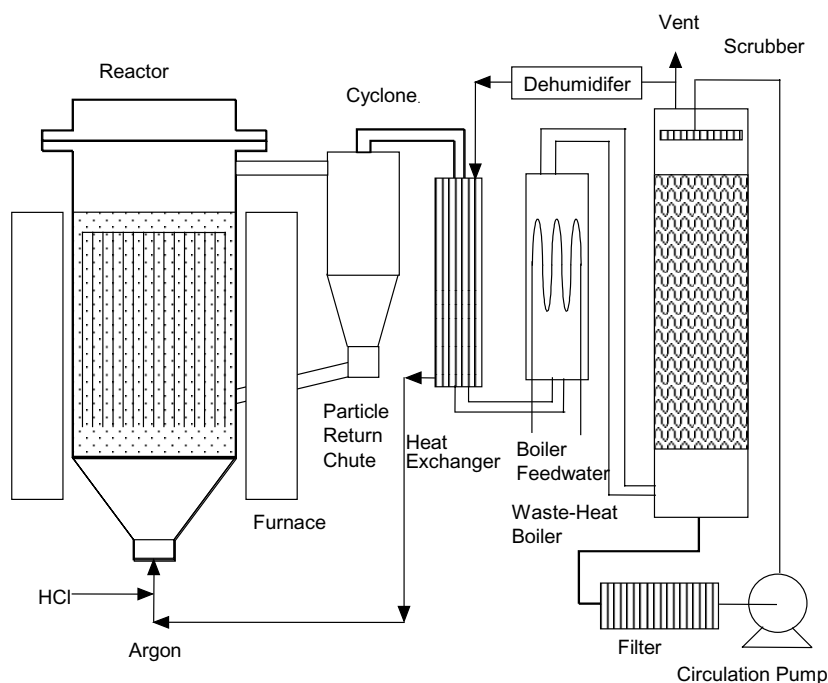


Figure 54. Schematic Diagram for the Fluidized Bed Chromizing Process

Fluidized Bed Reactor and Furnace

The reactor vessel (ID of 21 inch, or 53 cm) is made of oxidation- and heat-resistant materials such as RA 330 alloy. This alloy has good strength and oxidation resistance up to 1200°C (2200°F). We assumed that the resistance to HCl vapor in the fluidizing gas would be promoted by a diffusion coating of Cr formed during the coating process. The tubes (typically 1.25 inches, or 3.2 cm) to be coated are suspended in the fluidized bed from the top or placed inside a wire basket. We calculated that a reactor with an ID of 21 inches (53 cm) could accommodate about 100 tubes per batch, each tube separated from the others by about ¼ inch (0.6 cm). Such an arrangement would allow the tubes to be coated on both the inside and the outside. The reactor is heated by an electrical furnace.

We also calculated the minimum fluidization and elutriation velocities as a function of particle size for both alumina and chromium. The minimum fluidization, U_{mf} , and the elutriation velocity, U_t , for a 150- μm alumina particle are 1 and 100 cm s^{-1} , respectively, at a temperature of 927°C (1700°F). These velocities for chromium particles are about twice that of alumina particles because of the high density of chromium. In the experimental work conducted at SRI, the gas velocity was 20 cm s^{-1} (925°C, 1 atm), which was within the range between U_{mf} and U_t for both alumina and chromium particles. The U_{mf} and U_t do not change significantly with temperature because of the compensating effects of changes in the gas viscosity and gas density. We calculated that U_{mf} and U_t are changed by about 5% when the temperature is changed by about 100°C.

The height of the fluidized bed measured from the distributor is about 36 inches (91 cm), the void fraction of the bed is estimated to be about 0.6, and the total volume of the solids is about 204 L. If the bed consists of 97 wt% alumina and 3 wt% chromium, then the amounts of alumina and chromium are about 317 and 18 kg, respectively.

Cyclone to Capture Entrained Particles

Although the velocity of the gas through the fluidized bed is less than the elutriation velocity for the nominal, initial particle sizes of both alumina (150 μm) and chromium (50 μm), elutriation of small particles may continue to occur. The particle size of alumina may decrease due to attrition, and the size of chromium particles may decrease because of the reaction with HCl and vaporization of chromium chlorides. Hence, a certain fraction of the bed solids can be expected to entrain the gas stream leaving the fluidized bed reactor. A cyclone is installed at the outlet of the reactor to capture the majority of the entrained particles above 5–10 μm in size. As with the reactor, the cyclone will be constructed using Alloy RA 330 or a similar material. The particles collected in the cyclone will be returned to the fluidized bed.

Heat Exchanger and Waste Heat Boiler

When the reactor operates at about 925°C with 11.2 L s⁻¹ gas flow, the sensible heat in the gas stream (excluding the sensible heat of the entrained particles) is about 14 kW. The gas must be cooled down to less than 100°C before it enters the scrubber. Several alternatives are possible to recover the heat from the hot exhaust gas stream. A heat exchanger can be used to transfer a fraction of the heat to the reactor inlet gas stream. Another option is to recirculate the exhaust gas back to the inlet of the fluidized bed reactor with additional HCl vapor, as needed. Or a heat exchanger and a waste heat boiler can be installed downstream of the cyclone and the low-pressure steam generated in the boiler can be used for space heating or other applications.

Scrubber System

The exhaust gas leaving the boiler or recirculator contains HCl vapor and other contaminants that must be removed before the gas can be vented. We propose to use a scrubber that circulates an aqueous solution of caustic soda that would neutralize the HCl vapor. In this environment, chromium chloride vapor is hydrolyzed and converted to chromium oxides. The entrained or precipitated solids are captured in a filter press before the solution is recirculated. The solids are disposed of in an appropriate manner.

Suggested Operating Procedure

The reactor is designed to operate in a batch mode. The tubes to be coated are arranged in an open mesh container and inserted into the preheated reactor. Initially, the reactor is purged with argon gas to remove air. After purging, hydrogen is added to the feed gas to reduce any oxide scale present on the surface of the tubes. After the tubes attain the reactor temperature, hydrogen chloride gas is introduced to initiate the coating reactions. At the end of the coating period, hydrogen and hydrogen chloride gases are turned off from the

gas stream and the reactor is purged with argon. Then the lid of the reactor is opened and the tubes are taken out of the reactor. A new batch of tubes is inserted and the next cycle is initiated. We estimate that each cycle takes about 8 h.

Capital Costs

The cost of the equipment was estimated from existing publications and vendor quotes. Table 12 lists estimated capital costs of about \$442,000 for coating 150,000 tubes per year. These costs include the installed equipment cost (TIC), which is estimated to be 200% of the total equipment costs. Because the process scheme is relatively simple and small in size, a smaller than normal installation cost factor can be assumed. The costs of installation of utilities and other facilities are assumed to be about 5% and 1.5% of the total installed costs, respectively. The construction is assumed to take about 1 year, and the interest on the capital during this construction period is assumed to be 12%. The startup costs are assumed to be about 10% of the fixed capital costs.

Table 12. Capital Cost of the Chromium Coating Process (150,000 Tubes Per Year)

<u>Equipment</u>	<u>Quantity</u>	<u>Cost (\$)</u>
Furnace	1	\$100,000
Reactor	1	20,000
Waste heat boiler	1	10,000
Absorption tower	1	20,000
Heat exchanger	1	10,000
Miscellaneous		10,000
Total equipment cost		170,000
Total installed cost (TIC)		340,000
Utilities		17,000
General service facilities		5,355
Fixed capital costs (FCC)		362,355
Interest during construction		43,483
Startup costs		36,236
Total capital cost (TCC)		\$442,073

Annual Operating Costs

The estimated annual operating cost is shown in Table 13. For these calculations, we assume an on-stream factor of 90% and 350 days per year of operation. The annual maintenance cost is assumed to be 2% of the total installed cost. The cost of maintaining a laboratory for quality control is about 20% of the operating labor.

We also assume that a major portion of the elutriated alumina powder will be captured by the cyclone and returned to the reactor. Thus, the attrition loss of alumina is assumed to be 0.1% of the load per hour. The consumption and loss of chromium powder is assumed to be about 1% of the load per hour. Because argon and most of the hydrogen are not consumed, we assume that about 90% of the argon-hydrogen mixture will be recycled. The un-reacted hydrogen chloride and chromium chlorides will be absorbed in the absorption tower, through which a dilute stream of caustic soda is circulated. Any solids that are captured by the liquid are filtered and disposed of in an appropriate facility.

The assumptions used to calculate the plant overhead, taxes and insurance, and general and administrative costs are shown in Table 13. The cost of capital was assumed to be 25% of the fixed capital costs. Based on these assumptions, we calculate that the cost of the chromium coating will be about \$3.32 per pound. The labor cost of the process is high (71%), followed by capital costs (16.5%). The materials costs are only about 12.5% of the total cost.

Table 13. Annual Operating Costs (150,000 Tubes Per Year)

	Basis	Rate (\$)	Units		Cost (\$)
Operating	2 men/shift	15 /h	8	h/shift	226,800
Maintenance	2%/yr TIC				6,800
Quality control lab	20% OL				45,360
Total Labor					278,960
Alumina	0.1% /h	1 /kg	0.4	kg/h	3,024
Chromium	1% loss/h	12.5 /kg	0.4	kg/h	37,800
Carrier gas	10% flow	0.05 /kg	6.56	kg/h	2,481
Hydrogen chloride	0.25% carrier gas	3 /kg	0.21	kg/h	4,851
Hydrogen	25% flow	2.8 /kg	0.12	kg/h	2,481
Caustic soda		3 /kg	0.05	kg/h	1,063
Maintenance materials	2% TIC				6,800
Disposal of spent materials		0.35 /kg	0.8	kg/h	2,117
Miscellaneous					
Total Materials					60,618
Waste heat boiler water		1 /m ³	0.06	m ³ /h	454
Electricity		0.1 /kWh	45	kWh	34,020
Total Utilities					34,474
Total Direct Costs					374,051
Plant overhead	80% total labor				223,168
Taxes and Insurance	2% of fixed capital				7,247
G&A	10% operating cost				37,405
Depreciation	10% of fixed capital				36,236
Total Indirect Costs					304,056
Gross Production Cost	(Direct + Indirect)				678,107
Cost of capital	25% of fixed capital				90,589
Total Operating Cost					768,696
Cost of Coating/tube (\$)					5.12
Cost of Coating/lb (\$)					3.32

6.3. Licensing

6.3.1. Selection of a Commercialization Partner

As part of our feasibility study for scaling up the coating process, we contacted several industrial coating companies about collaboration. We received favorable responses and details of their production facilities. The best candidate was Quality Heat Technologies (QHT) in Australia, which specializes in fluidized bed coatings and heat treatments to improve wear resistance of metal components. QHT routinely performs fluidized bed heat treatment of very large components, as shown in Figure 55. They are well positioned to exploit coating markets for the low-cost metal diffusion coating process. We thought the expertise of this company would be appropriate for commercialization of our FBR-CVD technology. In discussions with GTI and SRI, QHT recognized a long-term commercial opportunity for the process: it could provide a Cr coating service to industry, produce Cr-coated tubing for a specific market, and/or sell equipment for the process. In September 2001, we licensed the SRI FBR-CVD Cr coating technology to QHT for scale-up and commercialization.



Figure 55. Heat Treatment of Large Gear Assembly in a Fluidized Bed Furnace.

6.3.2. Market Analysis by Quality Heat Technologies

QHT conducted an independent economic analysis to determine the cost of applying the SRI developed FBR-CVD Cr diffusion coatings to both the insides and the outsides of steel tubes. QHT needed to confirm the preliminary economic analysis data from SRI and the feasibility of converting the laboratory developed process to a large and competitive production operation. Based on QHT's market analysis and estimation of sales, the cost of Cr coating of 409 SS tubes is graphically shown in Figure 56. The numbers reflect the direct costs of producing Cr coatings in a 600-mm-diameter × 2000-mm-deep furnace with a coating time of 2.5 h.

Table 14 compares tubing costs for three super alloys with the cost of coated alloys, and potential margins. Clearly, there is a significant potential margin for Cr-coated low-cost alloys. According to our sources, one US heat exchanger factory alone uses 200,000 lb of AL6XN per year, at an average price of US\$ 6.50 per pound (= US\$ 1,200,000 per year). This is a significant potential market for Cr-coated low-cost steels.

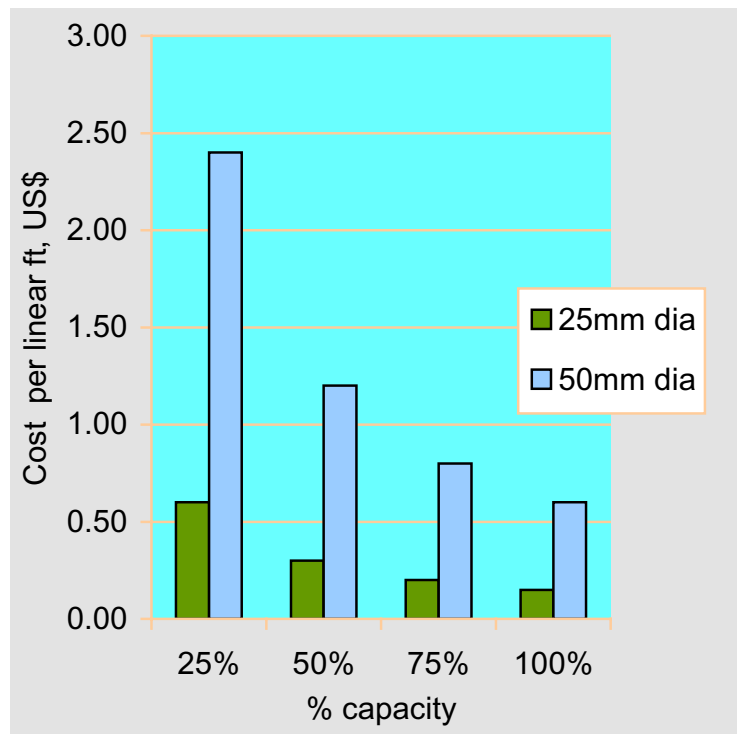


Figure 56. The Cost of Cr Coating of 409 SS Tubes by the FBR-CVD Process

Table 14. Comparison of 1-Inch-Diameter Tubing Costs per Linear Foot

Material	Cost (US\$)^a	Potential Margin (US\$)^b
AL6XN	4.04	2.54
SEA-CURE	2.80	1.30
AL29-4C	2.24	0.74
Cr-coated 409 SS	1.50	-

^aPrice for AL6XN and SEA-CURE based on quote from Trent Tube for 10,000 ft. Price for AL29-4C based on ASHRAE and Cr-coated tube on 50% utilization.

^bMargin contribution to labor overheads etc.

7.0 Technology Transfer and Commercial Production Process

In collaboration with QHT, we established a development program to transfer SRI's Cr diffusion coating process to a production scale for coating 409 SS tubes for the prototype generator and commercial exploitation of the Cr coating technology. The main tasks in the development program were performed by Mr. Ray Reynoldson at the QHT coating facilities in Australia. The initial objectives of the development program were to:

- Select low-cost metal powders from bulk suppliers and perform a set of laboratory scale coating experiments to determine their suitability for the Cr coating process.
- Establish the parameters needed to produce Cr-coated 409 SS tubes in a metal-lined pilot scale fluidized test bed (300 mm diameter × 600 mm deep) with a Cr diffusion profile similar or identical to that obtained in SRI coating experiments.
- Design and build a production scale, metal-lined fluidized bed specialized for the Cr coating process.
- Establish coating parameters for the production metal-lined fluidized bed (600 mm diameter × 1200 mm deep), using the pilot scale operation as the reference.
- Produce 50 meters of 38.1-mm-diameter 409 SS tubes (in lengths of 1000 mm) for a prototype generator to be built by Broad USA.
- Process additional test samples of 409 SS tubes for marketing and testing in other applications such as condensing heat exchangers in residential gas furnaces.

The results of the commercial Cr coating development program are discussed below.

7.1. Selection of Metal Powders and Suppliers

To make the coating process most economical, we carefully looked into a number of details, such as metal powder suppliers, required purity, required particle size, and gas suppliers. We performed a number of laboratory experiments with materials obtained from bulk suppliers to confirm that the resulting coatings meet necessary specifications. In one set of experiments, bulk quantities of chromium and several chromium alloys obtained from F.W. Winter, a metallurgical powder supplier to QHT, were used to coat metal specimens. The commercial Fe/Cr alloy powder is much less expensive than Cr/X (proprietary) alloy, so the coating material cost would be substantially reduced if we could use this alloy powder in place of Cr/X alloy. Therefore, a coating experiment was performed using Fe/Cr alloy powder and the proprietary additives in the same way as in our previous experiments. The other experimental conditions such as gas flow rates, temperature, and time of coating were also kept the same. Figure 57 shows the diffusion profile of Cr in 409 SS prepared using Fe/Cr alloy powder. Clearly, the diffusion depth is much lower than that obtained with Cr/X alloy powder (Figure 58). We believe that the high concentration of FeCl_x suppresses the vapor pressure of CrCl_x and thus reduces the rate of Cr deposition. Evidently, deep Cr diffusion requires the use of Cr alloy powder.

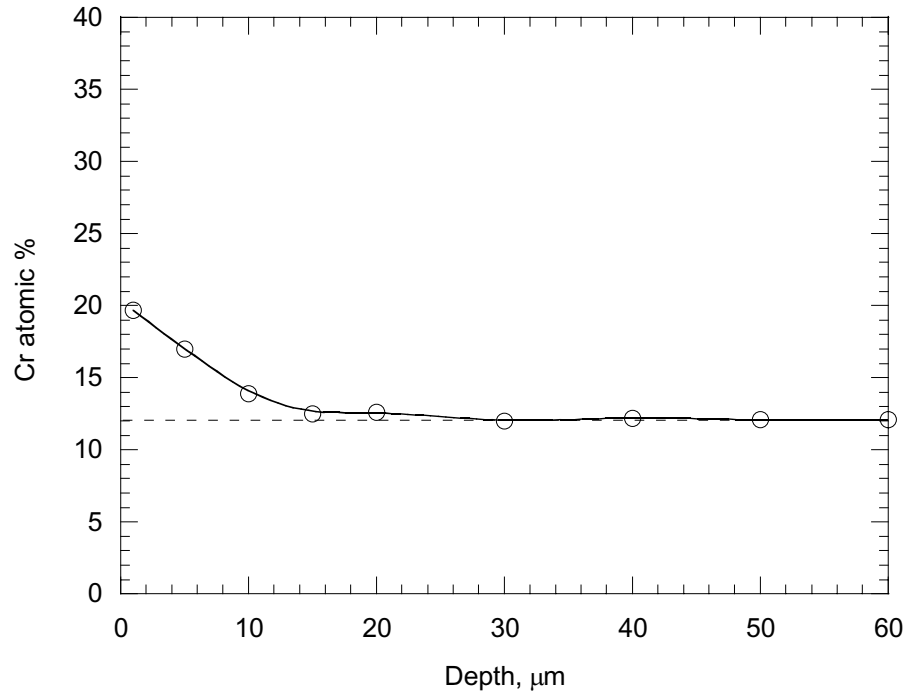


Figure 57. Diffusion Profile of Cr in 409 SS Prepared by Using Fe/Cr Metal Powder

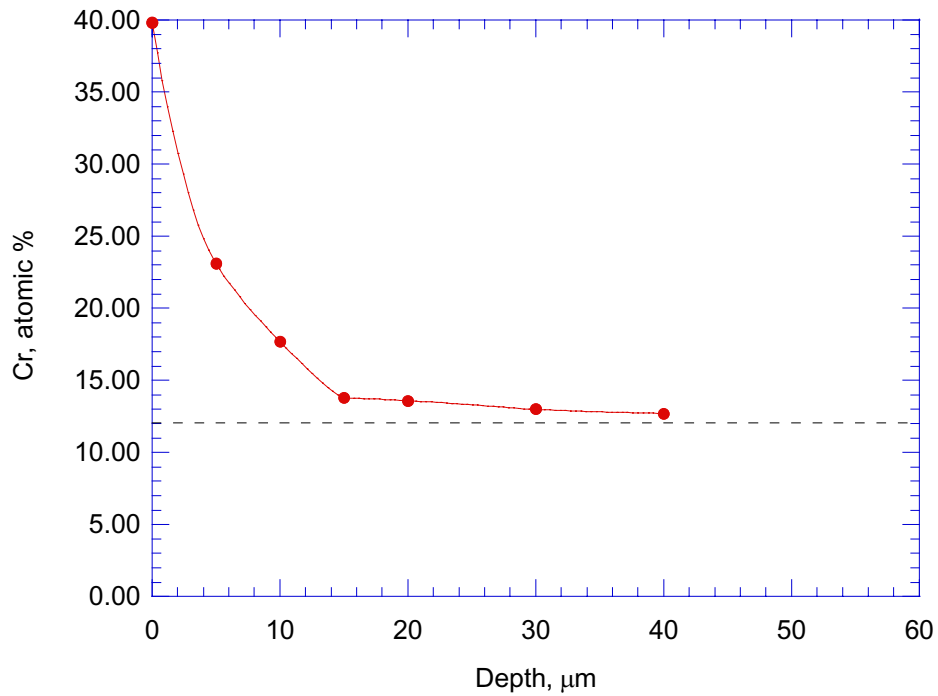


Figure 58. Diffusion Profile of Cr in 409 SS Prepared by Using Cr/X Alloy and Cr Metal Powders

7.2. Establishing Process Parameters In A Metallized Pilot Scale Fluidized Bed

The Cr coating process involves optimizing the following key variables to control the uniformity and reproducibility of the diffusion coating, and the surface finish of the coating (e.g., bright gray or dull green).

- Chromium metal powder composition
- Alumina powder
- Argon gas flow rate
- Hydrogen gas flow rate
- HCl gas flow rate
- Temperature profile of the process, i.e., heat up, time at coating temperature, and method and rate of cooling.

Each of these process variables has an influence on the performance and the outcome of the Cr coating process, and thus they must be properly established. SRI and QHT worked together to establish the parameters for the large-scale diffusion coating operation at QHT. This process included a number of laboratory experiments with materials obtained from bulk suppliers to confirm that the resulting coatings met necessary specifications, followed by a number of Cr coating experiments in the QHT pilot scale furnace. Bulk quantities of metal powder for these coating experiments were obtained from F.W. Winter, a metallurgical powder supplier to QHT.

The original parameters for the Cr diffusion coating process as established by SRI laboratories using a glass reactor and glass distributor (through which the mixed gases were introduced into the fluidized bed) are detailed in Table 15.

Table 15. SRI Parameters for Cr Coating

Item	SRI		Notes
Aluminum Oxide 105 μ M	200.5 G	98.04%	Bed Weight Percent
Chromium Alloy Powder	4 G	1.96%	Bed Weight Percent
Argon M ³ /H 400° - 1000°C	180 L/H	bal	Gas Flow Percent. Oxygen Purity Important.
Nitrogen To 400°C	Not Applicable		
Processing Temperature	975-1000°C		
Hcl Gas	0.78 L/H	0.40%	
Hydrogen	18 L/H	10%	Ratio 25/1 SRI
Processing Time	2.5 H Plus 0.5 H		
Time To Heat Tube To Temperature	75 Min		
Cooling Time To 30°C	45 Min		Cooled In Bed Under Ar/H ₂ Flow
Retort	Glass		
Diameter Of Furnace	2.7 In. (68 Mm)		
Microstructure After Processing	Fine Grained Annealed		

Although we tried to use SRI procedures as closely as possible in the initial runs at QHT's furnaces, there are some differences in the tube loading and unloading method between the SRI process and the QHT commercial process. In the SRI process, because of its small-scale nature, tubes were loaded and unloaded at room temperature, i.e., the fluidized bed was heated and cooled down in each coating cycle. In the QHT process, the fluidized bed is usually kept at temperature for economic and practical reasons, and the tubes are transferred to and from the bed at the operating temperature. The sequence of the QHT coating process is as follows:

- Load tubes at Load/Unload bay into basket.
- Pick up basket with tubes by protective atmosphere hood (PAH) and move PAH over the top of the furnace.
- Purge PAH with nitrogen until oxygen level is below 10 ppm, open the furnace lid and lower parts into furnace at a temperature of 975°-1000°C.
- Process tubes and basket as per recommended cycle.
- Purge PAH at end of cycle.
- When purged, remove tubes and basket from the furnace into PAH.
- Move hood to quenching fluidized bed.
- Purge and then lower tubes into quenching fluidized bed for cooling.

- When cooled, remove tubes from quenching fluidized bed and transfer back to Load/Unload bay.

We performed 17 trials in the pilot scale furnace (300 mm diameter × 600 mm deep) at Knoxfield, Australia. The major problems arising from the transfer of the SRI parameters to the QHT fluidized bed design can be categorized into process parameter issues and equipment design issues, which are discussed in detail below.

7.2.1. Process Parameter Issues

Initially QHT performed trials in accordance with the SRI coating procedures and parameters provided to QHT. The first results indicated that the same profile of chromium distribution could not be achieved in the QHT furnace with the SRI parameters. Subsequently, a Cr diffusion profile identical to the SRI profile was achieved by increasing the chromium powder concentration and HCl gas concentration. The differences in the parameters in the QHT furnace and at SRI are shown in Table 16. Figure 59 shows a representative Cr diffusion profile of a coating prepared in the pilot scale furnace using the parameters given in Table 16.

Table 16. Comparison of QHT and SRI Cr Coating Parameters

Item	QHT	%	SRI	%
Alumina 105 μm	70 kg	95%	200.5 g	98.04%
Chromium alloy powder	4 kg	5%	4 g	1.96%
Argon m ³ /h 400° - 1000°C	3 m ³	76%	180 L/h	90%
Nitrogen to 400°C	Room temperature to 400°C		Not applicable	
Processing temperature	975°C		1000°C	
HCl gas	0.035 m ³	1 %	0.78 L/h	0.40%
Hydrogen	0.80 m ³	23%	18 L/h	10%
Processing time	2.5 h plus 0.5 h w/o HCl		2.5 h plus 0.5 h	
Time to heat tube to temperature	3 min		75 min	
Cooling time to 30°C	10 min		30- 45 min est.	
Retort	MA253 Alloy		Glass	
Diameter of furnace	12 inches (300 mm)		2.7 inches (68 mm)	
Microstructure after processing	Very coarse grained		Fine grained annealed	
Results	Increase Cr up to 40%		Increase Cr up to 40%	
Differences	Ratios of gases Heat-up rate Metal retort vs. glass Higher temperature No use of nitrogen by SRI			

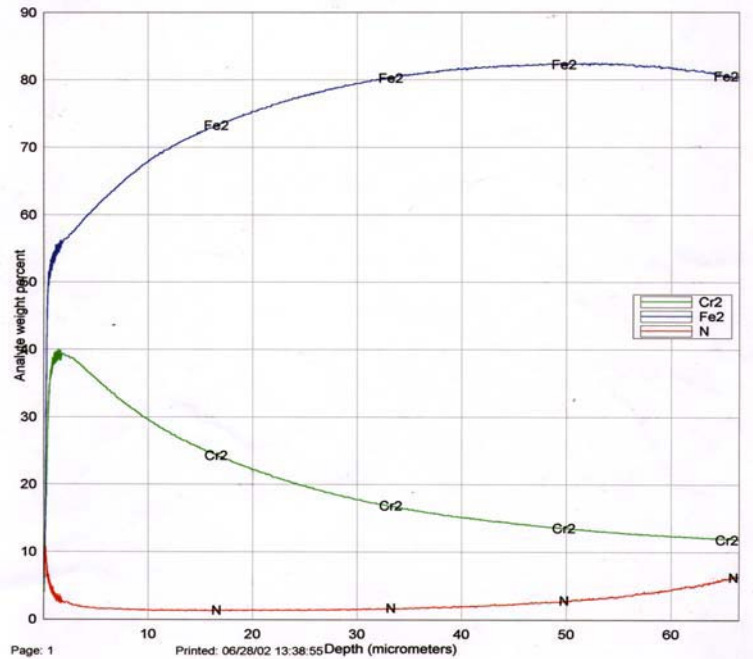


Figure 59. Representative Cr Diffusion Achieved in QHT Fluidized Bed at Knoxville

7.2.2. Equipment Issues.

In obtaining Cr profiles similar to those of SRI samples with the experimental parameters shown above, we encountered two process equipment problems. First, the powder immediately above and on the distributor was sintering for approximately 10–15 mm distance, as shown in Figure 60 and Figure 61, blocking the distributor. This would reduce the efficiency of Cr coating process and, furthermore, would significantly affect the quality of subsequent runs in a continuous operation. Second, the fluidizing particles were sticking to the samples being coated, i.e., the bed powder was not draining out of the tubes as they were removed from the bed. This would result in poor fluidization and unnecessary loss of fluidized bed powder in a continuous operation. We had not observed these problems in SRI fluidized beds. The fundamental design differences between the SRI fluidized bed and the QHT fluidized bed are given in Table 17.

Sintering at the base of the bed was thought to be related to the purity of the gases, and the mixing of the HCl gas. Powder sticking was thought to be related to excessive usage of HCl gas with the result that too much chromium chloride was being produced and not being removed from the parts before they were removed from the bed. The excessive usage of the HCl gas was also thought to be necessary to compensate for the purity of the gases then being used. Therefore, in later trials we modified the distributor and used higher purity argon and hydrogen. With these changes, both the sintering and sticking were significantly reduced but not completely eliminated.

We performed further tests with varying HCl to eliminate the powder sintering problem above the distributor plate. Tests 15 and 16 in the furnace provided a suitable Cr profile

with no significant sticking of the powder. In these trials, careful attention was paid to avoid contamination of oxygen by modifying the loading sequence. In the modified loading sequence, the tubes were immersed in the bed at 400°C and heated to operating temperature (1000°C) and treated, then cooled in the top chamber. These tests indicated that contamination of the bed from oxygen was critical, and that if the bed was not contaminated, a lower percentage of HCl gas could produce satisfactory results and eliminate sintering and severe sticking of the powder to the parts.

Table 17. Comparison of SRI and QHT Fluidized Bed Process

Item	SRI	QHT	Comments
Retort	Glass	Metal	Glass Would Be Totally Inert To Gas Reactions; Metal Is Not
Diffuser Construction	Glass	Metal - 2 Stage Distributor	Glass Diffusers Cannot Be Scaled Up Successfully
Diffuser Temperature	Hot Close To Operating Temp	Cold For Two Reasons: 1. Can Be Scaled Up 2. Reactions With Corrosive Gases Escalate At High Temps	
Diffuser - Gas Mixing	Gas Premixed	Two Diffusers Used, One For Inert Gases And The Other For Corrosive Hcl Gas With Carrier Gas	Gas Enters Bed Relatively Cold Gas Premixing Not As Good
Purity Of Gases	High Purity Used	Industrial Grades Used Except For Hcl	
Tube Samples	In Bed From Room Temp To Room Temp	Loaded And Removed At Temps Above 950°C	



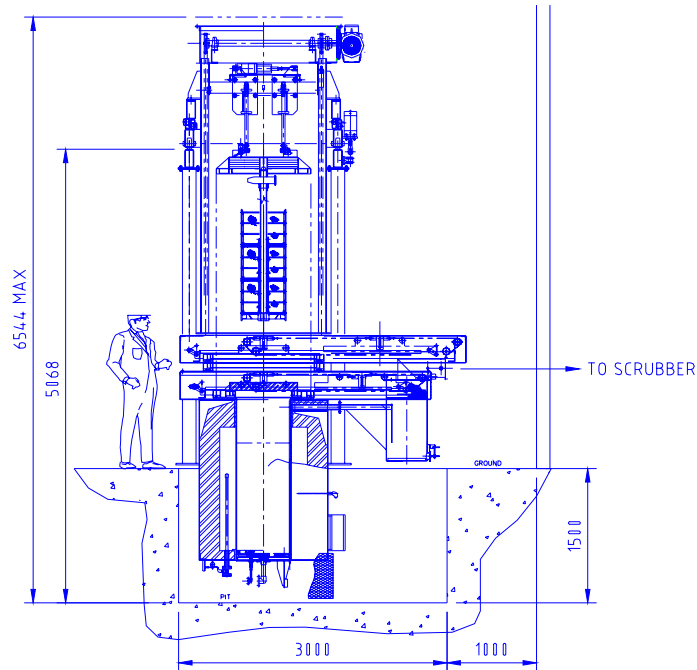
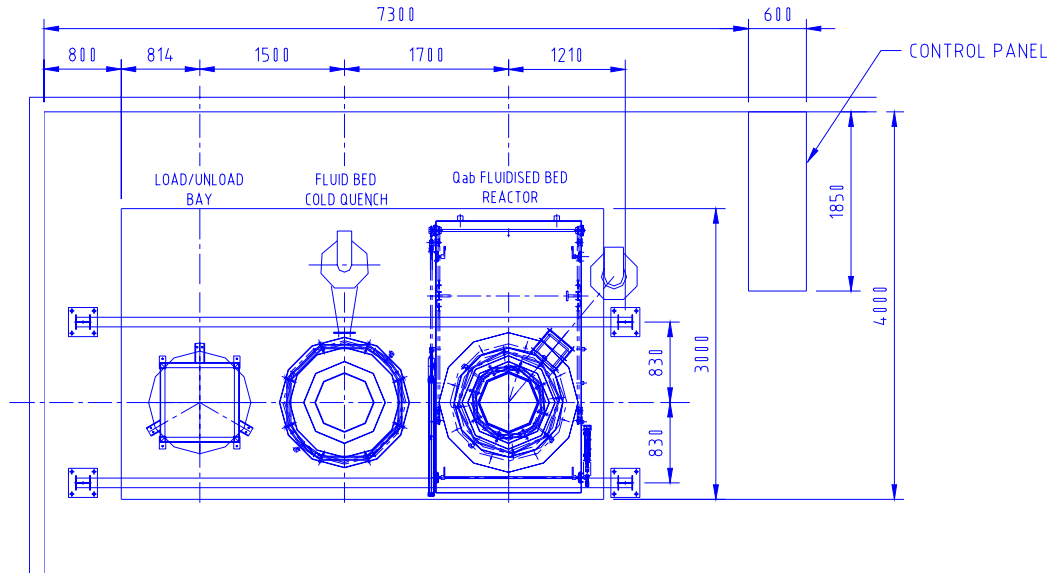
Figure 60. Top Distributor Showing Coarse Grit and Sintering



Figure 61. Sintered Cr Powder Recovered from Above the Flexible Tile

7.3. Designing And Building Of Commercial Fluidized Bed Plant For Chromium Coatings

QHT designed and built a commercial fluidized bed treatment plant for the Cr coating process based on the Cr coating technology developed by SRI and GTI. QHT completed the installation of this industrial scale fluidized bed reactor at Bayswater, Australia, in April 2002. Figure 62 is a schematic diagram of the QHT furnace at Bayswater. Figure 63 shows a photograph of the new plant. This plant would combine conventional heat treatment with the new diffusion coatings, the conventional heat treatment supporting the “acceptance time” needed to introduce the new coatings such as Cr coatings on 409 SS to the industry. The Bayswater plant furnace has a useful working bed of 600 mm diameter × 1500 mm deep.



UNLESS OTHERWISE STATED ALL DIMENSIONS IN MILLIMETRES. GENERAL TOLERANCES TO BE AS SPECIFIED BELOW		 3rd Angle Projection		QUALITY HEAT TECHNOLOGIES Pty. Ltd.	
LINEAR FINISHING: UP TO 50mm ±1 50 TO 100mm ±2 100 - 300mm ±4 300 - 1000mm ±8	LINEAR FABRICATION: UP TO 300mm ±1 300 - 1000mm ±1.5 1000 - 2000mm ±2 2000 - 4000mm ±3 4000 - 10000mm ±5 OVER 10000mm ±5			Drawn SON PHAM Checked Approved Client Approval Drawing Size B1 Scale 1:25	Drawing Title Project & Client Project Number Material
ANGULAR -90° ±1° -91° ±2° This drawing is the property of QUALITY HEAT TECHNOLOGIES PTY. LTD. and includes certain proprietary designs and patents and must not be used in any way detrimental to their interests.				-	-
				Drawing Number	Rev
				ED12228-004	1

Figure 62. Schematic Diagram of the Fluidized Bed Furnace



Figure 63. QHT's New Plant for Fluidized Bed Coating at Bayswater, Australia

7.4. Establishing Parameters for the Production Metal Lined Fluidized Bed at Bayswater

7.4.1. Technical Parameters

Using parameters identical to those for the 300 mm diameter furnace, we processed 409 SS tubes in the production furnace. Figure 64 shows the loaded basket ready for processing in the furnace. The furnace can accommodate 50 tubes of 38.1 mm diameter \times 1 m long in a single load. The bed needs about 300 kg of alumina powder for a single trial.

The first trial in the production furnace had to be abandoned because of a blocked exhaust line. In the second trial, we managed to obtain up to 20% Cr, as shown in Figure 65. We believe the lower Cr content was due to 'retort conditioning' and insufficient HCl. Also, we observed Cr powder sintering at the base of the bed in the area of the distributor (Figure 9), similar to what happened in our pilot scale trials. We believe these problems were due to poor mixing of HCl with the carrier gas. To minimize this problem, the furnace was modified so the distributor was placed in the coarse grit immediately above the main distributor and additional inert gas was added to the HCl so as to ensure uniform flow of the HCl gas out of each of the distributor holes (i.e., higher velocity and premixed before exit). This significantly improved the uniformity of processing in the bed, i.e., tubes located at various positions within the bed exhibited uniform diffusion. This has overcome the problem with the second distributor, but the problem of sintering above the coarse flexible grit still remains and the cause has not been accurately identified, although the purity of the incoming gases has significantly reduced the problem. Unfortunately, QHT management decided to stop the technical development effort at this point.



Figure 64. Loaded Tube Basket Ready for Processing at Bayswater

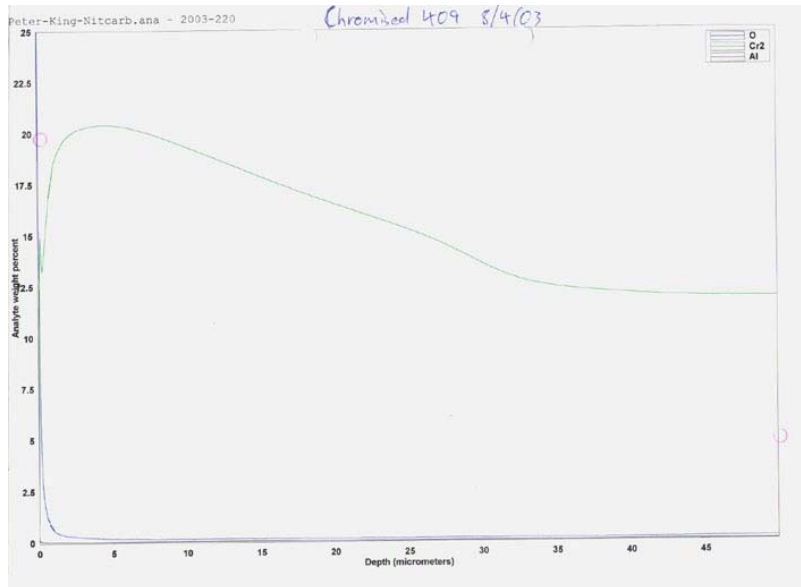


Figure 65. Cr Profile of Coated 409 SS Tube Resulting from a Trial at Bayswater



Figure 66. View of Distributor Showing Sintered Powder and Sticking of Powder to Distributor

7.4.2. Consumable Cost Estimates

Table 18 estimates the consumables cost for the process based on the QHT 24-inch-wide × 48-inch-deep reactor. The first case (9.5 h per cycle) is included to heat up and cool down the tubes in the main reactor, in case the purity of the atmosphere in a hot transfer hood cannot be assured. The second case (3.75 h per cycle) is based on the transfer hood being suitable and tubes processed continuously. These costs lead to savings over using expensive alloys such as AL294C and super austenitic stainless steels, on the order of 30% to 60%, including the equipment cost.

Table 18. Cost of Various Consumables in Cr Coating of Steel

Consumable	Stage 1A	Stage 1B	Stage 2	Stage 3	Total	%	Cost/ Unit	Notes
Heating up and cooling down cycle over 9.5 h								
Electricity	\$17.90	\$0.00	\$10.00	\$0.00	\$27.90	11.41%	\$0.10	Stage 1: Heating up the bed to 1000°C
Argon	\$0.00	\$56.00	\$32.00	\$10.00	\$18.00	7.36%	\$1.50	Stage 1B : Changeover to argon at 400°C
Hydrogen	\$0.00	\$3.20	\$19.14	\$0.00	\$22.34	9.14%	\$1.80	Stage 2: Actual Cr coating time
HCl	\$0.00	\$0.00	\$13.00	\$0.00	\$13.00	5.32%	\$23.00	Stage 3: Cr coating without HCl gas
Chromium powder	\$0.00	\$0.00	\$120.00	\$0.00	\$120.00	49.09%	\$20.00	Assume 1% of bed weight consumed for Cr
Nitrogen purging	\$10.50	\$0.00	\$0.00	\$3.00	\$13.50	5.52%	\$0.30	Purging in hood plus start up
Nitrogen quench	\$0.00	\$0.00	\$0.00	\$5.00	\$5.00	2.05%	\$0.30	Nitrogen in quench bed
Nitrogen cooling	\$0.00	\$0.00	\$0.00	\$14.70	\$14.70	6.01%	\$0.30	Cooling furnace from 1000° - 600°C
Miscellaneous	\$0.00	\$0.00	\$0.00	\$10.00	\$10.00	4.09%		Baskets etc.
Total	\$28.40	\$59.20	\$194.14	\$42.70	\$244.44	100.00%		

Table 18. (continued)

Consumable	Stage 1A	Stage 1B	Stage 2	Stage 3	Total	%	Cost/ Unit	Notes
Cost of cycle with bed at temperature for 3.75 h								
Electricity	\$0.00	\$0.00	\$10.00	\$0.00	\$10.00	4.57%	\$0.10	Stage 1: Heating up the bed to 1000°C
Argon	\$0.00	\$8.00	\$21.25	\$6.50	\$35.75	16.33%	\$1.50	Stage 1B: Changeover to argon at 400°C
Hydrogen	\$0.00	\$3.00	\$19.14	\$0.00	\$22.14	10.11%	\$1.80	Stage 2: Actual Cr coating time
HCl	\$0.00	\$0.00	\$13.00	\$0.00	\$13.00	5.94%	\$23.00	Stage 3: Cr coating without HCl gas
Chromium powder	\$0.00	\$0.00	\$120.00	\$0.00	\$120.00	54.82%	\$20.00	Assume 1% of bed weight consumed for Cr
Nitrogen purging	\$0.00	\$0.00	\$0.00	\$3.00	\$3.00	1.37%	\$0.30	Purging in hood
Nitrogen quench	\$0.00	\$0.00	\$0.00	\$5.00	\$5.00	2.28%	\$0.30	Nitrogen in quench bed
Nitrogen cooling	\$0.00	\$0.00	\$0.00	\$0.00	\$0.00	0.00%	\$0.30	Not applicable
Miscellaneous	\$0.00	\$0.00	\$0.00	\$5.00	\$10.00	4.57%		Baskets etc.
Total	\$0.00	\$11.00	\$183.39	\$19.50	\$218.89	100.00%		

7.5. Summary and Future Plans for Production of Large Coated Components.

We have shown that tubes up to a length of 1050 mm can be uniformly (within acceptable limits) Cr coated both internally and externally. The parameters for performing the process, while not completely optimized, can be used to produce a satisfactory corrosion-resistant coating. For competitive commercial scale production, we need to overcome the problem of powder sintering above the distributor and determine the allowable contamination of the gases used in the process. Also, we need to determine the ability to process loads by loading and unloading the fluidized bed at operating temperature, i.e., the possibility of contamination of the bed with oxygen and the effectiveness of the transfer system to maintain atmosphere integrity during loading and unloading. For the production of longer tubes, we need to confirm the uniformity of internal and external chromium diffusion and the relationship of diameter to length over which the uniformity can be maintained.

The transfer of IP from SRI international to QHT took longer than expected due to necessary modifications to the equipment and variables associated with the different types of fluidized bed equipment, as previously discussed. Furthermore, QHT management decided to stop the development work in the late stages of the program, and thus optimization of the process and delivery of Cr-coated tubes for fabrication of the prototype chiller within the project performance period was hampered. We are currently working with QHT management to get them to agree to complete the coating of 409 SS tubes for the prototype triple-effect generator. We recently negotiated an agreement with QHT that they would perform two more coating trials to produce tubes for the prototype chiller at a substantially higher cost. SRI and GTI are absorbing the additional expenses in order to complete the project and commercialize a research product that will benefit California ratepayers. We were not able to complete a prototype generator before completion of the project. However, we will continue to interact with the Commission as appropriate and keep the Commission informed of the progress of the commercialization effort.

GTI and SRI have terminated the exclusive license with QHT in Australia and are seeking a new licensee for the Cr diffusion coating process. We are also seeking several other avenues to produce Cr-coated tubes for the prototype chiller if QHT fails to succeed in their final trials. Mr. Ray Reynoldson, as a non-paid consultant, is contacting various manufacturers to produce coated tubes up to 4 ft long using the fluidized bed coating process. GTI and SRI are assisting this effort. GTI is also evaluating the possibilities of producing the tubes on site. The ability to produce large scale coated specimens will significantly shorten the market acceptance time. SRI and GTI could use coated tubes for promotional activities. The market penetration of Cr coatings would be much easier if we can provide full scale coated tubes to equipment manufacturers for field evaluation. Table 19 summarizes the options thus far identified. We will continue our commercialization and field testing efforts and will keep the Commission informed of the progress. The Cr coated low cost steel production readiness plan is envisioned as follows.

Cr Coated Tube Production Plan

- Finalize Development Of Process
 - This is very close to being finalized. But parameters for materials to be processed as well as all incoming gases need to be further optimized.
 - Effect of alloy additives (accelerant)
 - Usage of chromium per cycle purity of gases
 - Produce tubes for Broad prototype
- Finalize development of Equipment.
 - Overcome the distributor problem
 - Purity level of transfer Hood
 - Quality control tests need to be conducted
- Trials on chiller tubes
 - Field test tubes in the Broad prototype chiller
- Produce marketing plans
 - Establish existing market for Cr coating by other techniques
 - Analyze the oil and gas industry as well as aerospace
 - Segment market for tubing and prepare list of contacts
 - Study competition such as diffusion alloys etc.
 - Talk with market researchers on needs and requirements
 - Contact existing interested Companies
 - (e.g., Modene, Lennox)
 - Prepare publicity
 - More details about equipment and costs and methods of processing
 - Issue letters publicity and press releases
 - Include technical papers on process and corrosion etc- List journals applicable to corrosion etc.
- Prepare samples for potential users
- Arrange visits to interested parties
- Seek out subcontractor heat treat facility to perform trials

Table 19. Options for Full Scale Cr-Coated Tube Production

Option	Equipment or Alternative	Est. Budget Cost (US\$)	Notes
1	Fund Arvin to modify and reactivate equipment. Time line 3 – 6 months	50 – 100 K	Arvin to allow use and modification of equipment by outside party, i.e. RWR or SRI
2	Purchase equipment from Arvin. Remove and reinstall complete line at a contract heat treater on a lease arrangement. Time line 6 – 9 months	350 – 400 K, but some of the costs recoverable from the heat treater over 5 years	The contract heat treater could take the complete line of equipment and use it for other purposes as well as finishing off the CEC project.
3	Arrange for a heat treater, e.g., Dynamic Metal Treating, to modify their furnace and process tubes. Time line 9 months	75 – 125 K	If agreeable to modifying equipment.
4	Arrange for a proprietary contact underway to install equipment and produce the tubes. Time line 9 – 12 months	Cost could be <50 K, as the manufacturer would purchase the equipment for other purposes.	Conceivably they could also license the technology.
5	Build a new piece of equipment 20 inches diameter x 48 inches effective depth. Install at SRI or GTI. Time line 9 – 12 months	Cost 300 K	This would be for a basic turnkey installation of just the furnace without a top chamber, which means the tubes would be heated up and cooled down in the bed.
6	Add a top cooling and protective hood chamber. Time line same as Option 5	Cost 200 K, making total 500 K	This would enable the loads to be processed one after another without having to cool down and reheat for the next load.
7	Negotiate with GCD/QHT to purchase equipment. Time line 6 months	300 K for equipment purchase - reinstalling and commissioning at SRI or GTI is another 200-250 K	Cost of operating a larger diameter furnace, i.e., 24 inches vs 20 inches, is 50% higher. Plan foregoes \$100 K in royalties etc.
8	Build furnace as per Option 5 and install in Australia at Deakin University. Time line 6 – 7 months	Cost 350 - 400 K	Furnace owned by SRI/GTI. Possibly fund other research work at Deakin University.

8.0 Component Testing in Prototype Machine

8.1. Broad Prototype Design for Cr-Coated 409 SS

Broad USA has planned to design and fabricate a prototype direct-fired absorption generator with Cr-coated 409 SS tubes to be provided by QHT. The prototype generator will be of 25 cooling ton capacity, with water/LiBr/ZnBr₂ absorption fluid operating up to a temperature of 205°C (400°F). The pressure and flow-rate will be typical of a triple-effect generator with bromide absorption fluids. Broad will use a mix of tubes in the generator – 409 SS tubes coated by QHT under an SRI-GTI license, and also some SeaCure® tubes – for direct comparison of the performance of coated materials in the triple-effect generator environment. The emphasis will be on corrosion resistance behavior of coated components, and not on thermodynamic data collection.

Figure 67 illustrates the prototype triple-effect absorption chiller system designed by Broad USA. The steam from the generator is used by a double-stage, steam absorption chiller, which is a separate part of the triple-effect absorption chiller system. The triple-effect generator is related with the second-stage chiller only as a heat source, and there is no internal exchange of any fluids. The triple-effect generator and the second-stage chiller have two different control systems. An auxiliary circulating device is also included to facilitate the normal fluid circulation within the triple-effect generator. Figure 68 shows a drawing of the triple-effect generator with dotted lines showing the flue tubes. Some of these tubes will be coated 409 SS and others will be SeaCure® alloy used as a control.

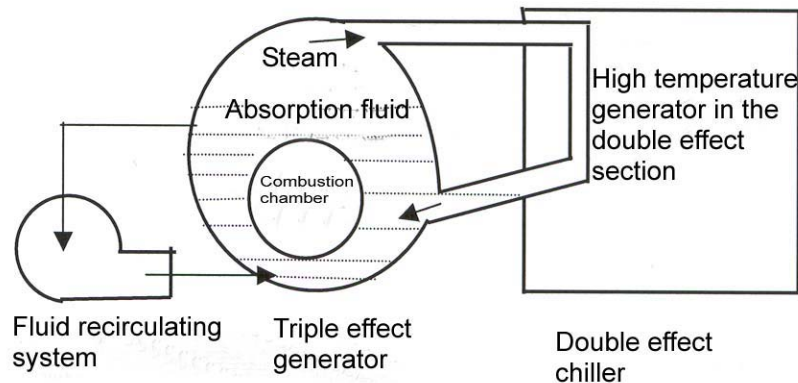


Figure 67. Simplified Diagram of a Broad Triple-Effect Advanced Absorption Chiller

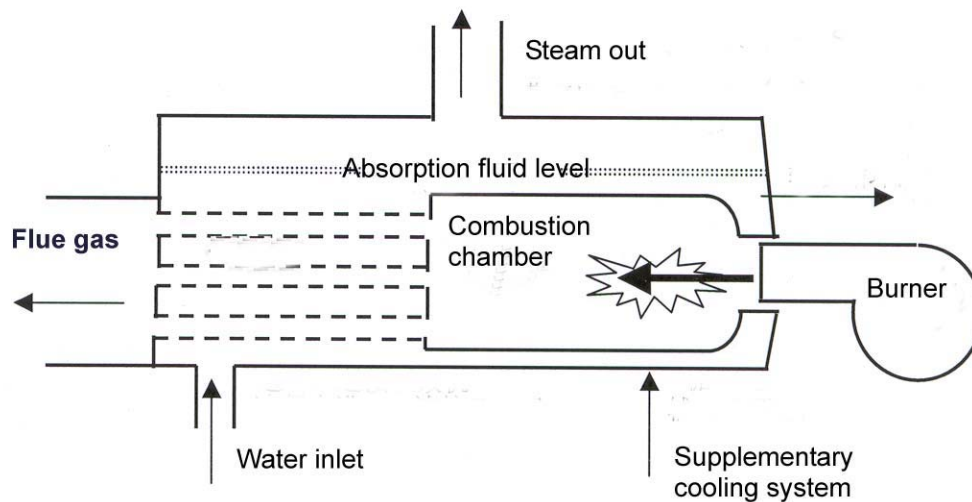


Figure 68. Simplified Diagram of the Broad Triple-Effect Generator

Broad's prototype design calls for coated tubes 1219 mm in length, 38 mm in outside diameter, and about 4 mm in thickness. The coated tubes will be made to size by welding. The welding rod materials will be AISI316L or 309L. Broad will weld the tubes to the tube sheet by the tungsten inert gas welding process (TIG).

8.2. Prototype Generator Test Plan

The test plan for the prototype generator design, fabrication and testing is as follows:

- a. Broad will finalize the design of the generator and process procedures according to GTI's schedule for providing coated tubes.
- b. Design control system for the generator, paying special attention to pressure, temperature, and safety.
- c. Prepare the test station, including cooling tower, arrangement of heating and cooling loads, consumption, fuels, etc.
- d. According to the design, prepare all materials, control parts, and other components other than the coated tubes.
- e. Make a 30-ton double-effect steam chiller with its energy input connection modified to facilitate the triple-effect generator.
- f. Manufacture about 300-500 kg of solution according to the fluid composition provided by GTI.
- g. With the coated tubes, begin to make the triple-effect generator for test.
- h. Purchase test equipment and instruments for measurement of temperature, pressure, time, flow-rate, etc.
- i. Select and train test personnel (for data collecting).

- j. Test, collect data, and make phase reports.
- k. When the test hours are completed, disassemble the generator and take samples of the tested tubes.
- l. Analyze samples and send samples to GTI.

The test data to be recorded and the order of analysis are given below:

- a. Take records of temperature, pressure, and flow-rate of fluid at set time intervals.
- b. Compare and analyze tube material before and after test.
- c. Compare and analyze solution contents before and after test (Fe, Ni, Cr, Mo, etc).

9.0 Summary And Conclusions

Advanced absorption cycles, which include double-effect, triple-effect, and generator absorber heat exchange cycles, offer significant advantages over conventional heating systems. As advanced cycles operate at much higher temperatures than conventional cycles, and as concentrated corrosive solutions consisting of salts such as LiBr, LiCl, and ZnBr₂ are used absorbents/refrigerants, many common alloys suffer significant corrosion attack in these systems. Selection of a suitable alloy that is stable under these aggressive conditions is a major issue, and chromium/molybdenum super alloys such as AL6XN® and SeaCure®, which are 6-7 times more expensive than 409 SS, are the currently available choices. As a result, the capital costs of the equipment are high; offsetting the economic gain from high performance efficiency, and thus market acceptance is slow.

To overcome this problem and remove the key technical barriers to market penetration, our efforts were focused on development of corrosion-resistant metallic coatings, which have surface compositions similar to those of super alloys, on less-expensive alloys. Fluidized bed reactor chemical vapor deposition technology (FBR-CVD), developed by SRI, can be used to produce metallic diffusion coatings with gradient compositions, in a shorter deposition time than is required in standard CVD techniques. More importantly, since the coating-substrate interface is diffused, mechanical and thermal stresses are minimal, resulting in a strongly anchored coating. Because of the low time-temperature budget, the grain growth during the coating process is minimal compared with the pack cementation process. Diffusion-coated low-cost alloys can be prepared with proper optimization procedures and careful selection of coating metals, to provide surface composition and corrosion-resistant properties similar to those of the much more expensive super alloys. Our goal was to produce coated 409 SS material to replace AL6XN® and SeaCure® components (tubes and sheets) in triple-effect cycles, as designed in Trane prototype units.

Our past experience and thermochemical analysis led us to the idea that metals such as Cr, Ni, Si, Ti, W, and Mo can be coated on 409 SS and C 1018 alloys to produce corrosion resistant diffusion coatings. Preliminary optimization experiments showed that Cr coatings with diffusion lengths > 50 µm can be successfully prepared on 409 SS at 1000°C in 2 h, followed by a 30-min annealing time. Similar coatings on pure iron and C 1018 have diffusion depths more than 25 µm, and the coated material showed adequate corrosion resistance in double effect advanced absorption cycle environment (in LiBr/LiOH at 165°C)

An important aspect of the FBR-CVD technique is that, it can easily be used for coating more than one metal (e.g., Ni and Cr, W and Cr), providing tailored compositions for the exposure environment. As some elements are difficult to deposit by FBRCVD, alternative approach to obtain highly specialized multi-element diffusion coatings for extremely aggressive applications is to use combination of electrodeposition and FBR-CVD. The electrodeposited overlay coating can be diffused in to the substrate during the fluidized bed treatment. This approach was used to prepare Cr + Ni, Cr + Ni + Mo, Cr + Ni + W diffusion coatings on 409 SS. The rates of corrosion of these multi-metal coated specimens were significantly lower than those of as-received ones in triple-effect conditions (LZB at 260°C).

Many advances in the direction of using coated samples in field applications were successfully completed in this project. Cr-coated coupons did not show any sign of

corrosion at the welds, indicating that Cr-coated components can be safely welded to form large, complicated equipment. The 409 SS specimens coated with research grade Cr powder as well as commercial bulk metal powders did not show any sign of corrosion in the triple-effect environment. Furthermore, the ASTM G48 - 76 test (conc. FeCl_3), recommended for the investigation of pitting and crevice corrosion, did not initiate any pits on Cr-coated 409 SS specimens. The rate of corrosion of Cr-coated 409 SS specimens in the FeCl_3 medium was a factor of 40 lower than that for as-received 409 SS. Furthermore, the critical pitting temperature of Cr-coated 409 SS tubes was similar to that of AL29-4C super alloy. All these tests demonstrate that Cr-coated 409 SS can be used to replace super alloys in advanced absorption environment.

As the first step toward commercialization, SRI's FBR-CVD technology was licensed to Quality Heat Technologies (QHT) in Australia, a company specializes in fluidized bed coatings and heat treatments to improve wear resistance of metallic components. After a series of optimization processes, QHT was able to produce Cr coatings on larger tubes with very impressive diffusion depth profiles, which is a major achievement in the scaling-up operation. QHT has issued press releases in this regard. The last step of the project is to test the tubes coated by QHT in the prototype unit designed by Broad USA, to demonstrate the industrial applicability of the SRI coating process.

As mentioned in Section 0, QHT management decided to stop the development work in the late stages of the program because of poor economic conditions of the company. However, we are currently working to get QHT to agree to complete the coating of 409 SS tubes for the prototype triple-effect generator. We recently negotiated an agreement with QHT that they would perform two more coating trials to produce tubes for the prototype chiller. We were not able to complete a prototype generator before the end of this project, but we are exploring several options to accomplish this and complete the remainder of the commercialization program. Commercialization of this research product will provide low-cost alternatives to expensive super alloys for use in the highly corrosive double- and triple-effect environments, and the cost savings will benefit California ratepayers.

References

1. K.E. Herold, *Absorption Chillers and Heat Pumps*, CRC Press, 1996.
2. *1988 ASHRAE Handbook: Equipment* (American Society of Heating, Refrigerating, and Air-Conditioning Engineers, Inc., Atlanta, GA, 1988).
3. *1990 ASHRAE Handbook: Refrigeration Systems and Applications* (American Society of Heating, Refrigerating, and Air-Conditioning Engineers, Inc., Atlanta, GA, 1990).
4. *1993 ASHRAE Handbook: Fundamentals* (American Society of Heating, Refrigerating, and Air-Conditioning Engineers, Inc., Atlanta, GA, 1993).
5. B.A. Phillips, "Development of an Advanced-Cycle Absorption Heat Pump for Residential Applications," *Proceedings of the 2nd DOE/ORNL Heat Pump Conference: Research and Development on Heat Pumps for Space Conditioning Applications*, prepared by Oak Ridge National Laboratory, Oak Ridge, TN, for U.S. Department of Energy, Report No. CONF-8804100 (1988), pp. 111-116.
6. R.C. Reimann and B. Melikian, "Development and Proof-Testing of Advanced Absorption Refrigeration-Cycle Concepts - Phase II," *Proceedings of the 2nd DOE/ORNL Heat Pump Conference: Research and Development on Heat Pumps for Space Conditioning Applications*, prepared by Oak Ridge National Laboratory, Oak Ridge, TN, for U.S. Department of Energy, Report No. CONF-8804100 (1988).
7. R.J. Modahl and F.C. Hayes, "Evaluation of a Commercial Advanced Absorption Heat Pump Breadboard," *Proceedings of the 2nd DOE/ORNL Heat Pump Conference: Research and Development on Heat Pumps for Space Conditioning Applications*, prepared by Oak Ridge National Laboratory, Oak Ridge, TN, for U.S. Department of Energy, Report No. CONF-8804100, (1988), pp. 117-125.
8. G.B. Naumov et al., *Handbook of Thermodynamic Data*, U.S. Geological Survey, Menlo Park, CA, 1974.
9. P. Jayaweera, A. Sanjurjo, K. Lau, G. Krishnan, N. Priyantha, D. Lowe, and N. Jiang, "Corrosion Protection of Low-Cost Alloys in LiBr/Water Advanced Absorption Cycles," Final Report, SRI Project PYH 1184 (GTI Contract 5095-260-3561).
10. P. Jayaweera, D.M. Lowe, A. Sanjurjo, K.H. Lau, and L. Liang, *Surf. Coat. Technol.* **86-87** (1996) 522.
11. A. Sanjurjo, S. Hettiarachchi, K.H. Lau, P. Cox, and B. Wood, *Metallurgical Coatings and Thin Films 1992*, Vol. 1 (Elsevier, 1992), p. 224.
12. B. Wood, A. Sanjurjo, and S. Swider, *Surf. Coat. Technol.* **49** (1991) 228.
13. Sanjurjo, K.H. Lau, and B. Wood, *Metallurgical Coatings and Thin Films 1992*, Vol. 1 (Elsevier, 1992), p. 219.

14. N. Priyantha, P. Jayaweera, A. Sanjurjo, K. Lau, F. Lu and K. Krist, *Surf. Coat. Technol.*, (in print, 2004)
15. O. H. Kessler, F.T. Hofmann and P. Mayr, *Surf. Coat. Technol.* **120-121** (1999) 366.
16. A. Cabrera et al., U.S. Patent 4,822,642, April 18, 1989
17. Cabrera et al., U.S. Patent 4,714,632, December 22, 1987
18. P. Jayaweera, D.M. Lowe, A. Sanjurjo, K.H. Lau and L. Liang, *Surf. Coat. Technol.* **86-87** (1996) 522.
19. M. Itoh, H. Midorikawa, and A. Minata, "Hermetically Circulating Absorption Type Refrigerator," U.S. Patent 4,311,024 (January 19, 1982).
20. B.R.W. Hinton, "Corrosion Inhibition with Rare Earth Metal Salts," *J. Alloys Compds.* **15** (1992) 180.
21. S. Hettiarachchi, K.C. Irwin, A. Nigam, and S.C. Narang, "Synergistic Corrosion Inhibitors for Heat Pump Vapor Absorbents-Phase II," Final Report, SRI International, SRI Project PYC 6862 (1989), Client Private.
22. S. K. Kim and H.J. Yoo, *Surf. Coat. Technol.* **108-109** (1998) 564.
23. Vitina, V. Rubene, M. Lubane, V. Belmane, A. Krumina and A. Knipele, *Surf. Coat. Technol.* **120-121** (1999) 430.
24. M. Schlesinger and M. Paunovic, *Modern Electroplating*, 4th ed., Wiley & Sons, 2000,
25. O. Younes and E. Gileadi, *J. Electrochem. Soc.* **149** (2002) C100.
26. E.J. Podlaha and D. Landolt, *J. Electrochem. Soc.* **143** (1996) 885
27. K. Murase, H. Ando, E. Matubara, T. Hirato and Y. Awakura, *J. Electrochem. Soc.* **147** (2000) 2210.
28. J.L. Cao, L.T. Li, Y.L. Wang and Z.L. Gui, *J. Electrochem. Soc.* **148** (2001) F180
29. J.L. Coa, L.T. Li, Y.L. Wang, J.Q. Zhao and Z.L. Gui, *Mater. Res. Bull.* **36** (2001) 2103.
30. F.E. Rasmussen, J.T. Ravnkilde, P.T. Tang, O. Hansen and S. Bouwstra, *Sensors Actuators* **92** (2001) 242.
31. J.H. Russel, B.S. Covino, Jr. and S.J. Bullard, *Corrosion* **57** (2001) 360. ASTM Test G48 - 76, American Society for Testing and Materials, (reapproved 1980), pp. 280-283.